NASA CONTRACTOR REPORT

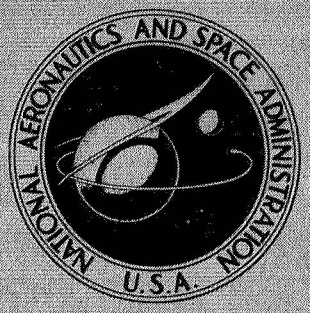

NASA CR-2110

NASA CR-2110

MAIN ROTOR FREE WAKE GEOMETRY EFFECTS ON BLADE AIR LOADS AND RESPONSE FOR HELICOPTERS IN STEADY MANEUVERS

Volume I — Theoretical Formulation and Analysis of Results

by S. Gene Sadler

Prepared by
ROCHESTER APPLIED SCIENCE ASSOCIATES, INC.
Rochester, N.Y. 14618
for Langley Research Center

NATIONAL AERONAUTICS AND SPACE ADMINISTRATION • WASHINGTON, D. C. • SEPTEMBER 1972

1. Report No.	2. Government Accession No.	3. Recipient's Catalog No.
NASA CR-2110		

4. Title and Subtitle	5. Report Date
MAIN ROTOR FREE WAKE GEOMETRY EFFECTS ON BLADE AIR LOADS AND RESPONSE FOR HELICOPTERS IN STEADY MANEUVERS. VOLUME I – THEORETICAL FORMULATION AND ANALYSIS OF RESULTS	September 1972
	6. Performing Organization Code
7. Author(s)	8. Performing Organization Report No.
S. Gene Sadler	RASA Rep. No. 71-13
9. Performing Organization Name and Address	10. Work Unit No.
Rochester Applied Science Associates, Inc. 140 Allens Creek Road Rochester, N.Y. 14618	11. Contract or Grant No. NAS 1-8448
	13. Type of Report and Period Covered
12. Sponsoring Agency Name and Address	Contractor Report
National Aeronautics and Space Administration Washington, D.C. 20546	14. Sponsoring Agency Code

15. Supplementary Notes

16. Abstract

A mathematical model and computer program was implemented to study the main rotor free wake geometry effects on helicopter rotor blade air loads and response in steady maneuvers. Volume I contains the theoretical formulation and analysis of results. Volume II (NASA CR-2111) contains the computer program listing.

17. Key Words (Suggested by Author(s))	18. Distribution Statement
Rotor wake Blade loads Maneuvers Math models	Unclassified – Unlimited

19. Security Classif. (of this report)	20. Security Classif. (of this page)	21. No. of Pages	22. Price*
Unclassified	Unclassified	108	$3.00

*For sale by the National Technical Information Service, Springfield, Virginia 22151

CONTENTS

MAIN ROTOR FREE WAKE GEOMETRY EFFECTS ON BLADE AIR LOADS AND RESPONSE FOR HELICOPTERS IN STEADY MANEUVERS

VOLUME I - THEORETICAL FORMULATION AND ANALYSIS OF RESULTS*

By S. Gene Sadler
Rochester Applied Science Associates, Inc.

SUMMARY

Rotor wake geometries were predicted by a process similar to start-up of a rotor in a free stream. An array of trailed and shed vortices was generated with vortex strengths corresponding to stepwise uniform radial and azimuthal blade circulations. The array was limited to an arbitrary number of azimuthal steps behind each blade, and the remainder of the wake model consisted of an arbitrary number of trailed vortices behind each array. Vortex elements were allowed to be transported by the resultant of the free stream and vortex-induced velocities. Blade angles of attack and relative motion between the rotor and its previously deposited wake were influenced by maneuvers. Wake geometries were computed, as were wake-induced velocity influence coefficients for use in the calculation of nonuniform downwash in the blade loads calculations.

Blade loads and response computations assumed steady-state (periodic) conditions, and included maneuver effects, the effects of nonuniform inflow, nonlinear airfoil characteristics, gravity loading, gyroscopic loading, and the response of flexible blades to the applied loads. The resulting nonlinear equations were solved by an iterative process, and computed data was compared with measured data, where available. The measured turn maneuvers were approximately steady maneuvers, the pull-ups were not steady, and no roll data was available. An alternate vortex-blade interaction model was used for one pull-up case.

Vortex-blade interactions were clearly indicated in the calculated wake-induced velocities. Air loads calculated with the use of static aerodynamic stall characteristics did not reflect many of these vortex-blade interactions, and were particularly unresponsive to high frequency angle of attack changes in the static stall region of angle of attack for an airfoil representation which included detailed Mach number effects in that region. Effects of both angle of attack rate and compressibility are required to predict air loads for such conditions. Computed blade response quantities were consistent with computed air loads and the normal modes used to represent the blades.

---

*VOLUME II - PROGRAM LISTINGS is contained in NASA CR-2111.

INTRODUCTION

Maneuver capabilities currently represent an undesirable limit on the operational envelope for most helicopters. These limitations are often a result of severe oscillatory air loads and helicopter response. There is an increasing need for an understanding of the causative physical phenomena, and there has recently been an increased effort to develop tools and to perform experimental and theoretical investigations to gain an understanding of these phenomena and to develop methods to overcome the existing limitations.

Accurate prediction of the aerodynamic flow field in which the helicopter rotor operates is critically important in the calculation of helicopter air loads, blade response, and vibration levels. There are indications that vortex-blade interactions are often dominant sources of high frequency air loads of sufficient magnitude that severe oscillatory response results. Such interactions have been discussed in references 1 through 4, among others. Methods for predicting the rotor's aerodynamic flow field have recently undergone extensive refinement, primarily due to the need for improved predictions and the availability of high-speed, large-capacity digital computers. These refinements have resulted in more realistically detailed models for calculation of nonuniform wake-induced inflow. Some of these models are discussed in references 5 through 9. Corresponding blade air load and blade response models have been developed, so that compatible blade loading and response models are used. The improved models for the wake-flow prediction have provided a good qualitative approximation to average measured wake flows (refs. 5, 10) and are expected to permit improved prediction of higher harmonic air loads and blade response.

Reference 5 discussed some of the difficulties associated with the prediction of vortex-induced inflow, and described a model which was developed to predict wake geometry and associated wake-induced flow and wake-induced velocity influence coefficients. This model showed good agreement with the measured average wake flows reported in reference 10, but was restricted to steady level forward flight operating conditions. The model discussed in this report is an extension of that discussed in reference 5, and includes effects of steady maneuvers on both wake geometry and blade load and response calculations. The computer program which has been implemented for this investigation is a modification of that of reference 5, and is operational for single rotor helicopters only. Wake geometries, wake-induced velocity influence coefficients, blade air loads and blade response were computed. Blade response (motions, shears, and moments) were computed in terms of a finite set (up to 12) of normal modes. The loads/response calculations were implemented for fully articulated rotors, teetering rotors or for rotors with (assumed) rigid hubs.

The blade loads/response model assumes periodicity of loads and response, so is inherently limited to analysis of steady-state level and maneuver flight conditions, and cannot be extended for analysis of non-steady flight conditions. The flight conditions analyzed herein include comparisons with some experimental cases which were not steady maneuvers, but which were intended to provide a measure of the acceptability of the programs as presently implemented.

The wake model program uses a forward-time integration method of solution. Vorticity is defined in terms of straight vortex elements with uniform properties along their lengths. The present wake program treats only steady-state level and maneuver flight conditions but could be extended to predict wake geometries, wake-induced inflow, and approximate blade loads and response for non-steady flight conditions as well, such as gust loading, transient maneuvers, etc. The extension of the wake program to include calculations of loads and response would necessitate a set of subroutines which would compute blade loads and response with a forward time integration method. It is anticipated that such extensions would increase the core storage requirements significantly, but would not greatly increase running times.

ANALYSIS

The computer programs were implemented as two main programs and preliminary calculations corresponding to convenient divisions in the theoretical representation of the helicopter rotor system and its wake, referred to hereafter as the model formulation and solution of governing equations. The program usage flow is indicated by the diagram in figure 1. The blade loads and response program uses input generated by the wake program as well as normal modes and natural frequencies defined by a previously developed blade frequency program. Both the wake and the blade loads and response programs require input specifying operating conditions, trim control settings, etc. These inputs may be obtained from experimental data or from appropriate preliminary calculations. The combined analyses and programs were directed toward prediction of blade air loads and response for helicopters in steady-maneuver flight conditions, in which the effects of a free wake and flexible blades have been included. (One flight condition calculation was performed with an empirically developed vortex-blade interaction model implemented for use in defining aerodynamic lift and moment coefficients. This was an exception to the usual procedure. Results of this case are noted at appropriate parts of the report.) As presently implemented, only one rotor may be modeled, blade-wake and wake-wake interactions were allowed, but no mass nor elastic coupling through the hub between blades was allowed. (The computer programs used for forward flight conditions could model two

arbitrarily located rotors, but core storage requirements and other considerations resulted in the present single-rotor model implementation for maneuver conditions.) All blades on the rotor were assumed to be identical, and all blades' motions, loads, etc., were also assumed to be the same.

Wake Model and Formulation

The wake geometry is calculated by carrying out a process similar to the start-up of a rotor in a free stream. The blades are located at a specified azimuthal and flapping position, without any wake. The blades then rotate through an azimuthal increment, $\Delta\psi$, and shed and trail vortex elements of unknown strength, but with known positions. The strengths of the vortices that are shed immediately behind the blade are then determined, and include the effect of their own self-induced velocities. (If it is desired, an estimate of the blade loads that result can then be determined, without the effects of blade flexibility being included.) All vortex element end points not attached to the blade are then allowed to translate as the blade is stepped forward for a time Δt with velocities as determined by the free stream and induced velocities. Here, $\Delta t = \Delta\psi/\Omega$, where Ω is the rotational speed. This completes the first step in the wake geometry calculation.

Subsequent steps are similar. The blades are rotated through an angle $\Delta\psi$ to new (specified) flapping angles. The vortices at and just behind the blades have unknown strength, while those in the wake have known strength. The strengths of the vortices attached to the blade are then computed, induced velocities at vortex element end points are computed, and end points not attached to the blade are allowed to translate with the resultant velocity due to the free stream and induced velocities. (Again, if desired, approximate blade loads may be computed, once blade circulations are known.) After the blade circulation values are determined for a given azimuthal location of the blades, vortex-induced velocities are computed at all vortex element end points in the wake. The blades are then advanced through an azimuthal increment, $\Delta\psi$, and each vortex end point which is not attached to the blades is allowed to translate for the time period $\Delta\psi/\Omega$, with the resultant velocity due to the free stream and induced velocities and with the position changes due to maneuvers, if any. The entire computational process for the new rotor blade positions is then repeated. That is, new wake-induced and free stream velocities at the blades are computed and used to determine new blade circulations. Then new vortex end point locations are computed, etc. Each blade advance results in an additional set of shed and trailed vortices being added to the wake. The number of revolutions of wake retained for actual computational purposes is specified by an input to the computer program. For practical use, the number of revolutions required is given by $N \geq 1/\mu\pi$.

In the manner described above, arrays of discrete shed and trailing vortices are generated immediately behind the blades with strengths which correspond to approximate blade loads. These arrays have stepwise radial and azimuthal strength variations so that total circulation is conserved. The arrays of shed and trailing vortices which are generated immediately behind the blades are referred to as the full mesh wake. Comparisons of wake flows predicted using this wake model for the entire wake with experimental measurements indicated that retention of shed elements with a coarse mesh resulted in poor induced velocity predictions, and that use of a fine mesh increased running time to an unacceptable level. Therefore, the full mesh wake was used to represent the wake immediately behind the blades, and a modified wake model was developed and implemented for use in the representation of the remainder of the wake, as shown in figure 2.

The modified wake consists of trailing vortices only, so vorticity is not conserved. The locations, circulations, core sizes, etc. of the trailing vortices in the modified wake are determined in terms of the full mesh wake's last sets of trailing vortex locations, circulations, etc. The wake-induced velocities, wake distortions, and other calculations are essentially the same for both the full mesh wake and for the modified wake portions of the wake model.

The wake and blade vortices are assumed to have finite-sized cores of rotational fluid, and the core sizes at the blade are controlled by an input parameter so as to be adjustable to improve agreement between calculated and experimental or theoretical core size data as desired. All elements are assumed to be straight for purposes of calculations, except where induced velocity calculations are performed for an end point of a vortex element due to an element with one end at that point. At such a point the neighboring elements are assumed to be arcs with curvature determined by three appropriate end points.

The basic mathematical formulations of the wake geometry program are those related to determination of blade motion, calculation of vortex-induced flow, and calculation of blade circulations including self-induced effects.

Blade motion.-The determination of approximate (steady and first harmonic) blade flapping motion is accomplished by using experimental data if available, or data from performance type calculations. If cyclic and collective pitch values and appropriate blade properties are known but blade coning and flapping motions are not known, a program option is available to compute approximate steady and first harmonic flapping motions internally. This option is described in detail in reference 5, and does not include maneuver effects.

Vortex-induced flow.-Vortex induced flow is computed at blade aerodynamic load points for calculation of bound circulation, and at vortex element end points for calculation of wake distortions. The Biot-Savart law (see ref. 11, for example) is the basic relationship used for calculating vortex induced flow exterior to vortex elements' rigidly rotating cores. At calculation points located inside a rigidly rotating vortex, the vortex induced velocity is determined from the rigidly rotating core velocity at that point. Flow at a vortex element end point due to the adjoining vortex elements accounts for curvature in the manner developed by Crimi in reference 7. At points where calculated velocities from an individual element are unrealistically high the velocities are restricted to be less than rotor tip speed; the total calculated velocity at a point is restricted to be less than a specified (by input) percentage of rotor tip speed. This type of limit is physically realistic, since the application of a very high velocity to a calculation point for a finite time increment, Δt, results in a larger motion than would result from a truly continuous type of calculation. That is, due to the finite nature of the model, calculation of wake distortions from vortex-induced velocities is unrealistic when very large velocities are permitted to remain over finite times, but are reasonable when velocities are limited. (In practice the limits were applied infrequently, as indicated by the program output.) The method of calculation of vortex-induced flow, i.e., the Biot-Savart law, is not directly influenced by the maneuver flight condition model requirements. Other effects of maneuvers on wake geometry, etc., are included in other parts of the model.

Maneuver effects on wake position.-The wake-induced and free stream velocities, together with a velocity due to the relative rotation between the rotor and the wake which accompanies the steady-state maneuvers are then computed to give each wake element end point its particular total velocity. The blades are then stepped forward through an angle $\Delta\psi$, and the wake element end points are transported by their respective velocities for a time Δt, where $\Delta t = \Delta\psi/\Omega$. Relative rotations and translations between the wake-oriented (inertial) coordinate system and the rotor-oriented coordinate system, as shown in figure 3, may be described by a coordinate transformation of the form

$$\begin{Bmatrix} x \\ y \\ z \end{Bmatrix}_{i+1} = \begin{Bmatrix} R \\ \end{Bmatrix} + \begin{Bmatrix} S \\ \end{Bmatrix} \begin{Bmatrix} x \\ y \\ z \end{Bmatrix}_{i} + \begin{Bmatrix} x \\ y \\ z \end{Bmatrix}_{I} \tag{1}$$

where the first term represents the translation due to helicopter motion, the second term represents the rotation due to helicopter motion, and the third term represents the wake-induced translations. Here (x, y, z) are the rectangular coordinate locations of the point. The definitions of R and S for the steady-state forward flight and maneuver flight conditions are given below for coordinated

turns, pull-ups, and rolls.

For coordinated turns with a rotation rate of $\dot{\delta}$ about a vertical axis (+ for nose-to-right turns)

$$\left[R\right] = \left[A\right]\left[P(\Lambda)\right]\left[D\right]R_c$$

$$\left[S\right] = \left[A\right]\left[P(\Lambda)\right]\left[P(0)\right]^{-1}\left[A\right]^{-1} \qquad (2)$$

where

$$\left[A\right] = \begin{bmatrix} 0 & +\cos\alpha_s & +\sin\alpha_s \\ 1 & 0 & 0 \\ 0 & -\sin\alpha_s & \cos\alpha_s \end{bmatrix}$$

$$\left[P(\Lambda)\right] = \begin{bmatrix} -\cos\Lambda\cos\Phi_c & -\sin\Lambda & -\cos\Lambda\sin\Phi_c \\ -\sin\Lambda\cos\Phi_c & \cos\Lambda & -\sin\Lambda\sin\Phi_c \\ \sin\Phi_c & 0 & -\cos\Phi_c \end{bmatrix}$$

$$\left[D\right] = \begin{bmatrix} \cos\Lambda - 1 \\ \sin\Lambda \\ 0 \end{bmatrix}$$

$\left[P(0)\right] = \left[P(\Lambda)\right]$ with $\Lambda = 0$

R_c = turn radius, meters

α_s = shaft tilt and positive aft, radians

$\Phi_c = \tan^{-1}(V_f^2/R_c g)$

V_f = helicopter velocity, meters/second (see fig. 4)

$\Lambda = \dot{\delta}\,\Delta t$

$\Delta t = 2\pi/N_s\Omega$

N_S = number of azimuthal steps per revolution

and other symbols have been defined previously. For a steady roll about a roll axis at roll rate $\dot{\phi}_R$, positive for right-side-down roll, the transformation matrices are defined as

$$\left\{R\right\} = \left\{B\right\}\left\{\Xi\right\}_1 \begin{Bmatrix} V_f \Delta t \\ Y \\ y,z \end{Bmatrix}_R$$

$$\left\{S\right\} = \left\{B\right\}\left\{\Xi\right\}_2 \left\{B\right\}^{-1} \tag{3}$$

where

$$\left\{B\right\} = \begin{bmatrix} \cos\alpha_R & 0 & \sin\alpha_R \\ 0 & 1 & 0 \\ -\sin\alpha_R & 0 & \cos\alpha_R \end{bmatrix}$$

$$\left\{\Xi\right\}_1 = \begin{bmatrix} 1 & 0 & 0 \\ 0 & \cos\phi_R & -\sin\phi_R \\ 0 & \sin\phi_R & \cos\phi_R \end{bmatrix}$$

$$\left\{\Xi\right\}_2 = \begin{bmatrix} 1 & 0 & 0 \\ 0 & 1-\cos\phi_R & \sin\phi_R \\ 0 & -\sin\phi_R & 1-\cos\phi_R \end{bmatrix}$$

the roll center is located at y_R, z_R in the shaft coordinate system, and

α_R = angle (about the y-axis) between the roll axis and the x-axis, radians

$\phi_R = \dot{\phi}\Delta t$.

Symmetrical pull-up at a rate $\dot{\alpha}_A$ with a radius R_p from the hub axis result in coordinate transformation matrices as defined by

$$\left[R\right] = \begin{bmatrix} \sin\alpha_A \\ 0 \\ 1-\cos\alpha_A \end{bmatrix} R_p$$

$$\left[S\right] = \begin{bmatrix} \cos\alpha_A & & -\sin\alpha_A \\ 0 & 1 & 0 \\ \sin\alpha_A & 0 & \cos\alpha_A \end{bmatrix} \tag{4}$$

where $\alpha_A = \dot{\alpha}_A \Delta t$.

Steady climb or steady forward flight with climb rate w_c and/or forward velocity V_f result in coordinate transformation matrices defined by

$$\left[R\right] = \begin{bmatrix} V_f \\ 0 \\ w_c \end{bmatrix} \Delta t$$

$$\left[S\right] = \begin{bmatrix} 1 & 0 & 0 \\ 0 & 1 & 0 \\ 0 & 0 & 1 \end{bmatrix}$$

The above forms of transformations are not limited by small angle approximations, so effects on wake location of maneuvers of any severity or time duration may be simulated. Effects of gravity loading and gyroscopic terms will be discussed in a later section, inasmuch as these maneuver effects primarily modify blade loads calculations.

Determination of bound circulation.-Blade circulations are dependent upon maneuver parameters, as determined by their aerodynamic effects. The velocities V and U, normal and tangential to the plane normal to the shaft axis, respectively, are given approximately by

$$V = V_f(\alpha_s - \alpha_\beta) + w + r(\dot{\alpha}_A \cos \psi + \dot{\phi}_R \cos \alpha_R \sin \psi) \quad (5)$$

$$U = \Omega r + V_f \sin \psi \quad (6)$$

where r = radial position, meters,

U = total tangential velocity, meters/second,

V = normal velocity, meters/second,

w = normal wake-induced velocity, meters/second,

$\dot{\alpha}_A$ = pitch rate, positive nose up, radians/second,

α_R = angle between roll axis and x-axis, radians,

α_s = shaft axis angle with respect to the free stream, positive aft, radians,

α_β = longitudinal first harmonic blade flapping, positive for flap up at $\psi=0$, radians,

$\dot{\phi}_R$ = roll rate, positive right-hand side down, radians/second,

ψ = azimuthal coordinate, positive counterclockwise and zero aft, radians,

Ω = rotor speed, radians/second.

Using small angle approximations and the definitions of lift per unit length, ℓ, in terms of bound circulation, Γ, density, ρ, and tangential velocity, U,

$$\ell \simeq \rho U \Gamma$$

and in terms of the angle of attack, $\alpha_p + V/U$, chord, c, lift curve slope $c_{\ell\alpha}$ and other previously defined quantities,

$$\ell \simeq \rho U^2 c c_{\ell\alpha}(\alpha_p + V/U)/2 .$$

By equating these expressions for lift the bound circulation may be defined as

$$\Gamma = c\, c_{\ell\alpha}(U\, \alpha_p + V)/2$$

or

$$\Gamma = c\, c_{\ell\alpha}[(\Omega r + V_f \sin\psi)\alpha_p + V_f(\alpha_s - \alpha_\beta) + w + r(\dot{\alpha}_A \cos\psi + \dot{\phi}_R \cos\alpha_R \sin\psi)]/2 \qquad (7)$$

where α_p is the sum of collective and cyclic pitch and blade twist, radians.

For a set of rotor blades which are assumed to have stepwise radial and azimuthal circulation variations, the above equations may be thought of as applying to each radial and azimuthal location. The normal component of wake-induced velocity on the blade, w, is made up of velocities due to known circulations in the wake and to unknown circulations at the blade, and may be written in the form

$$w(r_i,\psi_k) = w_K(r_i,\psi_k) + \sum_{\ell}\sum_{j} \sigma_{\ell j}(r_i,\psi_k)\Gamma(r_\ell,\psi_j) \qquad (8)$$

where $w_K(r_i,\psi_k)$ is the normal component of wake-induced velocity from known circulations

$\Gamma(r_\ell,\psi_j)$ is the blade circulation at (r_ℓ,ψ_j)

$\sigma_{\ell j}(r_i,\psi_k)$ is an influence coefficient which, when multiplied by the circulation $\Gamma(r_\ell,\psi_j)$ gives the induced velocity from the (r_ℓ,ψ_j) element of the wake at (r_i,ψ_k)

The summations over the indices ℓ and j indicate a summation over all radial sections of all blades at their respective azimuthal positions. Then a set of equations for all Γ's may be obtained, and is of the form

$$\Gamma(r_i,\psi_k) = \frac{c}{2} c_{\ell\alpha}\left[\sum_{\ell}\sum_{j} \sigma_{\ell j}(r_i,\psi_k)\Gamma(r_\ell,\psi_j) + \alpha_p(\Omega r_i + V_f \sin\psi_k) + V_f(\alpha_s - \alpha_\beta) + w_K + r(\dot{\alpha}_A \cos\psi + \dot{\phi}_R \cos\alpha_R \sin\psi)\right] \qquad (9)$$

This equation is solved with a simple iterative procedure (see ref. 5 for details).

Wake-induced velocity influence coefficients.-Calculation of input for the blade loads part of the program is done by adding together all σ's from the wake program which are multiplied by the same bound circulation, Γ, for computation of the wake-induced velocity at a blade load point in the blade loads calculation, and by properly subscripting the resulting numbers. These numbers are used in the solution of an equation in the blade loads program which is approximately equivalent to equation (9), except that small angles aren't assumed. The evaluation of the input to the blade loads program are computed only after a specified number of revolutions have been generated. Thus, the input (including both σ and Γ type quantities as discussed above) from the wake geometry program to the blade loads program is based on approximate (specified) blade motions and an approximately repetitive wake. The repetitive characteristic of wake-induced effects is presently determined on the basis of previous calculations which depended upon visual checking of data and resulting blade loads calculations.

Large-to-small step size transition.-A considerable savings in computer running times and storage was achieved by implementing a large-to-small step size option for "final calculations" in the wake geometry program. ("Final calculations" are those made during final steps, which are taken after the wake is assumed to be repetitive and during which wake-induced velocity influence coefficients and initial estimates for bound circulations are computed for use in the blade loads and response program.)

Investigation of the forward flight case wake geometries and subsequent preliminary calculations indicated that an increase in the number of azimuthal steps (or a corresponding decrease in the step size) would result in rapidly increasing running times. The cost of generating wake program output data for use in maneuver loads calculations could be prohibitive for most users. This is a consequence of the fact that the number of radial and azimuthal blade load points is necessarily much larger for calculations which are intended to simulate vortex-blade interactions than those which are not. It was determined during the analysis of the forward flight cases that an azimuthal step size on the order of 10° appeared to be reasonable, and that six or eight radial load points would provide considerably more data than the four used in the forward flight case calculations. Also, it was determined that blade load response at frequencies through the twelfth harmonic of rotor speed be calculated in order to permit comparison with measured data, which has response in that frequency range. This requirement for calculation of high frequency response necessitated the use of blade normal modes with correspondingly high frequencies. The use of high frequency flapping modes made the calculation of air loads at rather closely spaced radial aerodynamic

load points imperative in order to compute realistic generalized forces. That is, the air load spanwise distribution must have variations with the same or smaller spanwise length scale as the flapping mode shape variations, at least over the outer portion of the blade where high dynamic pressures are expected to occur.

Preliminary calculations and knowledge of the computer program structure and the types of computer systems which might be used to operate these programs led to the following conclusions:

1. The blade loads program for forward flight could be modified for maneuver flight calculations so as to have up to 8 radial and 36 azimuthal aerodynamic load points and up to 12 normal mode and natural frequency sets without unacceptable increase in running time but with a significant increase in the core storage required. The increased core storage is a combination of increased number of modes and increased number of azimuthal steps per revolution. Running time is relatively insensitive to the number of modes, and improved programming economics and better modeling of control system and lead-lag dampers was expected to improve convergence and compensate somewhat for the increased number of azimuthal steps per revolution. Storage requirements, using overlay methods, was expected to increase from under 70,000 octal to approximately 125,000 octal.

2. The wake geometry program for forward flight could be modified for maneuver flight calculations with small increases in the amount of core storage required, since only the "full mesh" wake had an increased number of elements per blade, and relatively few variables' dimensions were dependent upon the number of azimuthal steps per revolution. However, unless model modifications or other changes were made, running times would increase to the order of a few hours on the CDC 6600. The running time is a function of the number of elements in the wake model, which is approximately proportional to the number of trailing vortices (in the trailing vortex-only portion of the wake) times the number of azimuthal elements in a vortex times the number of blades. The running time increases with a power of this number, the power being between 3 and 4. The core storage requirements for the blade loads and response program was acceptable, but the running time expected for the wake geometry program was prohibitive for all but research-oriented use. As a result of these conclusions, it was determined that a change in wake model, or calculation procedure was necessary.

An investigation of wake geometry data for forward flight cases indicated that an acceptable approximation to the positions of the wake elements of a small step size model (say 36 steps per revolution) could be achieved by interpolation between element end points of a large step size model (say 12 or 18 steps per revolution). Preliminary calculations confirmed this conclusion.

The large-to-small step size option for the wake geometry program "final calculations" was implemented in the maneuver program, according to the following steps, which are indicated in figure 4 for clarity.

1. The program operates as for the forward flight cases until (NxN_s-N') steps have been made, and during these calculations large step sizes are used, as indicated in figure 4a. Here $N=1/\mu\pi$, N_s is the number of azimuthal steps per revolution, and N' is defined by

$$N' = 1 + \frac{\text{(number of full mesh steps behind each blade-1)}}{\text{number of small steps for each large step}}$$

2. The step size is reduced by a factor of 2 or 3, depending upon input data, so that by the time the rotor has completed the N revolutions the "full mesh" wake immediately behind each blade is all small step size, as indicated in figure 4b. All subsequent step sizes of the rotor are small.

3. The "final calculations" are done, with a large portion of the trailing-vortex-only wake being large step and a small portion immediately adjacent to the full mesh being small, as indicated in figure 4c. During these "final calculations" the program interpolates between large step wake element points and effectively approximates the large step portion of the trailing-vortex-only wake by small step size elements, as indicated by the broken line elements in figure 4c.

All wake program calculations for maneuver cases were done with this process. Use of this large-to-small step size option is believed to have significantly reduced program running time and, in addition, conserved core storage locations.

Distance-limiting.-The induced velocity from a vortex element at a point is approximately proportional to the length of the element divided by the square of the distance between the element and the point. Thus the "near neighbors" of a point have the dominant effect. Preliminary calculations and investigations of previous results indicated that all tip vortex elements further than approximately 0.5 to 1.0 rotor radius from a calculation point contribute less than 5% of the total wake-induced velocity at a point, yet require 50% to 90% of the calculations of this type, for typical wakes involved for these rotors and flight conditions. Therefore, a distance-limiting option was implemented in the wake geometry program. It is felt that this option reduced running time by a factor of 2 to 4, and required an insignificant number of additional core storage locations.

Blade Loads and Response Model and Formulation

The right-handed coordinate system used in the calculation of (periodic) blade circulations and blade response is located such that the z-axis is fixed to the shaft, directed upward, the x-axis is downstream, blade azimuth angle, ψ, is measured with respect to the x-axis, y is positive on the advancing side, and the distance radially outward from the axis of rotation on a given blade is denoted by r, as shown in figure 3.

Determination of aerodynamic loading.-The aerodynamic loading at a given radial and azimuthal station is derived from the flow experienced by the blade section, as sketched in figure 5. The geometric incidence of the section with respect to the rotor plane is the sum of the rigid body pitch angle $\theta_T(\psi)$, blade twist $\Gamma(r)$, and the torsional deflection $\phi_e(r,\psi)$. The velocity component tangent to the rotor plane, U, is given by

$$U = \Omega r + V_f \cos \alpha_s \sin \psi \tag{10}$$

and that normal to the rotor plane, V, is given by

$$V = - V_f \sin \alpha_s + \dot{h}(r,\psi) - w - w_c + r(\dot{\alpha}_A \cos \psi + \dot{\phi}_R \cos \alpha_R \sin \psi) \tag{11}$$

where $\dot{h}$ is the plunging velocity of the section due to the response of the blade, and w is the chordwise average wake-induced downwash, and is given by

$$w(r_i,\psi_j) = \sum_m \sum_n \sigma_{mn}(r_i,\psi_j)\ \Gamma\ (r_m,\psi_n)$$

where $\sigma_{mn}(r_i,\psi_j)$ is the wake-induced downwash at (r_i,ψ_j) due to unity bound circulation for blades which were located at (r_m,ψ_n), (r_m,ψ_{n+N_S}), etc., and w_c is the climb rate.

As is indicated in figure 5, the foil section is replaced by a vortex distribution of strength $\gamma(r,\delta,\psi)$ along the chord. This distribution is adjusted to make the flow at the section tangent to the chord, which relates Γ to the $\bar{w}$ and yields the basic relationships governing the aerodynamic loading. More details of the derivation of Γ are given in reference 5. The resulting equation for Γ is

$$\Gamma(r_i,\psi_j) = b_i(c_\ell u)_{ij} + \frac{\pi b_i}{2}(\lambda)_{ij} \tag{12a}$$

where b_i = blade semichord, meters,

c_ℓ = lift coefficient,

$u = (U^2 + V^2)^{1/2}$,

$\lambda = \theta_T(\psi_{j+1}) - \theta_T(\psi_{j-1}) + \phi_e(r_i,\psi_{j+1}) - \phi_e(r_i,\psi_{j-1})$,

θ_T = sum of collective and cyclic pitch angles, radians,

ϕ_e = torsional blade elastic deflection, radians.

In equation (12a) the lift coefficient, c_ℓ, is a function of angle of attack, α, and Mach number, M_N, as defined by aerodynamic coefficient subroutines. The total angle of attack, α, is defined by

$$\alpha(r_i,\psi_j) = \theta_T(\psi_j) + \phi(r_i,\psi_j) + \tau(r_i) + \tan^{-1}(V_{ij}/U_{ij}) \tag{12b}$$

where τ = built-in blade twist, radians. Equations (12) represent a set of nonlinear equations in the strengths, Γ. The nonlinearity is a result of nonlinear aerodynamic coefficient definitions, and of the nonlinear dependence of Γ upon itself (as contained in w and its contribution to V, then α, and finally c_ℓ). Solution of equations (12) is therefore accomplished in an iterative manner, and is discussed in detail in reference 5.

The lift, drag, and moment per unit span are readily calculated once blade circulations have been obtained. Resolving the forces into components normal and tangential to the rotor plane, F_z and F_x, respectively, results in the following expressions.

$$F_{z_{ij}} = \rho\, b_i \left[u(U\, c_\ell + V\, c_d)\right]_{ij} + \frac{\rho b_i}{2\Delta t}\left\{\Gamma_{j+1} - \Gamma_{j-1} + 2b\left[(c_m\, u)_{j+1} - (c_m\, u)_{j-1}\right]\right\}_i \tag{13}$$

$$F_{x_{ij}} = \rho\, b_i \left[u(-V\, c_\ell + U\, c_d)\right]_{ij} \tag{14}$$

where c_d = section drag coefficient,

c_m = section moment coefficient (about midchord),

$\Delta t = \Delta\psi/\Omega$.

The moment about midchord, M_0, is given by

$$M_0(r_i,\psi_j) = \rho b_i^2 \left\{ 2(c_m u^2)_{ij} - \frac{b_i}{8\Delta t}(\Gamma_{j+1} - \Gamma_{j-1})_i \right.$$

$$\left. - \frac{3\pi b_i^2}{8(\Delta t)^2} \left[\theta_{g_{j+1}} - 2\theta_{g_j} + \theta_{g_{j-1}} + (\xi_{j+1} - \xi_{j-1})/2 \right]_i \right\} \quad (15)$$

where θ_g = sum of collective and cyclic pitch angles, blade twist, and elastic torsional deflection, i.e., the total geometric angle of attack, radians,

ξ = local blade spanwise slope, radians.

The aerodynamic coefficients are computed from empirical approximations to experimental data. These empirical approximations are given in the Appendix A, for an NACA 0015 airfoil as equations (A-1), in Appendix B for an assumed particular vortex-blade interaction model, and in reference 5 for an NACA 0012 airfoil. The aerodynamic coefficients are, in general, nonlinear functions of Mach number and angle of attack.

Lumped loads.-Conversion of the aerodynamic loads to a form suitable for response calculations is done by lumping the distributed loads at the mass points of the lumped parameter blade model. The distributed aerodynamic moment is transferred to quarter-chord, then the distributed loads are integrated, using a straight-line approximation between load points, to obtain lumped loads at the mass points. The drag force at the i^{th} mass point, for example, is

$$f_{x_i} = \int_{R_i}^{R_{i+1}} F'_x(r)\, dr$$

where R_i and R_{i+1} are midway between masses m_i and m_{i-1}, and between m_{i+1} and m_i, respectively, and where $F'_x(r)$ is the straight-line approximation to the distributed drag load. Similarly the

lumped moment, m_{0_i}, and lift force f_{z_i} are computed from M_0 and F_z. Coordinate transformations are then applied which result in loads in the local blade coordinate system, and are given by

$$F_{v_i} = - f_{z_i} \cos \Phi_i - f_{x_i} \sin \Phi_i$$

$$F_{w_i} = f_{z_i} \sin \Phi_i - f_{x_i} \cos \Phi_i$$

$$M_{\phi_i} = m_{0_i} + z_{a_i} F_{v_i} \tag{16}$$

where z_{a_i} = distance of the elastic axis forward of quarter chord, meters

Φ_i = angle between chord and rotor plane, positive for airfoil rotated nose up, radians

The computation of the total force and moment at each mass, for every azimuthal and radial location is done according to the following relationships.

$$Q_v = m\Omega^2 \sin \Phi(h + \varepsilon \cos \Phi) + m\ddot{\theta}_c[\varepsilon + h \cos(\Phi - \theta_0)/\cos \Phi]$$
$$- 2m\Omega\dot{\Psi}\varepsilon \sin \Phi + F_v + mf_g(\cos \Phi \cos \alpha_s - \sin \Phi \sin \alpha_s \sin \psi) \tag{17a}$$

$$Q_\psi = m\Omega^2 \varepsilon r - 2\Omega\dot{\theta}_c[I_0 \sin \Phi + m\varepsilon h \sin \theta_0/\cos \Phi]$$
$$- 2\Omega\dot{\phi}I_0 + 2m\Omega\varepsilon(\dot{v} \sin \Phi + \dot{w} \cos \Phi) \tag{17b}$$

$$Q_w = m\Omega^2 \cos \Phi(h + \varepsilon \cos \Phi) - mh\ddot{\theta}_c \sin (\Phi - \theta_0)/\cos \Phi$$
$$- 2m\Omega\varepsilon\dot{\Psi} \cos \Phi + F_w - mf_g(\sin \Phi \cos \alpha_s + \cos \Phi \sin \alpha_s \sin \psi) \tag{17c}$$

$$Q_\phi = - \Omega^2 \sin \Phi[I_0 \cos \Phi + m\varepsilon h] - \ddot{\theta}_c[I_0 + m\varepsilon h \cos(\Phi - \theta_0)/\cos \Phi]$$
$$+ 2\Omega\dot{\Psi} \sin \Phi I_0 + M_\phi - m\varepsilon f_g(\cos \Phi \cos \alpha_s - \sin \Phi \sin \alpha_s \sin \psi)$$
$$+ \Omega(\dot{\alpha}_A \cos \psi + \dot{\phi}_R \sin \psi) I_0 \tag{17d}$$

$$Q_\theta = \Omega(- \dot{\alpha}_A \sin \psi + \dot{\phi}_R \cos \psi)(I_x + mr^2) \tag{17e}$$

where the Q's, $\dot{\Psi}$, ϕ, $\dot{v}$, $\dot{w}$ and the F's and M_ϕ are understood to be subscripted by i and j; m, h, ε, r, Φ, and I are understood to be subscripted by i, and θ_c and its time derivatives are understood to be subscripted by j. The cyclic pitch, θ_c, is given by

$$\theta_c = A_c \sin \Omega t + B_c \cos \Omega t$$

where A_c = lateral cyclic pitch, radians

B_c = longitudinal cyclic pitch, radians

Also, h_i is the horizontal separation between the elastic axis and the pitch axis at the $i^{\underline{th}}$ station, and Φ_i is the total average angle between the rotor plane and the chord at the $i^{\underline{th}}$ radial position, and r_i is the radius to the $i^{\underline{th}}$ mass. Reference 5 contains more details of equations 17, except that gravity and maneuver load terms were not included in the model for the steady level forward flight cases. The gravity loading terms are those in equations 17a, c, and d which occur as a factor of f_g, the gravity loading factor. Maneuver rate effects are included in equations 17d and e, and are those terms which are factors of $\dot{\alpha}_A$ and $\dot{\phi}_R$. The maneuver rate effects may be thought of as gyroscopic loading terms, with the gyroscopic moment being equal to the product of the rotor rotation rate, the appropriate mass moment of inertia, and the precessional (or in this instance, the maneuver) angular rate.

Generalized forces and coordinates.-The generalized forces acting on each normal mode are computed for each azimuth, according to

$$F_K(t) = \sum_J \sigma_{KJ} \dot{\zeta}_J + \sum_i \left(Q_{v_i} A_{v_i}^{(K)} + Q_{w_i} A_{w_i}^{(K)} + Q_{\phi_i} A_{\phi_i}^{(K)} + Q_{\psi_i} A_{\psi_i}^{(K)} + Q_{\theta_i} A_{\theta_i}^{(K)} \right) \qquad (18)$$

where $\dot{\zeta}_J$ is from the previous iteration,

$$\sigma_{KJ} = - c_{D_{\dot{\theta}}} A_{\phi_1}^{(K)} A_{\phi_1}^{(J)} \qquad \text{for } J \neq K$$

$$\sigma_{KK} = 2 \tilde{\sigma}_K \omega_K$$

$\tilde{\sigma}_K$ is the average aerodynamic damping coefficient for the $K^{\underline{th}}$ mode (read as input)

$A_{q_i}^{(K)}$ is the mode shape quantity for the "q" type of elastic deformation, at the $i^{\underline{th}}$ radial location, for the $K^{\underline{th}}$ mode

$c_{D_{\dot{\theta}}}$ is the damping associated with motion defined by $A_{\phi_1}^{(K)}$

The σ_{KJ} terms may be thought of as damping coupling terms.

The governing equation for the $K^{\underline{th}}$ generalized coordinate, ζ_K, is given by

$$\ddot{\zeta}_K + 2\sigma_K\omega_K \dot{\zeta}_K + \omega_K^2 \zeta_K = F_K(t) \qquad (19)$$

The damping term, σ_K, is presently defined in terms of the mode shape quantities and $\tilde{\sigma}_K$ as

$$\sigma_K = \tilde{\sigma}_K + c_{D_{\dot{\theta}}} \left[A_{\phi_1}^{(K)}\right]^2 \Big/ 2\omega_K$$

It should be noted that viscous-type damping of any motion (torsional, flatwise, or chordwise) may be represented by a similar expression. The solution of this equation is obtained in integral form. The solution assumes periodicity of both forcing function and response. The generalized coordinate, ζ_K, and its time derivatives are given in Appendix C for an overdamped system, $\sigma_K \geq 1$, and are given in reference 5 for an underdamped system, $\sigma_K \leq 1$. (It should also be noted that the present program is operable for $\sigma_K > 1$ as well as for $\sigma_K < 1$, which was previously not possible.)

The average aerodynamic damping coefficient term, $2\tilde{\sigma}_K\omega_K$, occurs on both sides of the governing equation for $\zeta_K(t)$. Since an iterative solution method is used in computing a compatible set of loads and responses, this term effectively cancels at convergence.

Blade response quantities.- Response variables are computed from

$$\dot{v}(t) = \sum_K A_v^{(K)} \dot{\zeta}_K(t)$$

$$\phi(t) = \sum_{K} A_{\phi}^{(K)} \zeta_K(t)$$

and similarly for $\dot{w}$, $\dot{\phi}$, $\dot{\Psi}$, ψ, and $\dot{\ell}$, where

v = flatwise blade deflection, meters

w = chordwise blade deflection, meters

ϕ = torsional blade deflection, radians

$\ell = \partial v/\partial r$, radians

$\Psi = \partial w/\partial r$, radians

Conversion of the response data to a form suitable for loads calculations is then done by computing loads quantities at aerodynamic load positions by linear interpolation of response quantities at the mass points. Thus, response quantities, i.e., the plunging velocity $\dot{h}$, the pitch θ, and slope ξ, are given by

$$\dot{h} = [\dot{v} \cos \Phi - \dot{w} \sin \Phi + z_a \dot{\phi} \cos \phi + (z_a - h)(\dot{\theta}_c - \Omega\xi)] + \xi V_f \cos \alpha_T \cos \psi \,, \qquad (20)$$

$$\theta_g = \theta_0 + \theta_c + \phi, \text{ and} \qquad (21)$$

$$\xi = -(\ell \cos \Phi + \Psi \sin \Phi) \,. \qquad (22)$$

These values of $\dot{h}$, θ_g, and ξ (computed at all aerodynamic radial and azimuthal load points) are used in the next iterative calculations of blade loads.

Once convergence has been established between blade loads and response, blade shears and moments are computed in terms of the normal mode and generalized coordinate quantities according to

$$T(t) = \sum_{K} A_T^{(K)} \zeta_K(t) \qquad (23)$$

for the torsional moment, and similarly for other moments, shears, and motions.

Determination of initial estimates.-Iterative methods of solution are used to solve a nonlinear set of equations, equations (12), as well as to determine a compatible set of load and response quantities. Due to the iterative solution for a compatible set of blade loads and blade response, good estimates of load and response

quantities are helpful to prevent divergence, and if properly chosen enhance convergence. A discussion of a particular case which diverged, and the method used to obtain convergence is discussed in the RESULTS AND DISCUSSION section.

Estimates of blade flapping motion for use in blade loads calculations may be computed by a method equivalent to that used in determining blade flapping motions for the wake geometry (see ref. 5) and wake-induced velocity influence coefficient calculation. When the shaft axis is chosen to be perpendicular to the tip path plane, blade flapping motions are assumed to be zero. Estimates for blade (bound) circulations for the blade loads program are input from the wake program, and are those values associated with the last steps of the wake program calculations, during which the wake-induced velocity influence coefficients were computed.

Blade natural frequency and mode shape model and formulation.- The program which calculates blade natural frequencies and mode shapes is an independent program which was developed by RASA and could be replaced by any approximately equivalent program. The necessary output for any such program in order that it might be used as input for the blade loads program are the natural frequencies together with the corresponding mode shape quantities, i.e., flapping and edgewise displacements, angles, shear forces, bending moments, and torsional deflection and torque. The mode shapes and natural frequencies used in the calculations reported here were fully coupled edgewise, flatwise, torsion modes. The modes need not be fully coupled but should be orthogonal for proper use in the blade loads and response program. These mode shape quantities are to be defined at the location of the point masses of the lumped parameter model, with mode shape magnitudes adjusted to give unity generalized mass. The lumped parameter model lengths, masses and inertias, mass eccentricities, offsets of elastic axis from pitch axis and midchord, twist distribution (as measured at mass points), but not model bending or torsional stiffnesses are used in the blade loads-response program.

Briefly, the model used for the real blade is a lumped parameter approximation consisting of uniform massless elastic beam sections under tension due to centrifugal loads, with point masses and inertias located at the ends of the massless lengths. A modified transfer matrix approach is used in determining the natural frequencies and mode shapes. (See, for example, ref. 12). The natural frequencies and corresponding mode shape quantities are used in the calculation of the response of the flexible blades to aerodynamic and inertia loads in the blade loads and response part of the program.

COMPUTER PROGRAM DESCRIPTION AND USE

The computer programs used for the implementation of the model constitute more than one separate program, and may be classified as those used for preliminary calculations, that used for wake geometry and wake influence coefficient calculations, and that used for computation of blade loads and blade response. The flow diagram shown in figure 1 indicates the general procedure used in the calculation of results. The preliminary calculations, some of which were done by computer programs, included determination of blade control inputs and determination of blade dynamic properties as described by a limited number of fully coupled free vibration mode shapes and corresponding natural frequencies. After available flight conditions, control settings, blade properties, etc. are obtained, this data is used to develop input to the wake program and the blade loads and response program. Experimentally measured or theoretically or empirically calculated data may be used for such data as blade cyclic and collective pitch settings, blade flapping motions, blade natural frequencies, etc. The blade control settings and approximate flapping motions for cases where such data is available may be taken from such data. Where experimental data isn't available, performance-type programs, charts, or tables may be used to provide this data, as appropriate. Blade mode shapes and frequencies may be computed by any method desired, but must give orthogonal mode shapes with a generalized mass of unity for use in the blade response calculations. The blade vibration characteristics used in the calculations discussed herein were obtained with a program which computes fully coupled (flapwise, edgewise, torsion) free vibration mode shapes and natural frequencies. Airfoil characteristics used in the calculations were defined in a subroutine by algebraic approximations to experimental data. If desired, this subroutine could be replaced by a similar subroutine or table look-up procedure for any airfoil section or for models which include rate effects, etc. The calculation or tabulation of airfoil data in a form suitable for use in the wake and loads programs may be thought of as a preliminary calculation, since at the present time it is operational for only NACA 0012 and NACA 0015 airfoil sections and one special vortex-blade interaction model, and any different models would have to be developed in a similar manner before being used.

After the necessary input quantities have been determined, the wake geometry program may be run to obtain wake geometry data and wake influence coefficients for use in blade loads. Estimates of blade bound circulations are also generated by the wake program for use in the blade loads program.

The blade loads and response program does not require wake influence coefficients for operation. Omission results in blade loads and response which do not include free wake effects; rather an assumed uniform wake-induced inflow is used. It is necessary

to input at least one natural frequency and mode shape from the blade free vibration analysis, as well as flight conditions, helicopter blade control settings, and program control variables. The blade loads and response program may be conveniently thought of as two large sections of which one computes blade loads, and one computes the response to those loads. Nonlinear effects are included in the model, so starting estimates for some quantities are made either by input or by the program, and iterations between load and response calculations are required in order to compute a compatible set of blade loads and response variables. The maximum number of iterations allowed is limited by input. Convergence within that number of iterations is determined by the relative change in bound circulation together with the relative change in motions as measured by the generalized coordinates, from one iteration to the next, as compared to input numbers. Output of load and response data is provided when any of the following situations occurs: (1) the convergence criteria between loads and response is satisfied, (2) divergence of loads from one iteration to the next occurs, or (3) the maximum number of iterations is reached. This output data in the first situation is the desired final output, while in the other cases the output serves as a source of information which may be used to determine reasons for failure to converge.

Listings of the program used to compute the wake geometry and wake-induced velocity influence coefficients, and the program used to compute blade loads and response are given in Volume II. It should be noted that the program input and output requires the use of English unit quantities, rather than metric unit quantities. Metric unit quantities are used in this report.

RESULTS AND DISCUSSION

The results of the preliminary calculation are presented and discussed in this section, as well as results of the wake program and blade loads and response program for maneuver flight conditions. All calculations of blade loads and response include the effects of a free wake. One case includes an empirical definition of lift and moment coefficients for a particular vortex-blade interaction model.

Preliminary Calculations

Preliminary calculations include those necessary to establish a numerical model of the helicopter, those necessary to calculate blade dynamic properties in terms of normal modes and natural frequencies, and those necessary to calculate helicopter flight condition and performance type parameters.

Helicopter model data.-Information necessary to develop a numerical model of the helicopter must be obtained from existing

sources. In particular, rotor blade dynamic and aerodynamic properties are required. While many rotor blades have the same aerodynamic shape, mechanical properties usually differ for each rotor. Sufficient geometrical and physical properties are needed to permit determination of blade dynamic properties, and a more complete discussion of normal modes and natural frequencies used in the calculations discussed in this report are presented in a subsequent section. When airfoil section data is not in a form suitable for use in these computer programs for defining aerodynamic coefficients, it must be developed.

Airfoil section coefficients for the NACA 0015 airfoil were developed by using standard curve-fitting techniques to fit low-degree polynomials to experimental data within several sections of the angle of attack range. The source for the experimental data was reference 13. Mach number effects were approximated by dividing the characteristics as obtained for the low Mach number data of reference 13 by the factor $\left(1-M_N^2\right)^{1/2}$. The resulting equations are given in Appendix A. It is suggested that polynomial approximations be used as they were here, rather than trigonometric approximations, as they are as easily developed, have as great an accuracy, and can result in somewhat shorter running times. Rate effects have not been modeled for the NACA 0012 or NACA 0015 airfoils, but such effects could be included in a similar manner.

Normal modes and natural frequencies.-It is necessary for operation of the blade loads and response program to have established a lumped parameter model of the rotor blades and the corresponding fully coupled torsion-flatwise-chordwise, natural frequencies and normal modes. (Lumped parameter model details for the H-34 and HU-1A helicopters are given in Appendix D.) These calculations were performed by an independent program, and resulting normal mode and natural frequency data was used as input for the blade loads/response program. Blade natural frequencies and tip mode shape quantities and mode identification are given in Tables 1 and 2. Mode shapes are given in figures 6, 7, and 8, and include modes with frequencies up to approximately 20Ω. All of these modes could have been used in the blade loads and response calculations. However, core storage requirements increase significantly with increased number of normal modes. Core storage limitations exist, and present a practical restriction on program size. The primary objective of this investigation was the modeling of vortex-blade interactions and predicting their effect on aerodynamic loading. Torsional response was expected to be significant for some flight conditions, as noted in reference 4. Based upon these considerations, it was decided to limit the number of modes. The following criteria were used in choosing the modes to be used in the calculations:

1. torsional response was of considerable interest so "torsional" modes or modes with significant torsional coupling were included,

2. "flatwise" modes with frequencies near torsional mode frequencies may be coupled aerodynamically and were included for this reason, and

3. modes necessary to describe expected steady and low harmonic gross blade motions were included, since these were expected to have a strong effect on the aerodynamics of the rotor.

Based on these considerations, modes denoted in Table 1 as F-1, F-2, F-3, F-4, T-1, T-2, and C-1 were used for H-34 blade representation. Those modes used for representation of the HU-1A teetering rotor are those denoted in Table 2 as symmetric modes F-1, F-2, F-3, F-4, T-1, and T-2; and as antisymmetric modes F-1, F-2, F-3, C-1, F-6, and T-3. The blades operate independently in torsion, for the model used in this program, for both rotors. Both teetering and fully articulated rotors have pitch bearings and may have torsional flexibility because of the pitch control mechanism. In the calculations of the H-34 normal modes, the control system stiffness was much higher than the blade torsional stiffness, so the torsional modes in figure 6 appear to be clamped at the hub. The HU-1A has sufficient control flexibility that significant torsional deflections occur at the pitch bearing, as may be seen from figures 7 and 8. Both symmetric and antisymmetric modes are needed to describe teetering rotor's flatwise and edgewise response but only pinned-free modes are needed for a fully articulated rotor. Thus, more modes were required for the HU-1A rotor than for the H-34 rotor. Early in the calculations runs were made for the H-34 model with modes selected according to the above criteria. Runs were also made with more modes in order to evaluate the effect of including additional modes. Details of the results of these runs are given in a later section.

Flight conditions and performance parameters.-Parameter values such as advance ratio, rotor speed, maneuver rate, air density, etc., were determined from experimental data for those cases where experimental data existed. For cases where calculated data was used as input, parameter values were chosen which were approximately the same as those for similar maneuvers where measured data existed, or which seemed to be reasonable values based on nominal helicopter maneuver capabilities and flight conditions. In general, the calculations represent maneuvers which are rather severe, and for some of the "calculated" data cases, may exceed helicopter maneuver capabilities.

Blade flap and pitch angles were taken from experimental maneuver data for cases where available. These values were used in calculations for Cases 1 through 6 and 11. It should be noted that these measured values did not result in thrust or drag trim. They were used because previous calculations indicated that vortex position was a more important factor than vortex strength, and vortex positions were expected to be reasonable with use of experimentally

measured values of pitch and flap angles. Computed results indicated that vortex-blade interactions were predicted, although they were not always in agreement with measured data, with respect to phase and magnitude. Furthermore, performance programs or charts for maneuver flight conditions with nonuniform wake effects were not available, and use of the wake and blade loads programs to obtain trim conditions would have required significant amounts of computer and personnel time with an unknown resulting improvement in predicted vortex-blade interaction effects.

For flight conditions where no experimental data was available, approximate values were computed. No performance type computer program or charts were known to be available which readily compute trim conditions for a helicopter in steady maneuver flight conditions. Computed trim settings were, therefore, determined by using performance charts for forward flight conditions as given in reference 14, extrapolating where these charts did not extend into the parameter range of a particular maneuver case, and altering these predicted forward flight values of pitch settings to approximately account for the aerodynamic and gyroscopic effects of maneuver flight conditions. Blade flap positions were computed by assuming that the shaft was perpendicular to the tip path plane, and that the tip path plane was determined by lift and drag trim requirements.

The calculated and measured rotor parameter values used as input in the final maneuver case calculations are given in Table 3. Of these, the collective angle values for Cases 10 and 12 were revised after initial blade loads and response calculations to improve the predicted thrust values. The blade flapping angles were used in the wake geometry program but were not required in the blade loads program. All runs were made with the same pitch control settings in both the wake geometry program and in the blade loads program.

Wake Geometry and Induced Velocity Calculations

The wake geometry numerical computations performed for maneuver flight conditions were done by essentially the same procedure as those reported in reference 5 for steady state, level, forward flight conditions. All cases required two rotor revolutions of wake, and running times were approximately 21 minutes CDC 6600 CPU time for the four-bladed H-34 and 8 minutes for the two-bladed HU-1A. (Running time is strongly dependent on the number of revolutions of wake required, as was discussed in more detail in reference 5.) All calculations were made with both large-to-small step size and distance limiting options, which were necessary to obtain results with acceptable run times.

Wake geometry plots.-Plots of location of the tip vortices of the model are useful in visualizing some of the effects of a freely distorting wake model. Free wake geometries as predicted by the model discussed in this report are significantly different from

fixed skewed helical geometries. Resulting wake-induced velocities may also differ significantly for a free wake model as opposed to a fixed helical wake model, particularly where vortex-blade interactions occur. A three-dimensional presentation of wake geometries would offer the best visualization, but many characteristics may be recognized by views such as those presented here. A more detailed presentation would include the rear view, and possibly views from different angles. It was not the intent of this work to make such a presentation. Rather, vortex-blade interactions are being studied, and such effects would not necessarily be more evident in more complicated or more complete presentations of wake geometry data. It is suggested that the most significant visualization for vortex-blade interactions would be the presentation of a series of wake geometries corresponding to one (or more) rotor revolutions by some means such as motion pictures or oscilloscope records. Data for such presentations could be most economically and reliably prepared by using computer graphics to display the appropriate wake geometry characteristics as determined by the wake geometry program. Plots of the wake geometry for an instant in time do not clearly display blade-vortex intersections, but they do imply that they occur. The use of color could allow more detail or clarity, but isn't essential for the purpose of this discussion. These plots do present qualitative information which is useful in the subsequent discussion.

The maneuver wake geometries do not appear to be significantly different from level forward flight geometries, especially as seen in the top view. Differences in the side and rear views are difficult to interpret in terms of vortex-blade interactions. Figure 9 shows the computed wake geometry for an H-34 coordinated right turn at an advance ratio of 0.225, which is referred to as flight 39, table 42 in reference 18. Only two tip vortices are shown in the figures 9(a) and (b) and these two plus those portions of the other two tip vortices which are near the rotor disk are shown in figure 9(c). The z-scale has been expanded by a factor of five to help improve the clarity of the side view plot. It should be noted that blade flapping angles are also increased. Inclusion of more vortices than these causes unnecessary additional complexity in the plots; omission of tip vortices in the rotor disk region would hinder some subsequent discussion of this plot. Approximately two rotor revolutions are presented in figure 9, which corresponds to the time required for vortices deposited near $\psi = 180°$ to be transported aft of the rotor disk. There is a gross rolling up pattern of the portions of the tip vortices which were deposited near the sides of the rotor disk (see points labelled "a" and "e") and a humping up of those portions of the tip vortices which were deposited near the forward portion of the rotor disk (see points labelled "c"). These characteristics are very similar to those observed for level forward flight cases.

There are several mechanisms which influence the wake geometry pattern, and which combine to give the resulting wake geometry,

such as that shown in figure 9. These include the free stream velocity, the wake self-induced velocity, induced velocity from the bound circulation, and the helicopter maneuver type and rate. In figure 9 the direction of the free stream for the rotor is indicated by the arrow labeled V_f. The path of the coordinate system origin, which is an indication of the effect of the maneuver, is shown by the line labeled "maneuver path". It can be seen that the maneuver rate and elapsed time are sufficiently small that the maneuver path is approximately a straight line.

Distortions from skewed helical-type curves in the plan view and in the z-direction in the side view are the result of blade-wake and wake-wake interactions. The blades appear to come close to previously deposited tip vortices on both the retreating and advancing sides of the rotor. The tip vortices appear to be intersected by the rotor blades in both the first and fourth quadrants, and are within 0.05R over considerable spanwise lengths in the fourth quadrant. In the first quadrant the tip vortices appear to go from above to below the rotor blades. (see vortex elements "c-d", for example.) In the fourth quadrant the tip vortices appear to have one or more local humps and dips. (See vortex elements "a-b-c", for example.) As a result, the tip vortex-blade interactions may be more severe in the fourth quadrant than in the first quadrant. It should be noted that both the first and fourth quadrants have approximately parallel orientations of blades and tip vortices, as seen from the plan fiew. The primary variables which could result in differences of interaction effects are thought to be vortex strength, interaction times, separation distance and/or geometrical orientation. For normal trim flight conditions the advancing side tip vortex strengths will be less than those on the retreating side. Interaction times are smaller and frequencies are higher on the advancing than on the retreating side due to forward velocity. It is felt that these effects, however, are of secondary importance with respect to induced velocity magnitude as compared to tip vortex-blade separation distance and geometrical orientation. The wake geometry shown in figure 10 is for a helicopter in a symmetrical pull-up ratio of 0.224. This flight condition was discussed in some detail in reference 4, and is referred to herein as Case 6. The general characteristics of the two geometries presented in figures 9 and 10 are similar, i.e., gross roll-up near the edges and local humps of vortices which were deposited near $\psi = 180°$. The free stream velocity has an upward component at the rotor disk, which is not the normal orientation for steady flight conditions. The generally lower position of the downstream vortex elements in figure 9, as compared to figure 10, is due to the relative change in direction of the free stream velocity. This upward component of the free stream velocity was present in the experimental data for two pull-ups and one turn flight condition. Such orientation indicates that the helicopter is decelerating in the forward direction, since the rotor thrust is perpendicular to the tip path and is acting in the drag direction.

Wake-induced velocities.-The magnitude and frequency of tip vortex-blade interaction effects are more clearly displayed and easier to interpret by wake-induced velocity variations than by plots of wake geometry. Wake geometry plots are difficult to interpret, and more importantly one plot represents only a small fraction of the time period of one revolution. The use of computer graphics could significantly enhance the utility of the wake geometry data by displaying the time-varying wake characteristics, as was mentioned previously. (The actual values of wake-induced velocities are computed in the blade loads and response program as the product of final bound circulations and wake-induced velocity influence coefficients. However, the wake-induced velocity influence coefficients used to establish these values are computed by the wake program and it is these influence coefficients which determine wake-blade interaction. For this reason the calculated wake-induced velocity distributions are discussed here rather than in the section on blade loads and response results.) Wake-induced velocities at the blade locations are shown for some of the flight conditions in figures 11 through 15 for Cases 1, 5, 6, 7, and 10, respectively. Other flight conditions had wake-induced velocities which were generally similar to those in these figures so no others are presented. The wake-induced velocities include contributions from all wake vortex elements, and are the most distinct representation of wake-rotor interactions available.

Some general characteristics which appear to be consistent for all flight conditions are evident from these figures. Maximum wake-induced velocities ranged between 0.1 and 0.16 of tip speed, which exceeds the inflow component due to V_f, for example. The azimuthal range for which wake-induced velocities are small and somewhat uniform is generally in the forward portion of the rotor disk and increases with radius. This is consistent with the fact that with forward velocity, the forward portion of the rotor disk has fewer vortices near it than the aft portion of the disk, i.e., the blades tend to be operating in "undisturbed" air in the forward part of the rotor disk. (See figures 9 and 10, for example.) In general, the forward third of the rotor disk appears to have very few high amplitude interactions in the high dynamic pressure region (outboard portion) of the rotor. The first and fourth quadrants show significant high frequency, high amplitude variations with some large variations occurring in the second and third quadrants near 90° and 270°, respectively. It should be noted that the peak values in these regions may not be the peak values as would be predicted by a "continuous" model. Any discrepancies due to the "finite time increment" nature of the present model tends to lower the peak values, i.e., "peak" velocities may not be computed, but may occur between calculation times. It is expected that there are not large magnitude variations due to tip vortex-blade interactions which have a higher frequency than those displayed in these plots. Average downstream spacing between tip vortices, which is primarily dependent upon forward speed and the rotor

speed, are known. These parameters then determine the approximate frequency of tip vortex-blade interactions. (See, for example, reference 4, where this frequency is referred to as ω_h.) For the advance ratios used in these cases the tip vortex-blade interactions in the fourth quadrant occur at about the twelfth harmonic of rotor speed. In the first quadrant the interaction frequency is higher, due to the fact that the vortices and blade are moving in the opposite directions. Note in figure 9(c), for example, that there could be three interactions in the fourth quadrant and five interactions in the first quadrant. (Downstream vortex motion should be taken into consideration; vortices move downstream approximately 0.056R during one-quarter rotor revolution.) First quadrant interactions have wake-induced velocities which have generally lower magnitude than fourth quadrant interactions for the same flight condition. (The induced velocity plots shown are machine generated, and are straight-line connections of data points which are separated by ten-degree azimuth intervals. Thus, frequencies up to the eighteenth harmonic of rotor speed are represented.)

Detailed variations are peculiar to each case, and some of these are noteworthy. Cases 5 and 10 (figs. 12 and 15) display higher magnitude variations than the others. Case 7 (fig. 14) appears to have more interactions in the third and fourth quadrants than the other cases. Case 10 (fig. 15) has one strong interaction in the fourth quadrant, where a tip vortex was nearly parallel to and within approximately 0.03R of the outboard portion (0.5R to 1.0R) of the blade. This resulted in a wake-induced velocity time history which approximates that expected for a parallel interaction with a "continuous" time history model of a finite core vortex. This case also had the highest computed wake-induced velocity value, $0.1584\Omega R$ or 34.75 meters/second.

Effects of wake-induced velocities on total angle of attack.- Wake-induced velocities affect aerodynamic loads through their contribution to the angle of attack. In the calculations, only normal, not in-plane, velocity components are computed from wake elements. Thus, the total effect of the wake on blade loads is that contained in equation (12b). Nonlinear airfoil characteristics, variations of the in-plane velocity due to forward velocity, blade cyclic and collective pitch, blade flapping, and blade elastic response also influence the total angle of attack. Thus, since induced velocities are only one of the contributors to angle of attack, some of the characteristics of the induced velocity plots are not evident, or are suppressed in the resulting plots of angle of attack. This is revealed in figures 16 through 19 which show computed angle of attack plots for Cases 1, 5, 6, and 10, respectively. Each of these figures, when compared with the appropriate one of figures 11, 12, 13 and 15, illustrate the contribution of wake-induced velocities to total blade element angle of attack. (It should be noted that positive wake-induced velocities make negative contributions to the angle of attack.) Figure 20 shows computed angles of attack for

Case 11 (wake-induced velocities were not printed for this case).

Wake-induced velocities generally have a reduced effect on angle of attack with increased radius, which results from the $1/\Omega r$ dependence of arctan (V/U). High frequency components of angles of attack and wake-induced velocities are in phase for all cases. Steady and low frequency components of angle of attack are primarily due to input cyclic and collective. Figures 16, 17, and 18 are for a four-bladed H-34 helicopter, and display more vortex-blade interactions than figures 19 and 20, which are for the two-bladed HU-1A helicopter. Figure 19 shows evidence of an interaction near $\psi = 290°$ with a parallel vortex-blade orientation and small distances between the vortex and the blade. No other figures display this characteristic. It appears from the plan view of the wake geometries that all flight conditions could have near parallel vortex-blade orientations, but such interactions are not clearly evident in the other figures. The other figures show indications of lower magnitude interactions, which resulted from non-parallel vortex-blade orientations or larger distances between the vortex and the blade than those which were calculated for the flight condition shown in figure 19. All figures show variations in the magnitude or number of interactions with radial location. For instance, figure 16 shows more interactions near $r = 0.819R$ than at other radial positions, while figure 17 has one strong interaction at that position and more weaker interactions at other positions. The differences for figure 16 are probably due to differing distances between the blade and the vortices, with minimum distances near $r = 0.819R$. For figure 17, there appears to have been a vortex which went from behind the blade inboard of $r \approx 0.8R$ to ahead of the blade outboard of $r \approx 0.8R$, with a corresponding phase change in the induced velocity. Figure 17 shows large magnitude interactions at the inboard positions of the rotor on the retreating side and noticeable but smaller and higher frequency variations on the advancing side. This figure, when compared with the corresponding wake-induced velocities of figure 13, clearly displays the influence of radius on the contribution of wake-induced velocities to angle of attack. Figure 20 shows calculated angles of attack for a pull-up flight condition, which appears to have one approximately parallel orientation interaction with relatively small magnitude effects in the fourth quadrant and several interactions with smaller magnitude effects in the first quadrant.

It should be noted that all calculated angles of attack are those determined by an iterative solution of equation (12), and with blade response effects included. Thus, airfoil aerodynamic characteristics such as stall have entered into the determination of the circulations, and directly affect the wake-induced velocities and angles of attack. Different airfoil aerodynamic characteristics (for example, effects of angle of attack rates on lift, etc.) would result in different bound circulations, different wake-induced velocities, and different angles of attack. The angle of attack and wake-induced velocity plots indicate that the radial and azimuthal spacing used was sufficient to isolate vortex interactions,

to indicate where vortex-induced flow reversed direction, and to show expected wake-induced velocity time histories for small separation distance near-parallel-type interactions.

Blade Loads and Response Results

The blade loads and response calculations performed for the maneuver flight conditions were basically similar to those reported in reference 5 for steady-state level forward flight conditions, but with certain additional considerations. There were gravity loading and maneuver gyroscopic loading as included in equations (17), maneuver effects on the velocity normal to the rotor plane as included in equation (11) and, for Case 6, the use of a special tip vortex-blade interaction model as previously discussed and as described analytically in Appendix B. Program operation was generally the same as for forward flight cases. (A slightly modified calculation procedure was used for one case in which a divergence occurred in the numerical iteration solution technique related to the solution of equation (12), which resulted from large wake-induced velocity effects. This modified procedure is discussed in the following section.) Running times ranged from two to ten minutes (CDC 6600 CPU time), with most runs taking about five minutes. Run time was strongly dependent upon the number of iterations required to obtain a converged solution, and was independent of the number of blades. The reasons that the run times were independent of the number of blades are (1) the program treats only one blade, (2) the same number of azimuthal and radial blade aerodynamic load points were used for both types of helicopters which were modeled, the H-34 and the HU-1A, and (3) the number of normal modes used in the response calculation has a negligible effect on the total program running time. The data from the wake program which is used as input to the blade loads program corresponds to the small-step model discussed previously. Radial and azimuthal aerodynamic load point spacing was intended to be close enough to display the effects of wake-blade interactions, especially as they influence higher harmonic loading. Blade load and response quantities which are computed and printed by this program include aerodynamic loads (forces parallel to and normal to the rotor disk, and applied pitching moments about the quarterchord), blade shears, moments, lineal and angular response motions, wake-induced velocities (which have been discussed previously) and angles of attack.

Solution for non-convergent case.-The solution of equation (12), which is a nonlinear equation for the bound circulations, depends upon the accuracy of initial estimates for the bound circulations. The normal operating procedure is to use the bound circulation estimates provided by the wake program as initial estimates for use in the blade loads calculation. This procedure was satisfactory for the maneuver flight conditions, with the exception of Case 11. This case did not converge using this method. The failure to converge appeared to be a result of large magnitude wake-induced velocity

influence coefficients (which are indicative of tip vortex-blade interactions) together with a poor initial estimate for the bound circulations.

The loads program has an option to limit the magnitude of the wake-induced velocity effects, so this was done, and a "revised" initial estimate for the bound circulations was obtained by using the wake program bound circulations as initial estimates for this "revised" set. The limit was then eased somewhat and the process repeated, using the "revised" initial estimates to generate a "second-level-revised" set of estimates. Although this process was continued for several steps, later analysis indicated that a series of two revisions of initial estimates (with decreasing limits) would have been sufficient to permit convergence. Further discussion of Case 11 results are presented in a subsequent section.

Aerodynamic loads for four-bladed rotor.-Measured section air loadings as reported in reference 15 were compared with those computed. Table 4 gives Case numbers as referred to in this report, and flight and table numbers as referred to in reference 15 for the H-34 helicopter and table and tabulation numbers as referred to in reference 16 for the HU-1A helicopter. Both measured and calculated blade loads data for some cases for the H-34 helicopter have high frequency variations of significant magnitude. It is believed that these variations may indicate the influence of wake-blade interactions. Comparing measured and calculated results, it was found that the phase and frequency of these variations are generally not in good agreement, although the azimuthal region where the interactions are indicated agree well for some cases. The calculated and measured air load variations agree fairly well at $r \approx 0.90R$ for the Case 1 flight condition shown in figure 21, but do not agree as well at $r \approx 0.75R$ nor for the flight condition shown in figure 22. (In all air load data presentation for the H-34, measured data at $r=0.90R$ and $r=0.75R$ are compared to calculated data at $r=0.917R$ and $r=0.760R$, respectively.) It is clearly evident from the calculated angle of attack variations as shown in figures 16 and 17, which correspond to these air load variations, that the angle of attack variations within approximately ± 0.1 radian range are reflected in air load variations, while those variations between approximately 0.1 to 0.3 radians do not appear to affect the air load variations. Specific details relating to this effect are discussed later. The mean level of the computed section aerodynamic loading is lower than the measured loading at all radial positions compared for all cases. This overall loading discrepancy is thought to be due to the use of measured pitch angles, which resulted in computed thrust values which varied between 0.63 and 0.975 of the measured thrust. It must be assumed that the helicopter maneuver rates were accurately measured.

The inclusion of Mach number effects on the NACA 0012 airfoil characteristics in the static stall angle of attack range greatly influenced air load calculations for the H-34 helicopter.

Vortex-blade interactions were most common in the first and fourth quadrants, as has been discussed previously. The tip Mach numbers of the retreating blade were in the range of 0.45 to 0.55, and were proportionately smaller with decreasing radius. For this Mach number range the lift coefficient is approximately constant for angle of attack variations between approximately 0.1 and 0.35 radians, as shown in the sketch below.

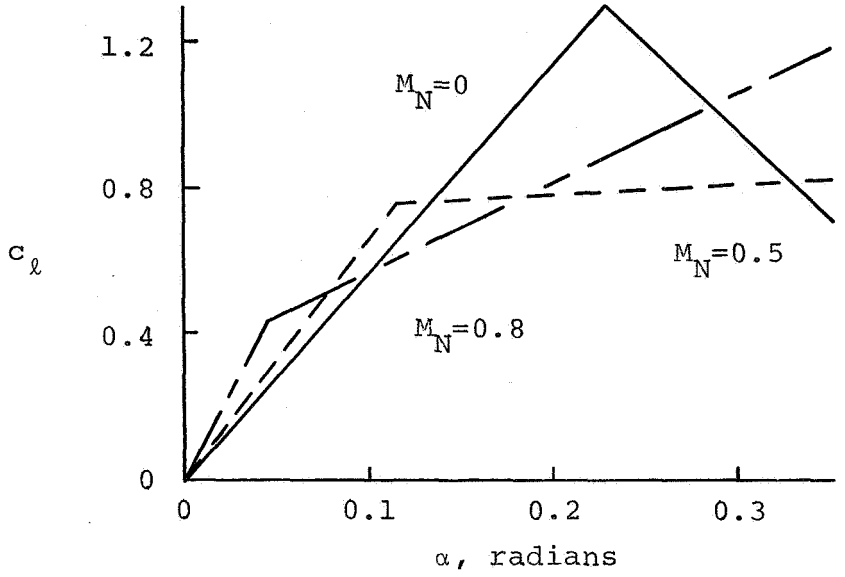

As a result, variations in angle of attack as shown in figures 16 through 18 have corresponding variations in air load only if they range between approximately ±0.1 radian; variations in angle of attack between 0.1 to 0.35 radians have very small resulting air load variations. Retreating blade angle of attack values tend to be higher than those for the advancing blade, due to lateral cyclic, and were frequently in the 0.1 to 0.3 radian range so that angle of attack variations due to wake-induced velocities are generally "masked" more on the retreating blade than on the advancing blade. While some of the differences between calculated and measured loadings may be due to the low calculated thrust (i.e., incorrect pitch angles), this trend was not observed to be consistent, as seen from the comparison of calculated and measured data for other flight conditions. For example, Case 5, which is a symmetrical pull-up at an advance ratio of 0.159 and with a gravity loading factor of 1.6 has aerodynamic loads as shown in figure 22. Here, the steady and low frequency components appear to be in better agreement than for Case 1. It should be noted that Case 5 had a calculated thrust which which was 0.975 of that measured. However, at both radial positions shown in figure 22 there appear to be more measured vortex-blade interactions in the fourth quadrant air loads than were calculated. Thus, in terms of the higher frequency aerodynamic loads, it appears that Case 1 provides a better representation than Case 5. The apparent calculated vortex-blade interactions near ψ=10°, 110° to 150°, and 270° to 310° as shown in figure 20 at r=0.75R are not

indicated in the measured data of reference 15. However, the pressure time history data at the 9% chordwise station as presented in reference 4 for this flight condition indicates that the calculated variations at $r \approx 0.75R$ near $\psi = 270°$ did exist. It should be noted that the data presented in reference 15 represents a chordwise integration of several pressure taps; and that the computed values are those determined by lifting line theory at the 25% chordwise position. The measured data points of reference 15 could lack sufficient resolution to show some such high frequency variations but it is felt that other likely reasons for the differences are that computed wake positions may be incorrect due to wake program limitations or pitch and flap angle inaccuracies and that very close vortex-blade interactions requires the use of lifting surface theory such as that developed (for some special orientations) in reference 6.

In figure 22, there is a general smoothing of calculated air loads as compared to measured air loads especially for $\psi > 210°$. The angles of attack at these radial positions had significant variations in this azimuthal range, as may be seen from figure 17. The frequency and phasing of computed angles of attack and measured air loads agree much better than do the frequency and phasing of the computed and measured air loads, at both radial locations. Angles of attack (which have significant contribution from wake-induced velocities) have variations in the fourth quadrant which do not influence air loads. The smoothing between calculated angles of attack and air loads is primarily due to Mach number static stall effects. Similar results were obtained for all other flight conditions where angle of attack variations occurred within the angle of attack range of 0.1 to 0.3 radians and near Mach numbers of 0.5. These airfoil characteristic representations effectively "insulate" the calculated air loads from the effects of calculated vortex-blade interactions. A secondary effect is that the wake-induced velocities are determined by using computed bound circulation values, and may be somewhat "smoothed" themselves, due to the Mach number static stall effects. It should be noted here that no angle of attack rate effects were included in the airfoil characteristic representations for either the H-34 or the HU-1A helicopter. The inclusion of such rate effects could significantly change the calculated air loads for cases where angles of attack had relatively high magnitudes as well as high frequency variations within the static stall regime. NACA 0012 airfoil characteristic representation did not have static stall Mach number effects, as did the H-34 airfoil characteristics, so there is a one-to-one correspondence between angle of attack variation and air load variations for the HU-1A helicopter. It appears that such calculated variations may generally agree fairly well with measured variations. Therefore, it appears that both angle of attack rate effects and Mach number effects on stall are important for a realistic representation of an airfoil. Furthermore, if rate effects are neglected, omission of Mach number effects on static stall may actually improve the representation of airfoil characteristics for vortex-blade interactions.

It should be noted that both coordinated turns and symmetrical pull-ups involve a combination of gravity loads greater than one and an overall motion which tends to rotate the aft half of the rotor disk downward and the forward half upward.

Measured shaft and flapping angles indicate that both Cases 1 and 5 are for transient conditions in which the helicopter is decelerating in the forward direction. Other calculated and measured data were not significantly different than these two cases so only a few additional plots of the air loads are presented.

Calculated and measured air loads for other radial positions for Case 1 are shown in figure 23. There appears to be a computed vortex-blade interaction near $\psi=90°$ at all radial positions but there is decreasing agreement between measured and calculated phase and magnitude with decreasing radius. The 9% chordwise pressure time history for the radial positions of r=0.55 and outboard all have evidence of vortex-blade interactions, and both the phasing and the number of interactions agree fairly well with the calculated loadings shown in figure 23. As previously mentioned, the chordwise integration used in reference 15 can result in loss of high frequency information which the analysis of reference 4 and the calculated data retain. The evaluated high frequency air load variations in the fourth quadrant on the outboard portion of the rotor are clearly evident in the measured load data of reference 15 at only the radial positions of r=0.85R and outboard. Again, this may be due to vortex position inaccuracies or data integrations as done in reference 15.

Computed and measured air loads for Case 6 are discussed later, in the section on use of a particular vortex-blade interaction model, and similar results for Cases 10 and 11 are discussed in the section on the two-bladed rotor.

Response of four-bladed rotor.-The response of the rotor as measured by the flatwise and chordwise bending moments, the torsional moment, and the pitch horn load all depend upon applied loads (inertial and aerodynamic) and upon blade stiffnesses. Blade properties are characterized by the blade normal modes and natural frequencies. Where a finite number of normal modes are used to represent the rotor blades, blade response is automatically limited to that which can be represented by a linear combination of these modes. The time history of the applied loads may or may not be properly reflected in the response, depending upon the modes which are used to represent the blade. For example, the amplitude of the response to a sinusoidal force with frequency, ω_F, of a particular mode varies with the dynamic amplification factor, $[1-(\omega_F/\omega_K)^2]^{-1}$, where ω_K is the $K^{\underline{th}}$ mode's natural frequency. (The response solution described in Appendix C is not derived in terms of forcing

function harmonics, but the same comment applies.) Thus, because the vortex-blade interaction effects on air loads is usually at approximately the twelfth to fifteenth harmonic of blade passage for the H-34, modes with natural frequencies in this frequency range could be expected to respond more than others. As was discussed previously, torsional response was a primary factor in determining the choice of blade modes to be used in the finite set. All torsional modes were included, as were modes needed for gross blade motions and flatwise modes with significant torsional mass coupling or with frequencies close to torsional mode frequencies (which could result in significant aerodynamic coupling between flatwise and torsional modes). (See the section on Preliminary Calculations for more details.) As a result, flapping modes which had frequencies near the twelfth harmonic were not included. This resulted in a general suppression of vortex-blade interaction effects in the flatwise moments where such variations in air loads were computed.

The flatwise bending moments for Cases 1 and 5 are shown in Figure 24, for a radial position at approximately 0.65 of the rotor radius. (The measured moment was at r=0.65R and the calculated was at r=0.63R for all H-34 flatwise moments.) In general, this is the approximate location for the maximum peak-to-peak bending moment for an articulated rotor blade. The trend of the calculated flatwise moment for Case 1 is in better agreement with the measured data than is that for Case 5. The peak values and the phase and frequency of higher frequency components are not well predicted. The suppression of high frequency variations in air loads due to the airfoil characteristic representation, as previously discussed, effectively eliminated many high frequency air load variations, and blade response would not be expected to show the effects of vortex-blade interactions in such cases. Case 1, however, had significant high frequency variations near ψ=270° on the outboard half of the rotor but had no such variations in the computed flatwise bending moment, primarily because of the modes used. In general, there were significantly more high frequency variations in the measured flatwise moments than in the calculated flatwise moments. The flatwise moment values as computed and measured for other cases were generally more similar to those presented for Case 1 than for Case 5. It should be noted that differences between the physical situation and the numerical model could combine to yield such results. Use of a limited set of normal modes and airfoil characteristic representation have been discussed. The relative orientation and location of blades and tip vortices which interact and the timing of interactions, as predicted by the wake program is another source of differences. Blade air loads and response, which are coupled by the nonlinear equations, are also strongly dependent upon pitch angles, shaft angle, and other experimentally determined inputs. Such input values in the calculations presented here did not yield the correct thrusts, and could be expected to also have significant effects on other computed values as well.

The azimuthal history of computed and measured chordwise bending moments at approximately 0.575 of the rotor radius is shown in figure 25 for Case 1. (The measured moment was at r=0.575R, and the calculated was at r=0.548R, for the H-34 chordwise moments.) The plot shown is typical of measured and calculated chordwise moments obtained for all cases for the H-34 rotor, a fully articulated rotor with a lead-lag damper. The measured data usually exhibits a large low frequency (second or third harmonic of rotor speed) oscillation, but the calculated data is nearly uniform and positive. Three reasons for this discrepancy are suggested. The actual H-34 lead-lag damper is highly nonlinear. For this damper, damping force is essentially proportional to velocity squared up to a specified value at which the force is limited by a relief valve. The damper constant as contained in reference 15 is considered to be too high over much of the damping rate-damping force range. Instead, a damper constant was used which was based on the energy dissipated per cycle by the actual nonlinear damper. This is still a linear representation, and may be part of the cause of the consistent discrepancies between measured and calculated values of chordwise moment for the H-34 helicopter. The chordwise dynamic response of the rotor blades also depends upon the normal modes and frequencies used for dynamic representation of the blades. As previously discussed, it was desired that high frequency torsional response (through the fifteenth harmonic of rotor rotational speed) would be permitted. However, core storage requirements precluded the use of some of the normal modes computed for the frequency range of 0 to 20Ω. A reasonable criteria was therefore established by which some modes were included and other excluded. The same criteria were applied to both the H-34 and the HU-1A rotors. One of those modes which were excluded was the second chordwise mode, denoted C-2, which has a frequency of approximately 3.3Ω. It now appears that this mode had significant response in the measured data. While exclusion of this mode may have adversely influenced the chordwise moment calculations, because of the weak coupling involved it is not thought to have had significant effect on air load calculations or on response displacement-type variables. (Discussion of the effects of the use of a larger subset of normal modes is continued in the next section.) The other possible reason for the large steady chordwise moment is a result of basic limitations of the blade frequency data which was used to model the blade flexibility. The equilibrium position of the blade was assumed to be flat and along a radial coordinate in the determination of blade normal modes and natural frequencies. The equilibrium position of the blade actually involves steady coning and lag. The steady lag does not contribute significantly to the chordwise moment in the real case, but does in the calculations. The assumed equilibrium position does not have this large of an effect on the flatwise bending moment because the blades are much more flexible in flapping than in chordwise bending, and because the coning angle is much smaller than the steady lag angle.

Torsional moments at mid-span and pitch horn loads for Cases 1 and 5 are shown in figure 26. (Both measured and calculated moments are at r=0.50R, and pitch horn loads are at the pitch horn for H-34 data.) The disagreements are significant as considered on the basis of general trends, peak values, and high frequency content. The peak values as measured in the first and fourth quadrants are underestimated for both the torsional moment and pitch horn load, and there is more high frequency content in the calculated pitch horn load within the second quadrant than was measured. These characteristics were common to all H-34 cases. Both torsional moments and pitch horn loads are strongly influenced by the previously discussed airfoil representation inaccuracies. As may be seen in figure 25, there do not appear to be significant frequency limitations in the calculated data. None were expected since the normal modes used included all torsional modes.

Computed and measured torsional moment and pitch horn load data are discussed in later sections for the special vortex-blade interaction model and for the HU-1A helicopter.

Use of additional normal modes.-More normal modes were calculated during preliminary calculations than were used in the blade loads and response calculations. The reasons for selection and the method of choice of the subset of modes used was discussed in the section on preliminary calculations. To investigate the effects of including additional modes, one blade loads run was made using Case 6 wake and loads data, except that additional modes were included. All other H-34 simulation runs had been made with seven modes, denoted in Table 1 as F-1, F-2, F-3, F-4, T-1, T-2, and C-1. The additional modes used for the one "Case 6" run only were F-5, F-6, C-2, and C-3. The air loads and high frequency response motions appear to have been very slightly altered by use of the additional modes. The maximum tip peak-to-peak oscillation in the higher modes was approximately 0.003 meter for flatwise motion and approximately 0.025 meter for chordwise motion. The C-2 mode had the largest response of any of the four additional modes by an order of magnitude. Because of the weak coupling, chordwise motions are the least important with respect to air loads (with the present model). The chordwise bending moment changed significantly with the inclusion of the additional chordwise modes as may be seen in figure 27. It can be seen that the frequency and magnitude of the variations of the computed moment are in relatively good agreement with the measured variations, but that the computed mean value is too high. Except for previously discussed items (such as possibly incorrect equilibrium position, pitch angles and lead-lag damper representation) the cause of apparent steady positive bias of the chordwise bending moment is not known. No runs with additional modes were made for any other cases.

It is recognized that use of a subset of the normal modes calculated by a single-blade natural frequency program may adversely affect results. Furthermore, the use of normal modes which do not

include effects of swashplate flexibility, inter-blade mechanical coupling, and other helicopter rotor system characteristics discussed in reference 17, for example, may have a significant effect on predicted loads and motions. However, within the intent and capability of the programs discussed herein, the subsets of modes used for the H-34 and the HU-1A appear to allow calculation of the dominant air load and response characteristics. (Program modifications to include modes such as those determined in reference 17 would be extensive, since such modes would, in general, be complex, and have complex eigenvalues. Extension of the model and program described in reference 17 are straightforward, and are being undertaken at the time of this writing.)

Use of special vortex-blade interaction model.- Some of the flight conditions for which calculations are reported here were the object of an extensive data analysis in reference 4. Based on that analysis, empirical relationships for lift and moment coefficients were developed for airfoils which undergo stall due to vortex-blade interactions. These relationships were implemented as described in Appendix B, and were used in computations for one flight condition with the blade loads and response program. This case, Case 6 (referred to as Case 2 in reference 4), was also computed without the special vortex-blade interaction model. Some of the results of the calculations are indicated on figures 28 through 30, where three sets of data are presented. They are:

1. measured data as reported in reference 15,

2. computed data without the special vortex-blade interaction effects and with even normal modes used in the blade response calculations, and

3. computed data with the special vortex-blade interaction effects and with twelve normal modes used in the blade response calculations.

The special vortex-blade interactions as modeled used a frequency ratio (ω_{he}/Ω) of 12, a c_{ℓ_u} of 1.0, a $\Delta c_\ell/2$ of 0.2, and values of $c_{m_{2D,stalled}}$ of -0.12. Possible vortex-blade interaction locations were determined by the magnitude of wake-induced velocity influence coefficients, and were restricted to the fourth quadrant. Interactions were permitted by the VBINT array at the following radial and azimuthal locations: for r/R=0.446 at ψ=300° and 350°; for r/R=0.597 at ψ=270°, 290°, 300°, 310°, and 350°; for r/R=0.689 at ψ=270°, 290°, 330°, 340°, and 350°; for r/R=0.760 at ψ=270°. 290°, and 310°; for r/R=0.819 at ψ=270°, 310°, and 320°; for r/R=0.871 at ψ=280°, 300°, 320°, and 340°; for r/R=0.917 at ψ=300°, 310°, and 350°; and for r/R=0.960 at ψ=300°, 310°, 340°, and 350°. The interaction criteria, as given in APPENDIX B, were satisfied for some of these load positions. The aerodynamic loads as given in

figures 28 do show some effects of such interactions. There are slightly larger high frequency variations of loading in the first quadrant with the special interaction model than without it, but this was at least partially due to blade response. (First quadrant air loads were not directly influenced by the special model.) There are significantly larger high frequency variations in the fourth quadrant, which are primarily due to the special vortex interaction.

Figure 29 shows the computed aerodynamic pitching moments at two radial load positions, both with and without the special interaction model. The effects of the interaction are clearly evident at r/R-0.760, 0.871, and 0.917, but are smaller at 0.960. The data presented in reference 4 indicated that strong interactions occurred at r/R=0.95. These differences may be due to inaccuracies in the wake model calculations or input data, as has been previously discussed. Figure 29 does show the frequency and severity of aerodynamic moments which may result from use of the special vortex-blade interaction model. Calculations were also made with a value of $c_{m_{2D,stalled}}$ of -0.24, with larger magnitude but otherwise similar air load variations as described above.

Figure 30 shows the blade response in terms of the blade torsional moment near r/R=0.50, pitch horn load, and flatwise bending moment near r/R=0.55. The vortex-blade interaction effects caused small differences between calculated response with and without the special vortex-blade interaction model. There are small, high-frequency variations in the first and fourth quadrants for the special vortex-blade interaction model. The number, location, and sign of the variations do not coincide with the measured data as given in reference 4. This is due to the locations of possible interactions as specified by the VBINT array and other calculation model inaccuracies. The type of response which may be expected from the use of the special model is apparent, however. Lack of larger magnitude high frequency variations in the torsional moment, as compared to the data in reference 4, may be due to the absence of a rotor system torsional natural frequency near the twelfth harmonic of rotor speed. Such a frequency could be due to mechanical coupling through the swashplate or other inter-blade coupling which was not part of the blade model as defined by the normal modes and natural frequencies used in this analysis. The flatwise moments shown in figure 30 show only low magnitude, high frequency variations with the use of the special vortex-blade interaction model. Similar characteristics were observed in the data of reference 4.

The use of the special vortex-blade interaction model appears to result in more realistic dynamic stall aerodynamic loads than use of static stall characteristics. The use of this or other models may be necessary to obtain realistic results for some flight

conditions, and requires no significant changes in running time, core storage, or input data. Thus, the basic program, and this special model, provide a basis for extending the aerodynamic representations to more complex forms than the two-dimensional, static stall representation previously used, and indicate the types of results which may be expected from such models.

Aerodynamic loads for two-bladed rotor.- Calculated and measured air loads (see ref. 16) and blade response for a symmetrical pull-up flight condition are shown in figures 31 through 33. This is the only type of maneuver for which comparisons with measured data for a two-bladed rotor were made. As with the H-34 rotor cases, the rotor control settings for this HU-1A simulation were obtained from measured data. The computed thrust was 0.88 of the flight value. This thrust value is in better agreement with that measured than was obtained for any of the H-34 cases except Case 5. The air load levels are in generally good agreement in the lower harmonics. The higher frequency content of the measured data is limited to six harmonics, so measured blade-wake interactions are not clearly evident, as may be seen from figure 30. It does appear that the calculated air loads near 0.75R and 0.90R have tip vortex interactions near 90° which the measured data does not contain, and that both measured and calculated data indicate an interaction near 300°. (The HU-1A calculated air loads near the measured air load positions of r=0.75R and r=0.90R are at r=0.761R and r=0.919R, respectively.) As may be seen in figure 32(a), the computed flatwise bending moment (measured at r=0.65R, computed at r=0.63R) has smaller variations than those measured, and approximately the same levels; the computed chordwise bending moment as shown in figure 32(b) has variations with approximately the same magnitude and frequency as those measured, but in contrast with the measured data, has essentially no steady component. (The chordwise bending moment was measured at r=0.60R and calculated at r=0.59R.) As with the standard H-34 cases, only one chordwise mode was used in these calculations, that denoted the antisymmetric C-1 mode, which has a frequency of approximately 1.5Ω. Inclusion of more modes may have significantly changed these results. In particular, a symmetrical mode, with frequency near zero exists. This would result in an approximately steady bending displacement due to steady drag loads, and could account for differences in the steady chordwise moment. The torsional moments at midspan agree reasonably well in the first and second quadrant but the measured results exhibit larger variations in the third and fourth quadrant than those calculated, as may be seen in figure 33(a). (Midspan torsional moments for the HU-1A were measured at r=0.50R and calculated at r=0.543R.) The pitch loads, as shown in figure 33(b), have very similar characteristics except that the calculated pitch load has a phase lag of approximately 40° compared to that measured, and the calculated load generally has a significantly higher level than that which was measured.

Calculated air loads for other HU-1A maneuver conditions were obtained, using calculated control angles as previously discussed. Both turn conditions had very similar aerodynamic loads and response. The air loads, bending moments, and torsional moment and pitch horn load are shown in figures 34 through 36 for Case 10. This is a left turn at an advance ratio of 0.24 and with a gravity factor of 1.5. As may be seen from the air loads near r=0.75R and r=0.90R, the tip vortex-blade interaction which was evident in the wake-induced velocities (as shown in figure 15) has a more noticeable effect at the outboard station. This is consistent with the computed angles of attack and airfoil model characteristics. The angle of attack has a downward "spike" at 0.9R, but stays below the stall region. The angle of attack at r≈0.75R goes into the stall region before the sudden dip, so air loads show much less effect at that radial position than at r≈0.9R.

Elimination of tip vortex.- Rapid dissipation of helicopter blade tip vortices has been the object of recent theoretical and experimental investigations. (See references 18 and 19.) Elimination of the downstream tip vortex in the computer model was done for the Case 10 flight condition by defining the tip vortex strength in the trailing vortex portion of the model to be zero. Figures 37 and 38 show computed quantities for this case with and without a tip vortex. The severe vortex-blade interaction near ψ=290° has been eliminated with removal of the tip vortex, with a corresponding change in air loads. High frequency air loads in the first quadrant were not eliminated, however. Wake-induced velocities and angles of attack in the first quadrant have relatively small variations which, together with the rapidly increasing dynamic pressure, result in high frequency air load components of significant magnitude. Wake geometry data for the calculation without a tip vortex showed that portions of the three inboard trailing vortices which were intended to model the vortex sheet have caused the small (but effective) wake-induced velocity variations in the first quadrant. Blade moments retain some high frequency content, probably due to the first quadrant air loads, but are generally smoother without than with the tip vortex.

Vortex blade interaction effect.- The rather strong reductions in the vortex-blade interaction effects as observed between the computed angles of attack and the computed air loads for the H-34 cases arises because of the static stall effects as contained in the airfoil model. These effects were more severe for some of the H-34 cases than for the HU-1A, primarily due to the inclusion of more realistic static stall dependence on Mach number for the NACA 0012 airfoil than was used for the NACA 0015 airfoil. Dynamic effects on the airfoil characteristics appear to be necessary in order to show the effects of vortex-blade interactions where the angle of attack ranges involved extend into the static stall region. Significant vortex-blade interaction effects were computed with the special model used here.

CONCLUSIONS AND RECOMMENDATIONS

The wake-induced velocities, angles of attack, aerodynamic loads, and blade response have been computed for helicopters in steady-state maneuvering flight conditions. Effects of a freely distorting wake, flexible blade response, and nonlinear airfoil characteristics, were included in the calculations. Computed and measured data showed general agreement with respect to the number of vortex-blade interactions and their approximate locations, but many details did not agree well. The following are specific conclusions obtained from the calculations, from comparison of calculated data with measured data, and from the associated analyses and interpretations of results.

1. Tip vortex-blade interactions are predicted in the azimuthal regions, and with frequencies as were expected for helicopters in steady maneuver flight conditions.

2. The time histories of interactions correspond to that of the blade passing near previously deposited tip vortices, which occurs primarily in the first and fourth quadrants near the blade tips, and over increasing portions of the azimuth with decreasing radial position.

3. Most interactions occur in the first and fourth quadrants. First quadrant interactions occur at a higher frequency than fourth quadrant interactions, and fourth quadrant interactions commonly yield angles of attack which extend into the static stall range.

4. Vortex-blade interactions with various orientations and distances were computed. Small-distance, near-parallel interactions yielded an induced-velocity time history which would be expected from a finite core vortex-blade interaction, and occurred primarily in the fourth quadrant. Interactions in the first quadrant usually had the vortex orientation going from above the rotor disk near $y=0$ to below the rotor with increasing distance starboard.

5. Total computed angles of attack clearly displayed wake-induced velocity effects, and these effects were approximately inversely proportional to blade radial coordinate. Air loads, of course, are proportional to velocity squared, so outboard angle of attack variations are more important in terms of blade loads than are inboard variations.

6. Calculated aerodynamic loads are dominated by stall effects for many conditions where vortex-blade interactions occurred. Effects of both angle of attack rate and Mach number must be included in aerodynamic representation of the airfoil if high frequency angle of attack variations which extend into the stall region are to be realistically reflected in computed air loads.

7. Due to the fact that reasonably accurate performance parameters were not available from performance type programs or tables, measured data or data computed by extrapolation and extension of level forward flight data was used for the required performance parameter variables. Measured input data inaccuracies or model limitations resulted in low computed thrust values, and yielded predicted vortex-blade interactions which seldom agreed in detail with measured interactions, as indicated by computed angles of attack and measured air loads.

8. Vortex-blade interaction locations (but not magnitudes) show better agreement between computed angles of attack and measured pressure tap data than between computed data and measured air loads. Lifting surface rather than lifting line representation of the airfoil may be necessary for accurate representation of small-distance interaction effects.

It is recommended that further refinements be made and calculations be performed which account for the following.

1. Angle of attack time history and compressibility effects should be more accurately represented. Program modifications to implement these changes in the blade loads and response would be primarily in airfoil aerodynamic representation subroutines.

2. Lifting surface theory effects should be developed for a range of vortex-blade orientations and approximated in so as to be able to be efficiently implemented in the existing program.

3. Computer graphic representation of wake geometries could be used to develop more easily interpreted free wake geometry data. Tip vortex-blade interactions could be indicated and time histories used to enhance understanding of this complex phenomena.

4. A performance-type program for calculation of performance parameter values for helicopters in steady maneuver flight conditions should be developed. Such a program could include the capability to model some of the major effects noted in existing studies of helicopter maneuver flight conditions.

APPENDIX A

NACA 0015 AIRFOIL CHARACTERISTICS

The following equations, referred to as equations (A-1), are based upon NACA 0015 airfoil data reported in reference 3 and give aerodynamic coefficients used in the definition of distributed airloads as a function of angle of attack and Mach number.

Angle of Attack Range	Aerodynamic Coefficients as Polynomial Function of Angle of Attack
$0.0 \leq \alpha \leq 0.17453$	$c_\ell = 5.4426\alpha$
	$c_d = 0.006+1.2578\alpha^2$
	$c_m = 1.4467\alpha$
$0.17453 < \alpha \leq 0.59305$	$c_\ell = -5.17552006+74.39225790\alpha-305.08426727\alpha^2$ $+510.05783752\alpha^3-300.69898135\alpha^4$
	$c_d = 1.00809827-13.2161593\alpha+60.24338928\alpha^2$ $-105.33915863\alpha^3+66.65706750\alpha^4$
	$c_m = -1.3120201+19.4541356\alpha-82.038638\alpha^2$ $+139.68468\alpha^3-83.7789094\alpha^4$
$0.59305 < \alpha \leq 2.79253$	$c_\ell = -1.1043+5.9103\alpha-5.2224\alpha^2$ $+1.3845\alpha^3-0.0895\alpha^4$
	$c_d = -0.3690+1.2002\alpha+1.4200\alpha^2$ $-1.0989\alpha^3+0.1671\alpha^4$
	$c_m = -0.1810+1.1369\alpha-1.1730\alpha^2$ $+0.3019\alpha^3-0.0120\alpha^4$
$2.79253 < \alpha \leq 3.05433$	$c_\ell = 19073.5635-26905.6199\alpha+14223.9143\alpha^2$ $-3340.04534\alpha^3+293.9323\alpha^4$
	$c_d = 4324.4195-6164.2224\alpha+3288.5370\alpha^2$ $-778.11679\alpha^3+68.89728\alpha^4$
	$c_m = 20060.7298-27914.6308\alpha+14560.552\alpha^2$ $-3374.20824\alpha^3+293.10403\alpha^4$
$3.05433 < \alpha \leq 3.141593$	$c_\ell = -27.057746+8.6127481\alpha$
	$c_d = 1.1263058-0.110658\alpha^2$
	$c_m = -13.846155+4.4073682\alpha$

For all ranges of α, the lift curve slope, $c_{\ell\alpha}$, is given by $dc_\ell/d\alpha$, and compressibility effects are approximated by dividing all quantities by $\sqrt{1-M_N^2}$ where M_N = Mach number.

APPENDIX B

VORTEX-BLADE INTERACTION MODEL

The symmetrical pull-up for the H-34 with advance ratio of 0.224 was analyzed in reference 4, and empirical relationships were developed which approximated the observed lift and moment variations. These empirical relationships were implemented according to the following procedure.

Vortex-blade interactions depend upon tip vortex-blade load point proximity and effective angle of attack. Tip vortex-blade proximity is reflected in the magnitude of the wake-induced velocity influence coefficients, σ. It was concluded in reference 4 that vortex-blade interactions occurred in the fourth quadrant due to vortices deposited in the third quadrant. Thus, from these experimental observations and by using theoretically calculated σ's an array was established which defined potential vortex-blade interaction locations. If the angle of attack magnitude exceeded a specified maximum, α_m, an interaction was assumed to have occurred. The tests and definitions were done as follows:

1. Is the current blade load position one with a possible vortex-blade interaction (as determined by the input array VBINT)?

2. Is $\alpha \geq \alpha_m$?

3. If either 1. or 2. are not true, no interaction is indicated, but if both 1. and 2. are true, an interaction is indicated and the lift and moment coefficients are defined as follows:

$$c_\ell(\psi) = c_{\ell_u} + \left(\frac{\Delta C_\ell}{2}\right) \sin\left(\frac{\omega_{he}}{\Omega}\right)\left(\psi - \psi_I\right) \tag{B-1}$$

$$\text{and } c_m(\psi) = \frac{1}{2}\left[1 - \cos\left(\frac{\omega_{he}}{\Omega}\right)\left(\psi - \psi_I\right)\right] c_{m_{2D,\text{stalled}}} \tag{B-2}$$

where ψ_I = angle at which vortex-blade interaction was first indicated, i.e.

$$\psi_I = \frac{\Omega}{\omega_{he}} \sin^{-1}\left(\frac{c_\ell(\psi_J) - c_{\ell_u}}{\Delta C_\ell/2}\right)$$

with $c_\ell(\psi_J)$ lift coefficient calculated from normal airfoil characteristics at ψ_J

$\left(\frac{\Delta C_\ell}{2}\right) \doteq 0.3$ (from ref. 4)

$c_{m_{2D,stalled}}$ = two-dimensional stall limit moment coefficient

$\left(\frac{\omega_{he}}{\Omega}\right)$ = ratio of vortex interaction frequency to rotor speed (referred to as ω_h/Ω in reference 4)

$c_{\ell_u} \doteq 1.0$ (for NACA 0012 and NACA 0015 airfoils)

Once an interaction was indicated, coefficients were defined for one complete cycle by the above method, i.e., for $\left(\frac{\omega_{he}}{\Omega}\right)(\psi-\psi_I) < 2\pi$.

APPENDIX C

SOLUTION FOR GENERALIZED COORDINATE OF AN OVERDAMPED SYSTEM

The governing equation for the $K^{\underline{th}}$ generalized coordinate, ζ_K, is given by

$$\ddot{\zeta}_K + 2\sigma_K\omega_K \dot{\zeta}_K + \omega_k^2 \zeta_k = F_K(t) \qquad \text{(C-1)}$$

The solution of this equation is obtained in integral form. The solution assumes periodicity of both forcing function and response. The generalized coordinate, ζ_K, and its first time derivative, $\dot{\zeta}_K$, are given below. The second time derivative of the generalized coordinate, $\ddot{\zeta}_K$, is obtained from the governing equation itself, after solution for ζ_K and $\dot{\zeta}_K$. Subscript K is understood on ζ , $\dot{\zeta}$, $\bar{\omega}$, ω, σ, F.

$$\zeta(t) = \left[\int_0^t e^{-\sigma\omega(t-\tau)} \sinh \bar{\omega}(t-\tau)\, F(\tau)\, d\tau - e^{-\sigma\omega t}(G \cosh \bar{\omega}t + H \sinh \bar{\omega}t)\right]/\bar{\omega} \qquad \text{(C-2)}$$

$$\dot{\zeta}(t) = -\sigma\omega\zeta(t) + \int_0^t e^{-\sigma\omega(t-\tau)} \cosh \bar{\omega}(t-\tau)\, F(\tau)\, d\tau + e^{-\sigma\omega t}(G \sinh \bar{\omega}t + H \cosh \bar{\omega}t) \qquad \text{(C-3)}$$

$$\ddot{\zeta}(t) = F(t) - 2\sigma\omega\dot{\zeta}(t) - \omega^2 \zeta(t) \qquad \text{(C-4)}$$

where $G = (SI + CJ)/(C^2 - S^2)$

$H = (CI + SJ)/(C^2 - S^2)$

$C = 1 - e^{-\sigma\omega T} \cosh \bar{\omega} T$

$S = e^{-\sigma\omega T} \sinh \bar{\omega} T$

$$I = \int_0^T e^{-\sigma\omega(T-\tau)} \cosh \bar{\omega}(T - \tau) \; F \; (\tau) d\tau$$

$$J = \int_0^T e^{-\sigma\omega(T-\tau)} \sinh \bar{\omega}(T - \tau) \; F \; (\tau) d\tau$$

$$\bar{\omega} = \omega\sqrt{\sigma^2 - 1}$$

$$T = 2\pi/\Omega$$

Computer program implementation to evaluate the integrals is done by trapezoidal rule.

APPENDIX D

BLADE MODELS DATA

The following tables give the properties of the blade models for the H-34 and HU-1A helicopters which were used to develop natural frequencies and normal modes with the blade frequency program (and which were also used in the blade loads and response program calculations). The tables give the section properties of the lumped parameter models, with details of the notation as given in references 12 and 13. The lumped parameter blade model begins at a radial coordinate at the inboard end of 0.3048 meter (1.0 foot) for the H-34 and 0.0 for the HU-1A. The length, bending and torsional stiffnesses, and mass are those associated with a section length. The other quantities are associated with the intersection, or ends, of sections. (The mass is lumped at the ends of sections by the computer program, one-half of each section's mass being lumped at each end of the section.)

The bending and torsional stiffnesses are used in the blade frequency program but not in the blade loads and response program. The Za (or ZA), which defines the chordwise dimension of the elastic axis ahead of quarter chord, is used only in the blade loads and response program.

H-34 BLADE PROPERTIES

I	Length feet	EIX $lb\text{-}ft^2$	EIY $lb\text{-}ft^2$	EIZ $lb\text{-}ft^2$	IX,IY $lb\text{-}sec^2\text{-}feet$	Mass $\frac{lb\text{-}sec^2}{feet}$	$\Delta\phi$ degrees	ε feet	ΔLZ feet	ZA feet
1	0.010	8.264×10^{5}	6.460×10^{6}	5.417×10^{5}	6.99×10^{-2}	0.21×10^{-1}	0.0	0.0	0.0	0.0
2	1.073	8.264	3.194	34.72	6.48	21.99	0.0	0.0	0.0	0.0
3	0.833	3.140	1.646	4.910	4.38	9.94	0.0	0.0	0.0	0.0
4	1.667	1.458	1.193	1.187	2.20	1.65	-0.28×10^{-1}	1.367×10^{-2}	6.835×10^{-3}	0.0
5	2.000	1.215	1.107	1.021	2.33	2.64	-6.81	1.367	0.0	0.0
6	0.917	1.215	1.107	1.021	2.98	1.66	-3.12	1.367	0.0	0.0
7	2.583	1.215	1.107	1.021	3.47	4.26	-8.80	1.367	0.0	0.0
8	1.500	1.215	1.107	1.021	3.53	2.72	-5.10	1.367	0.0	0.0
9	2.417	1.215	1.107	1.021	3.19	3.98	-8.23	1.367	0.0	0.0
10	1.333	1.215	1.107	1.021	3.30	2.42	-4.54	1.367	0.0	0.0
11	2.333	1.215	1.107	1.021	4.11	3.69	-7.94	1.367	0.0	0.0
12	2.500	1.215	1.107	1.021	2.83	3.96	-8.52	1.367	0.0	0.0
13	0.833	1.215	1.107	1.021	2.55	1.51	-2.83	1.367	0.0	0.0
14	2.000	1.215	1.107	1.021	3.47	3.30	-6.81	1.367	0.0	0.0
15	2.083	1.215	1.107	1.021	2.93	4.13	-7.09	1.367	0.0	0.0
16	1.167	1.215	1.107	1.021	1.70	2.00	-3.97	1.367	0.0	0.0
17	0.833	1.215	1.107	1.021	2.45	2.06	-2.84	1.367	0.0	0.0
18	0.917	1.215	1.107	1.021	0.55	1.51	-3.12	1.367	0.0	0.0

HU-1A BLADE PROPERTIES

I	Length feet	EIX $lb\text{-}ft^2$	EIY $lb\text{-}ft^2$	EIZ $lb\text{-}ft^2$	IX,IY $lb\text{-}sec^2\text{-}feet$	Mass $\frac{lb\text{-}sec^2}{feet}$	$\Delta\phi$ degrees	ϵ feet	ΔLZ feet	ZA feet
1	1.2210	0.1603×10^5	20.97×10^6	10.76×10^5	4.893×10^{-2}	7.280×10^{-1}	0.0	6.2640	0.0	-1.8080×10^{-1}
2	0.4458	18.75	20.97	10.76	1.787	2.658	0.0	5.5780	0.0	-1.7500
3	0.7467	17.36	18.58	9.514	2.882	4.067	-0.636×10^{-1}	4.9330	-75.0×10^{-3}	-1.6583
4	0.7083	6.875	14.58	6.944	2.776	3.089	-3.864	3.9610	2.585	-1.5833
5	0.6250	1.250	11.63	4.956	2.476	2.178	-3.409	0.1937	2.452	-1.5167
6	0.7000	1.250	9.896	3.542	2.584	1.957	-3.818	-0.6517	2.163	-1.4375
7	0.4500	1.250	8.750	2.587	1.533	1.048	-2.454	-0.1515	2.423	-1.3833
8	0.6500	1.250	7.986	1.997	2.070	1.326	-3.545	0.9583	1.558	-1.3084
9	0.9500	1.233	7.986	1.597	2.777	1.797	-5.182	0.1330	2.250	-1.2083
10	0.9000	1.198	7.847	1.567	2.582	1.685	-4.909	-0.5360	3.288	-1.1042
11	2.3000	1.198	6.597	1.589	5.751	4.221	-12.55	0.3062	3.115	-0.8417
12	2.3000	1.198	5.278	1.632	4.605	4.029	-12.55	1.0170	7.962	-0.5833
13	1.0000	1.198	5.243	1.667	1.889	1.736	-5.454	1.0480	7.962	-0.4833
14	0.9000	1.198	5.514	1.675	1.860	1.898	-4.909	5.7880	3.462	-0.3750
15	2.3000	1.198	5.556	1.684	5.221	5.143	-12.55	4.2470	3.115	-0.1208
16	2.2500	1.146	5.660	1.692	5.237	5.192	-12.27	4.9280	7.962	0.1291
17	1.7500	1.076	6.701	1.771	3.849	5.322	-9.546	6.2500	7.788	0.3291
18	1.8000	1.042	6.701	1.771	4.095	5.167	-9.818	4.7920	6.058	0.5333

APPENDIX E

SYMBOLS

A	coordinate transformation matrix (see eq. 2)
A_c	lateral cyclic pitch, radians
A_q	mode shape quantities representing the "q" type mode variable (see eq. 18)
B	coordinate transformation matrix (see eq. 3)
B_c	longitudinal cyclic pitch, radians
b	blade semichord, meters
C	generalized coordinate amplitude factor (see eq. C-4)
C-m	nomenclature for the $m^{\underline{th}}$ chordwise normal mode, m (an integer) increasing with frequency
c	chord, meters
c_d	drag coefficient
$c_{D_{\dot{\theta}}}$	torsional damping coefficient, newton-seconds
c_ℓ	lift coefficient
c_{ℓ_u}	lift coefficient limit for special stall model (see eq. B-2)
$c_{\ell\alpha}$	lift curve slope at 0° angle of attack
c_m	moment coefficient
$c_{m_{2D,\text{stalled}}}$	two-dimensional stall limit moment coefficient
D	coordinate transformation matrix (see eq. 2)
F_K	generalized force for the $K^{\underline{th}}$ mode, newton-meters
F_v, F_w	lumped aerodynamic forces acting at blade mass points, newtons

F_x, F_z	distributed aerodynamic forces per unit span, newtons/meter
F-m	nomenclature for the $m^{\underline{th}}$ flatwise normal mode, m (an integer) increasing with frequency
f_g	gravity load factor, thrust/weight
G	generalized coordinate amplitude factor (see eq. C-4)
g	helicopter acceleration, meters/second^2
H	generalized coordinate amplitude factor (see eq. C-4)
h	chordwise dimension of the elastic axis ahead of the pitch axis, meters
$\dot{h}$	blade response plunging velocity, meters/second
I	generalized coordinate amplitude factor (see eq. C-4)
I_0, I_x	blade element torsional mass moment of inertia about the elastic axis and c.g., respectively, kilogram meters^2
I_y	blade element chordwise mass moment of inertia about the c.g. ($I_y \equiv I_x$), kilogram meters^2
J	generalized coordinate amplitude factor (see eq. C-4)
ℓ	lift per unit span, newtons/meter
M_N	Mach number
M_0	distributed aerodynamic moment per unit span, newtons
M_ϕ	lumped aerodynamic moment acting at blade mass point, newton/meters
m	blade element mass, kilograms
N	number of revolutions, $N \geq 1/\mu\pi$
N_S	number of azimuthal steps per revolution
P	coordinate transformation matrix (see eq. 2)

Q_q	total "q-type" load at blade element mass point
R	coordinate transformation matrix (see eq. 1), or rotor tip radius, meters
R_C, R_P	maneuver radii for coordinated turns and symmetrical pull-ups, respectively, meters
r	radial coordinate, meters (see fig. 4)
S	coordinate transformation matrix (see eq. 1) or generalized coordinate amplitude factor (see eq. C-4)
T	torque, newton/meters (see eq. 22); or period, seconds (see eq. C-4)
T-m	nomenclature for the $m^{\underline{th}}$ torsional normal mode, m (an integer) increasing with frequency
t	time, seconds
U	velocity tangential to rotor plane, meters/second (see eq. 6)
u	$(U^2+V^2)^{1/2}$, meters/second
V	velocity normal to rotor plane, meters/second (see eq. 5)
V_f	helicopter velocity, meters/second (see fig. 4)
w_c	climb rate, meters/second
w	wake-induced velocity normal to rotor plane, meters/second
x,y,z	rectangular coordinates, meters (see fig. 4): x is positive aft, y is positive on the advancing side, and z is parallel to the shaft and positive up
α	total blade section angle of attack, radians
α_c	vortex interaction angle of attack limit, radians
α_A	pitch angle increment, radians (see eq. 4)
α_m	stall angle of attack (see APPENDIX B), radians
α_p	sum of pitch and blade twist angles, radians
α_R	angle between the roll axis and the x-axis, radians

α_S	shaft tilt angle, positive aft, radians
α_β	longitudinal first harmonic blade flapping angle, positive for flap up at $\psi=0$, radians
β_0	steady blade coning angle, radians
β_1	longitudinal first harmonic flapping angle, radians
β_2	lateral first harmonic flapping angle, radians
Γ	circulation, meters /second
γ	circulation per unit chord, meters/second (see fig. 5)
δ	chordwise coordinate, meters (see fig. 5)
$\dot{\delta}$	turn rate, radians/second
ε	distance of mass c.g. ahead of elastic axis, meters
ζ_K	generalized coordinate of the $K^{\underline{th}}$ mode
θ_c	cyclic pitch, radians
θ_g	total geometric angle of attack, $\theta_T + \tau + \phi_e$, radians
θ_0	collective pitch, radians
θ_T	$\theta_0 + \theta_c$
λ	$\partial v/\partial r$, radians
Λ	incremental turn angle, $\dot{\delta}\Delta t$, radians (see eq. 2)
λ	bound circulation term (see eq. 12)
μ	advance ratio, $V_f/\Omega R$
Ξ	coordinate transformation matrix (see eq. 3)
ξ	blade spanwise slope, radians/meter
ρ	air mass density, kilograms/meter^3
σ	wake-induced velocity influence coefficient, 1/meter (see eq. 8) or damping coefficient (see eq. 18)

$\tilde{\sigma}$	average aerodynamic damping coefficient
τ	blade twist, radians
Φ	angle between rotor plane and chord, positive for airfoil nose-up, radians
Φ_c	coning angle for turns, radians (see eq. 2)
ϕ_R	incremental roll angle, radians (see eq. 3)
ϕ_e	torisonal elastic deflection, radians
Ψ	chordwise elastic bending slope, radians/meter
ψ	azimuthal angle, radians (see fig. 4)
Ω	rotor speed, radians/second
ω	blade natural frequeny
ω_{he}	vortex interaction frequency
$\bar{\omega}$	$\omega\sqrt{1-\sigma^2}$, or $\omega\sqrt{\sigma^2-1}$ for underdamped or overdamped systems, respectively, radians/second (see eq. C-4)

Subscripts:

A	denotes pitch maneuver quantities
i	denotes radial location
J	normal mode number
j	denotes azimuthal location
K	normal mode number
k	denotes azimuthal location
ℓ	denotes radial location
n	denotes radial location
0	denotes a steady condition or parameter
q	a dummy subscript variable (see eq. 18)
R	denotes roll maneuver quantities
v	denotes flatwise blade load and response quantities

w	denotes chordwise blade load and response quantities
x	denotes quantities parallel to the x-axis or normal to the rotor shaft
z	denotes quantities parallel to the z-axis
θ	denotes spanwise slope type blade load and response quantities
ϕ	denotes torsional blade load and response quantities
ψ	denotes chordwise blade load and response quantities

Mathematical Notation

Δ	denotes an increment, i.e., Δt is an increment in t
$\cdot$	indicates time derivative, i.e., $\dot{v}=dv/dt$

REFERENCES

1. Rabbott, J.P.; Lizak, A.A.; and Paglino, V.M.: A Presentation of Measured and Calculated Full-Scale Rotor Blade Aerodynamic and Structural Loads. USAAVLABS Tech. Report 66-31, July 1966.
2. Scheiman, J.; and Ludi, L.H.: Qualitative Evaluation of Effect of Helicopter Rotor-Blade Tip Vortex on Blade Airloads. NASA TN D-1637, May 1963.
3. Ward, John F.; and Snyder, William J.: The Dynamic Response of a Flexible Rotor Blade to a Tip-vortex Induced Moving Force. AIAA/AHS VTOL Research, Design, and Operations Meeting. Paper No. 69-203, February 1969.
4. Ward, John F.: Helicopter Rotor Periodic Differential Pressures and Structural Response Measured in Transient and Steady-State Maneuvers. Journal of the American Helicopter Society, Vol. 16, No. 1, January 1971.
5. Sadler, S. Gene: Development and Application of a Method for Predicting Rotor Free Wake Positions and Resulting Rotor Blade Air Loads. NASA Contractor Report 1911.
6. Johnson, Wayne: A Comparison Between Experimental Data and a Lifting Surface Theory Calculation of Vortex Induced Loads. Massachusetts Institute of Technology, Aeroelastic and Structures Research Laboratory, TR 153-3, August 1970.
7. Crimi, P.: Theoretical Prediction of the Flow in the Wake of a Helicopter Rotor. Cornell Aero. Lab. Report No. BB-1994-S-1, Sept. 1965.
8. Scully, M.P.: A Method of Computing Helicopter Vortex Wake Distortion. Massachusetts Institute of Technology, Aeroelastic and Structures Research Laboratory, TR 138-1, June 1967.
9. Johnson, Wayne: A Comparison Between Experimental Data and Helicopter Airloads Calculated Using a Lifting Surface Theory. Massachusetts Institute of Technology, Aeroelastic and Structures Research Laboratory, TR 157-1, July 1970.
10. Heyson, H.H.; and Katzoff, S.: Induced Velocities Near a Lifting Rotor With Nonuniform Disc Loading. NACA Report 1319, 1957.
11. Robinson, A.; and Laurman, J.A.: Wing Theory. Cambridge Univ. Press, London, 1956.
12. Pestel, E.C.; and Leckie, F.A.: Matrix Methods in Elastomechanics. McGraw-Hill Book Co., Inc., 1963.
13. Critzos, Chris C.; Heyson, Harry H.; Boswinkle, Robert W.,Jr.: Aerodynamic Characteristics of NACA 0012 Airfoil Section at Angles of Attack from 0° to 180°. NACA TN 3361, January 1955.
14. Tanner, Watson H.: Charts for Estimating Rotary Wing Performance in Hover and at High Forward Speeds. NACA CR-114, November 1964.

15. Scheiman, James: A Tabulation of Helicopter Rotor-blade Differential Pressures, Stresses, and Motions as Measured in Flight. NASA TM X-952, 1964.
16. Burpo, F.B., et al: Measurement of Dynamic Air Loads on a Full-scale Semirigid Rotor. TCREC Technical Report 62-42, 1962.
17. Piarulli, Vincent J.: The Effects of Nonuniform Swash-plate Stiffness on Coupled Blade-Control System Dynamics and Stability. NASA CR-1817, 1971.
18. Rinehart, S.A.: Study of Modification of Rotor Tip Vortex by Aerodynamic Means. RASA Report 70-02 (available as AD-704804), 1970.
19. Rinehart, S.A.; Balcerak, J.C.; and White, Richard P. Jr.: An Experimental Study of Tip Vortex Modification by Mass Flow Injection. RASA Report 71-01, (available as AD-726736), 1971.

TABLE 1

H-34 FREQUENCIES AND MODE SHAPES
Ω=23.0 rad/sec, θ_0=13.6°
FULLY ARTICULATED

ω		Tip Deflection		Mode Type	Coupling, if important
rad/sec	X 1/Ω	ϕ/v	-w/v		
5.6804	0.2470	-0.0110	-9.60000	C-1	F-1
23.6361	1.0277	-0.0082	0.09230	F-1	0
61.2762	2.6642	-0.0010	-0.11300	F-2	0
75.6725	3.2901	-0.0163	5.39000	C-2	F-3
111.3324	4.8405	0.0114	-0.08870	F-3	0
163.2693	7.0987	780.8	0.63900	T-1	0
171.3437	7.4497	0.1345	0.12400	F-4	C-3
192.8873	8.3864	0.1175	-8.05000	C-3	F-3
250.5688	10.8943	-0.0301	0.00925	F-5	0
347.3836	15.1036	0.0224	0.05620	F-6	0
357.5299	15.5448	0.0129	-15.9300	C-4	0
444.9662	19.3464	-0.0928	-0.01510	F-7	0
484.3651	21.0594	57.74	-0.01160	T-2	0

TABLE 2

HU-1A FREQUENCIES AND MODE SHAPES
Ω=32.882 rad/sec, θ_0=10°

ω		Tip Deflection		Mode	Coupling,
rad/sec	X 1/Ω	φ/v	-w/v	Type	if important
symmetric modes (clamped flap, pinned chordwise)					
37.1260	1.1291	-0.0994	-.06200	F-1	0
104.9312	3.1910	-0.8530	-.06330	F-2	T-1
126.5499	3.8486	15.0600	-.06080	T-1	F-2
181.6353	5.5239	-0.8464	2.89000	C-2	F-3, T-1
200.2473	6.0899	-0.9613	-.34400	F-3	T-1, C-2
310.8473	9.4534	1.8440	+.01520	F-4	T-2
338.2845	10.2878	15.6800	-.01300	T-2	F-4
468.2712	14.2410	0.6758	-.05780	F-5	T-3
546.1555	16.6096	-0.1732	11.27000	C-3	0
621.0826	18.8882	-13.470	-.01220	T-3	F-6
636.4494	19.3556	-1.1700	-.06120	F-6	T-3
antisymmetric modes (pinned flap, clamped chordwise)					
32.0184	0.9737	-0.0725	-.34400	F-1	T-1
49.7393	1.5127	-0.1883	2.80000	C-1	F-1
90.3910	2.7490	-0.6168	-.19000	F-2	T-1, C-1
126.4704	3.8462	21.6900	-.07820	T-1	0
161.8563	4.9223	-0.9383	0.01600	F-3	T-1
271.1910	8.2474	0.0892	0.19700	F-4	C-2
288.7094	8.7802	0.2464	-4.39000	C-2	F-4
339.2609	10.3175	19.7800	-.05150	T-2	F-4
414.4594	12.6044	-0.3169	+.03120	F-5	T-2
601.8897	18.3045	4.081	-.01107	F-6	T-3
609.0193	18.5214	6.378	-.01620	T-3	F-6

TABLE 3

ROTOR PARAMETER INPUT VALUES

Case No.[1]	Maneuver Condition[2]	g-level	μ	Ω rad/sec	$\dot{q}^2$ rad/sec	Pitch Angles, °			Flap Angles, °			α_s deg.	ρ lb-sec^2/ft^4
						θ_0	A_c	B_c	β_0	β_1	β_2		
1	right turn	1.50	.185	23.2	.224	13.17	-4.41	2.06	5.17	-1.16	-.580	+1.68	.00213
2	left turn	1.52	.192	23.2	.221	12.73	-3.58	2.74	5.18	-1.13	-.670	-1.80	.00213
3	right turn	1.34	.225	22.8	.128	14.44	-6.72	3.04	4.49	-0.88	-.810	-2.90	.00210
4	left turn	1.35	.244	22.5	.127	14.30	-6.41	3.32	4.62	-1.22	1.090	-3.03	.00210
5	pull-up	1.60	.159	24.1	.250	16.02	-9.29	2.18	5.75	-1.55	2.380	-2.78	.00216
6	pull-up	1.40	.224	23.0	.150	13.74	-7.21	2.98	5.40	-0.76	-.410	+4.80	.00210
7	right roll	1.00	.200	23.2	.300	12.60	-4.14	-13.2	3.44	0	0	-3.00	.00214
8	left roll	1.00	.200	23.2	-.30	12.60	-2.96	15.6	3.44	0	0	-3.00	.00214
9	right turn	1.50	.240	32.9	.154	22.00	-8.00	2.0	0	0	0	-3.64	.00210
10	left turn	1.50	.240	32.9	.154	22.00	-8.00	2.0	0	0	0	-3.64	.00210
11	pull-up	1.15	.210	32.9	.115	16.94	-6.16	1.62	0	-0.64	-1.25	+2.35	.00207
12	right roll	1.00	.200	32.9	.300	19.20	-6.00	17.20	0	0	0	-3.75	.00210

[1]Cases 1 through 8 are for an H-34 helicopter, Cases 9 through 12 are for an HU-1A.

[2]$\dot{q}$ is $\dot{\alpha}_A$ for pull-ups and turns, $\dot{\phi}_r$ for rolls.

TABLE 4

CASE NUMBERS AND DATA SOURCES

Case Number[1]	Flight Condition	Data Sources Reference Number(s) - Nomenclature	Ratio of Computed to Required Thrust[2]
1	right turn	15 - Flight 36, Table 39 ; 4 - Case (4)	0.633
2	left turn	15 - Flight 37, Table 40 ; 4 - Case (3)	0.760
3	right turn	15 - Flight 39, Table 42 ; 4 - Case (6)	0.768
4	left turn	15 - Flight 40, Table 43 ; 4 - Case (5)	0.692
5	symmetrical pull-up	15 - Flight 87, Table 118	0.975
6	symmetrical pull-up	15 - Flight 89, Table 123; 4 - Case (2)	0.814
7	right roll	Computed	1.010
8	left roll	Computed	0.907
9	right turn	Computed	0.708
10	left turn	Computed	0.780
11	symmetrical pull-up	16 - Table 8a and IBM Tab 13c	0.879
12	right roll	Computed	0.967

[1]Cases 1 through 8 are for an H-34 helicopter, and Cases 9 through 12 are for an HU-1A helicopter.

[2]Required thrust is that measured, where reported; and that which would result from the specified load factor for "computed" cases.

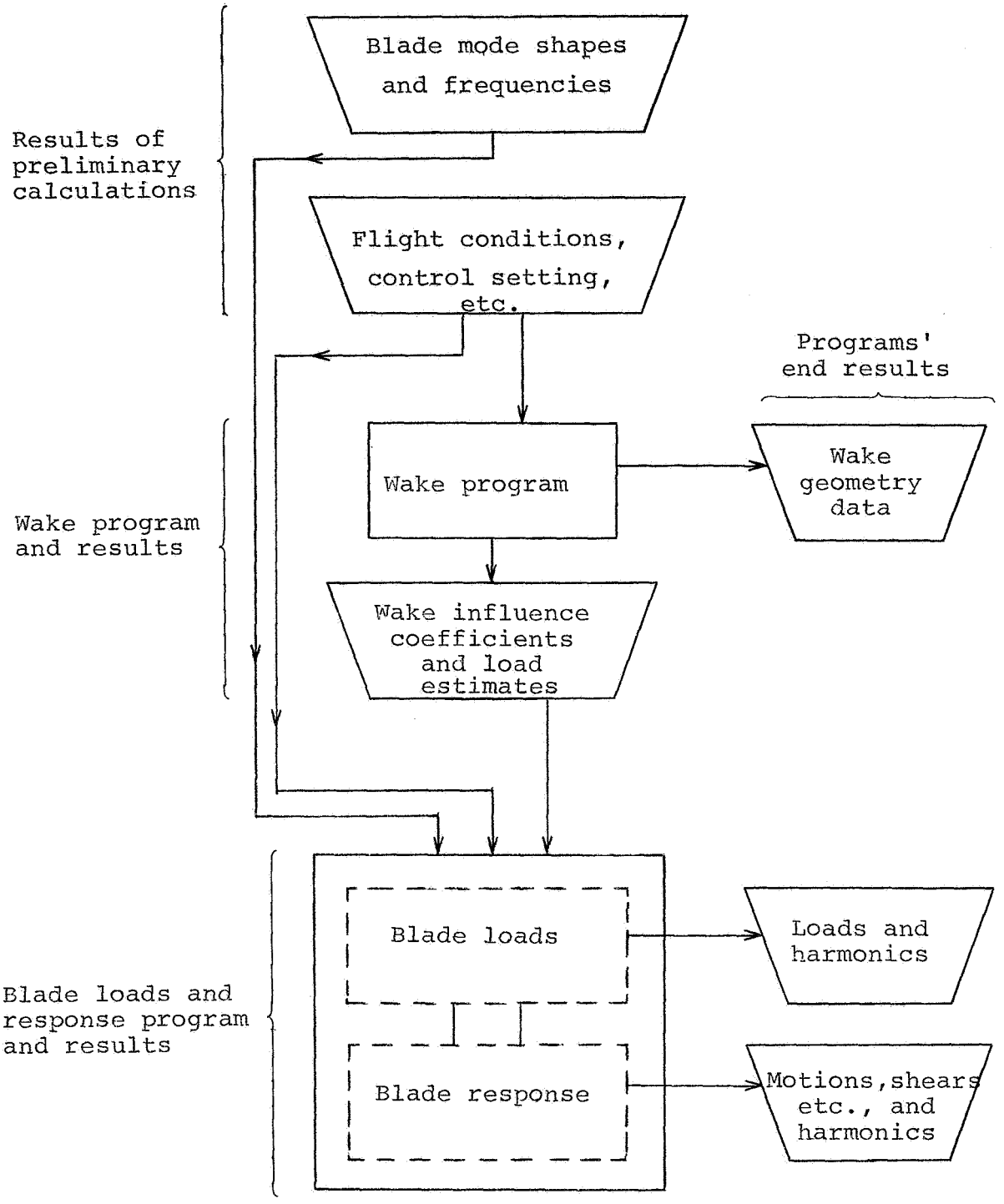

Figure 1. Program usage flow diagram

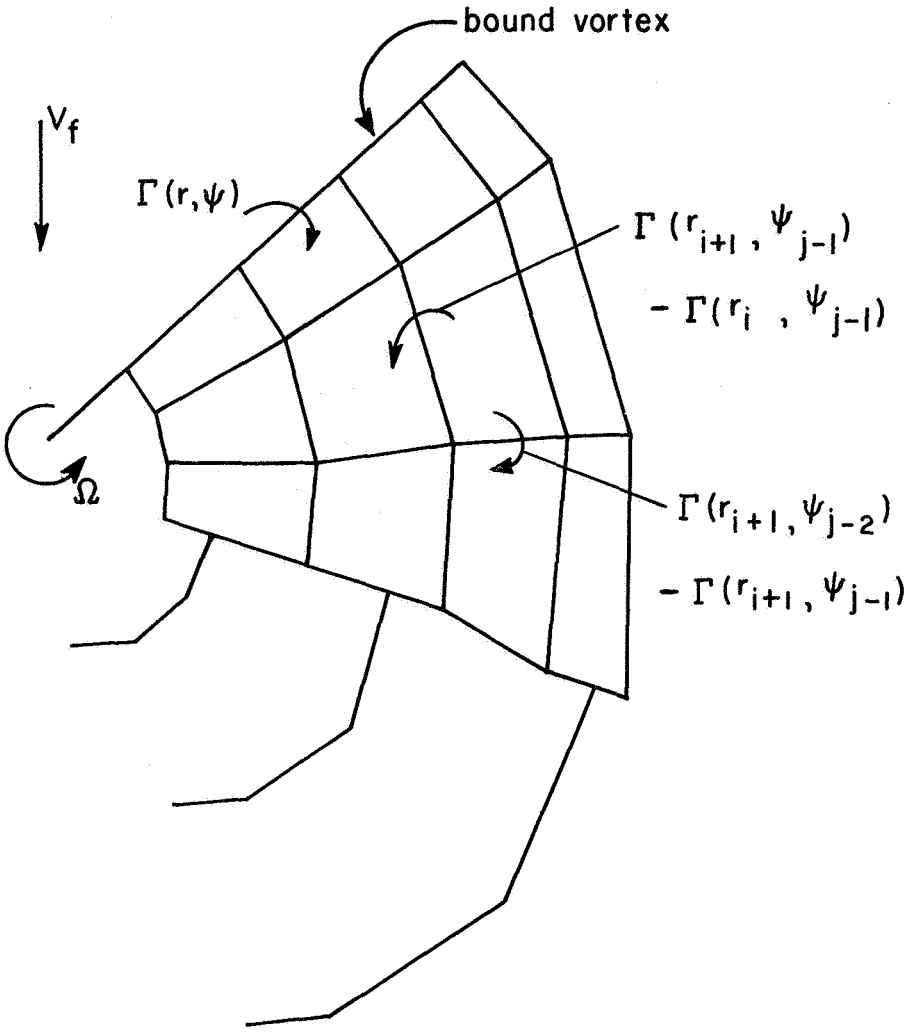

Figure 2. Wake model with combination of "full mesh" wake of shed and trailing vortices and "modified" wake of trailing vortices only

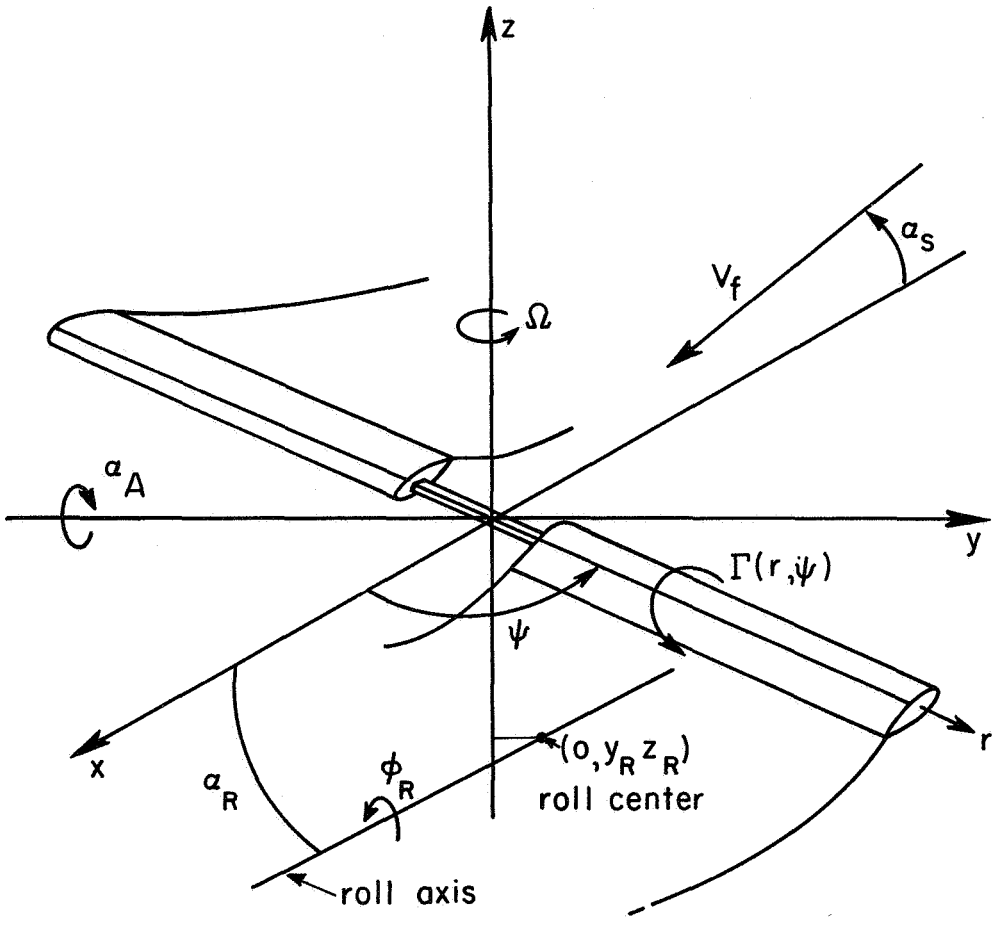

Figure 3. Rotor system coordinates

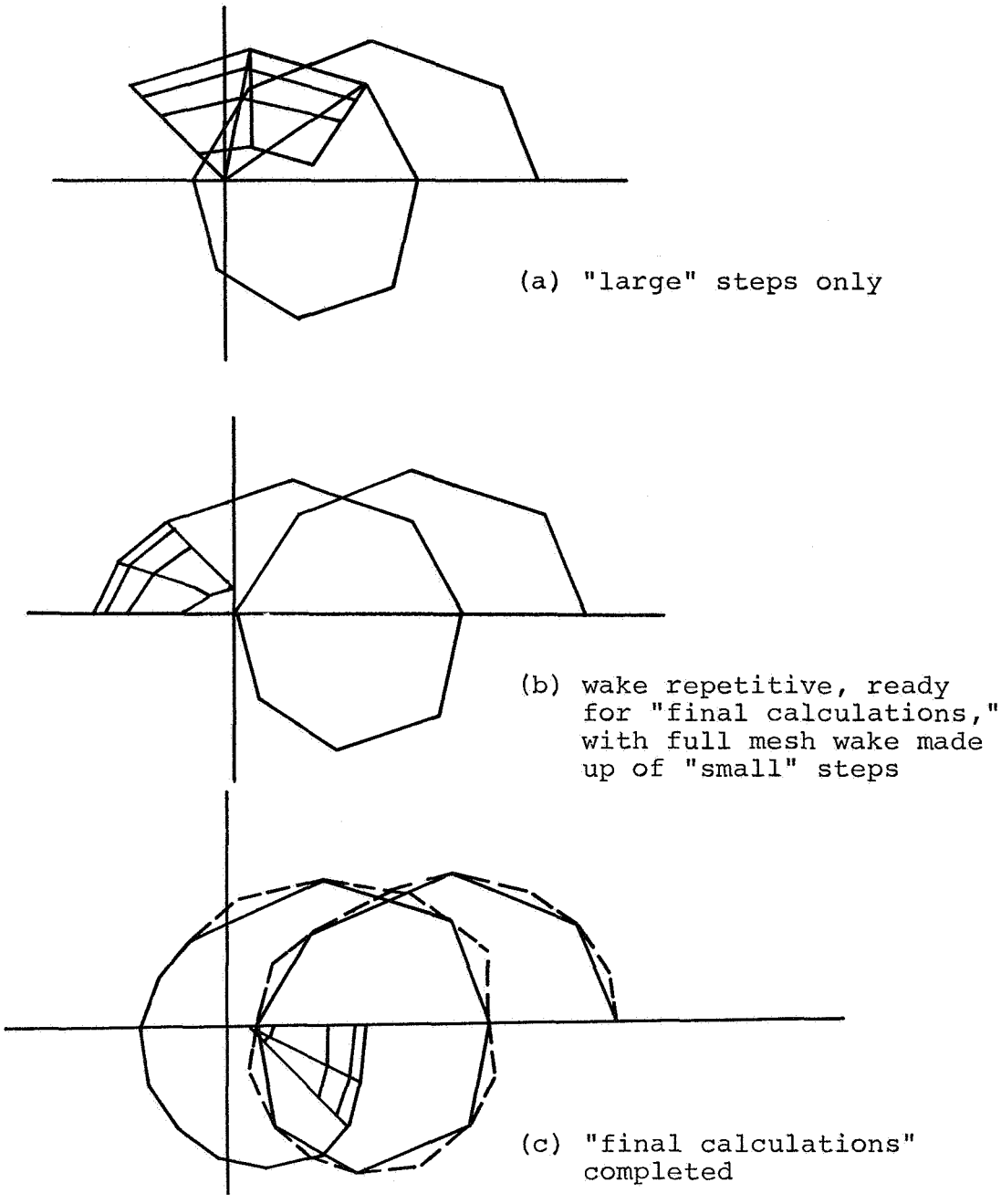

Figure 4. Large-to-small step size procedure, illustrated here for eight large steps and sixteen small steps per revolution. All calculations were performed with eighteen large steps and thirty-six small steps per revolution.

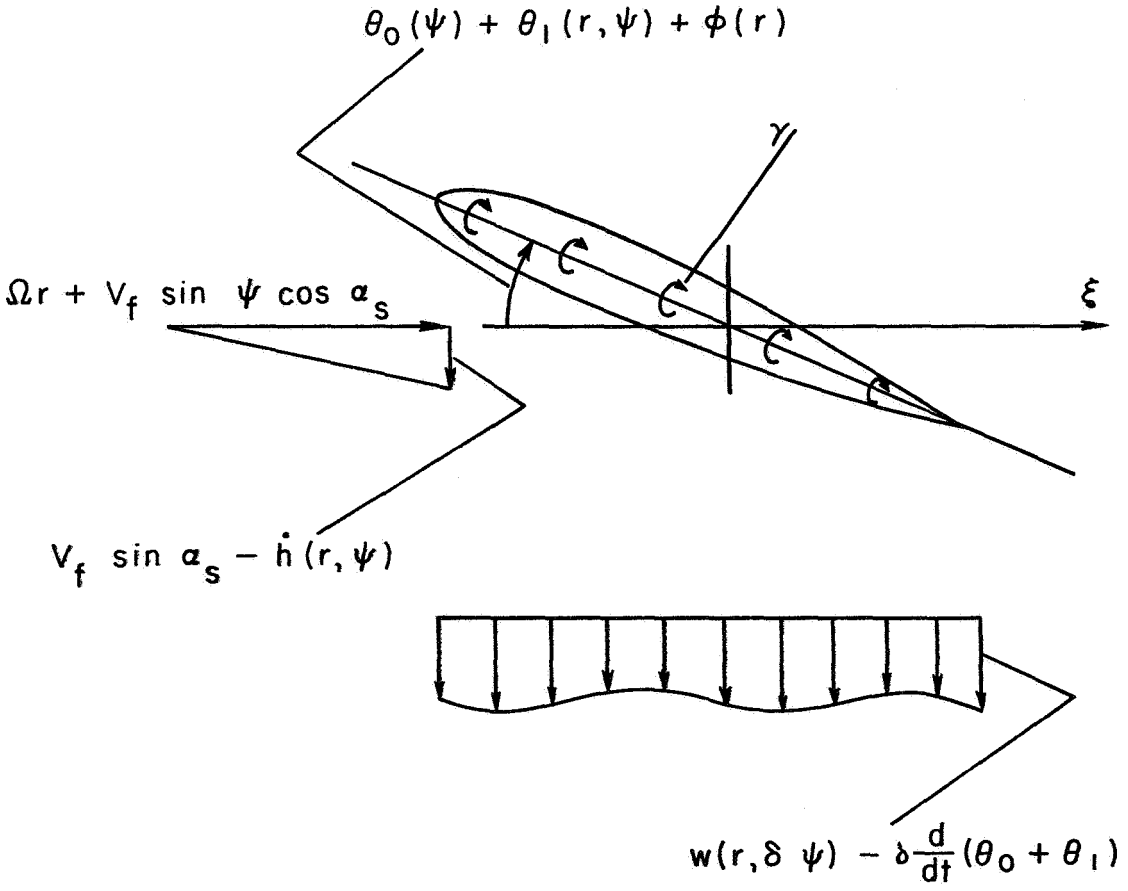

Figure 5. The flow at a blade section

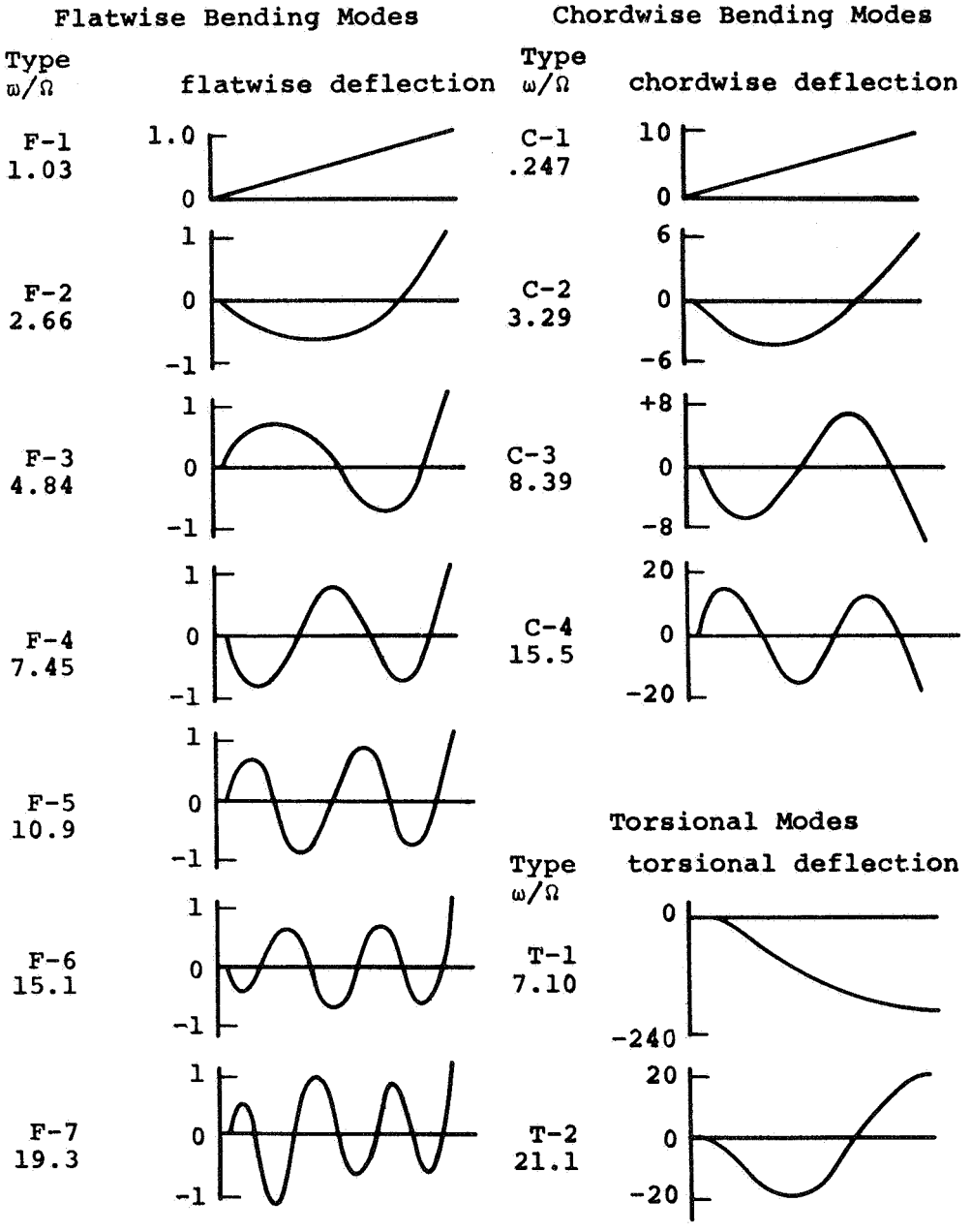

Figure 6. H-34 coupled mode shapes and frequencies, Ω = 23 rad/sec (Very weak coupling exists between mode types, so only major mode shape is shown and all mode shapes are for a tip flatwise deflection of unity.)

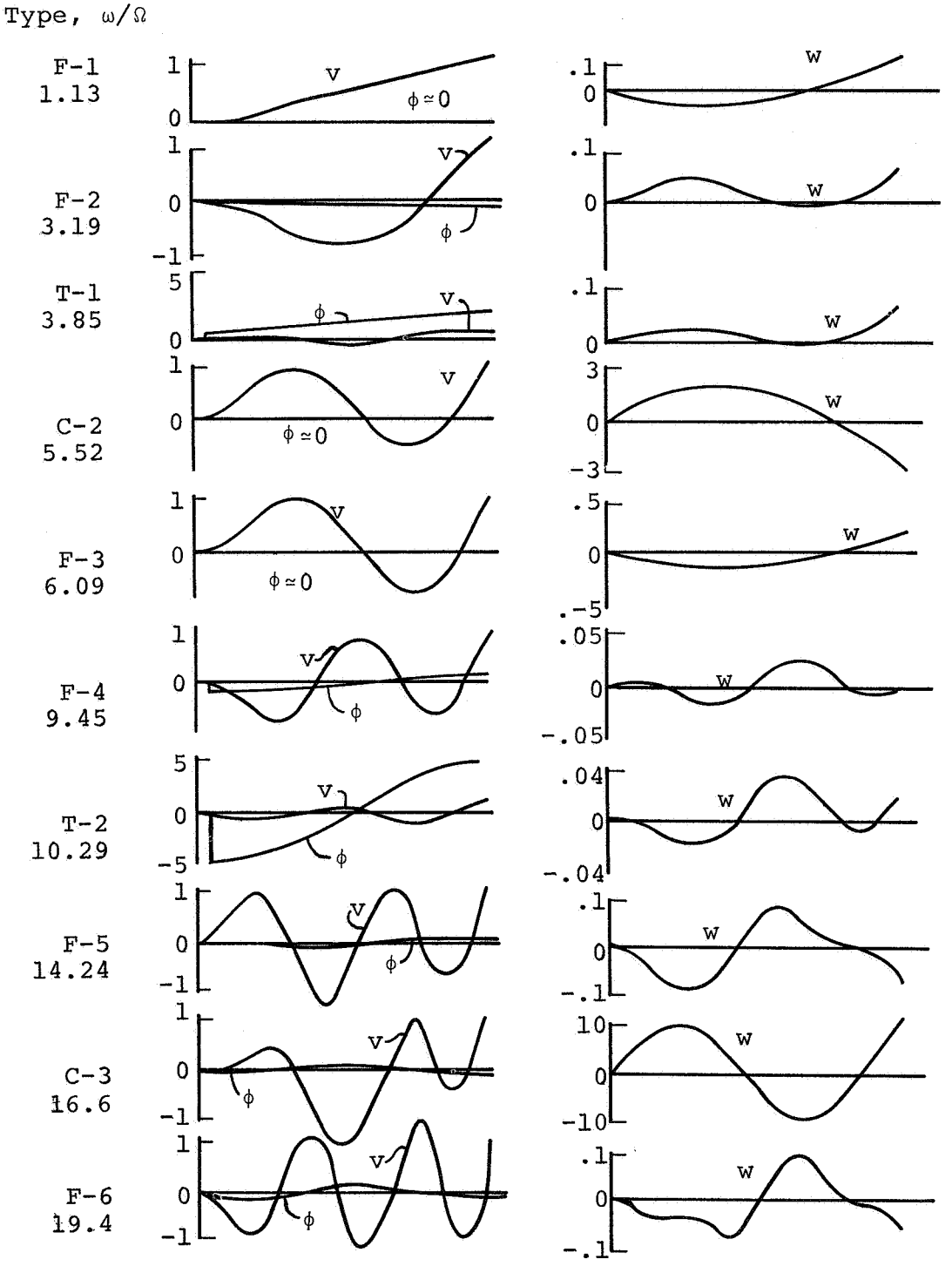

Figure 7. HU-1A coupled symmetric mode shapes and frequencies; v and w in $m/(m\ v_{tip})$, ϕ in $rad/(m\ v_{tip})$, Ω=32.88

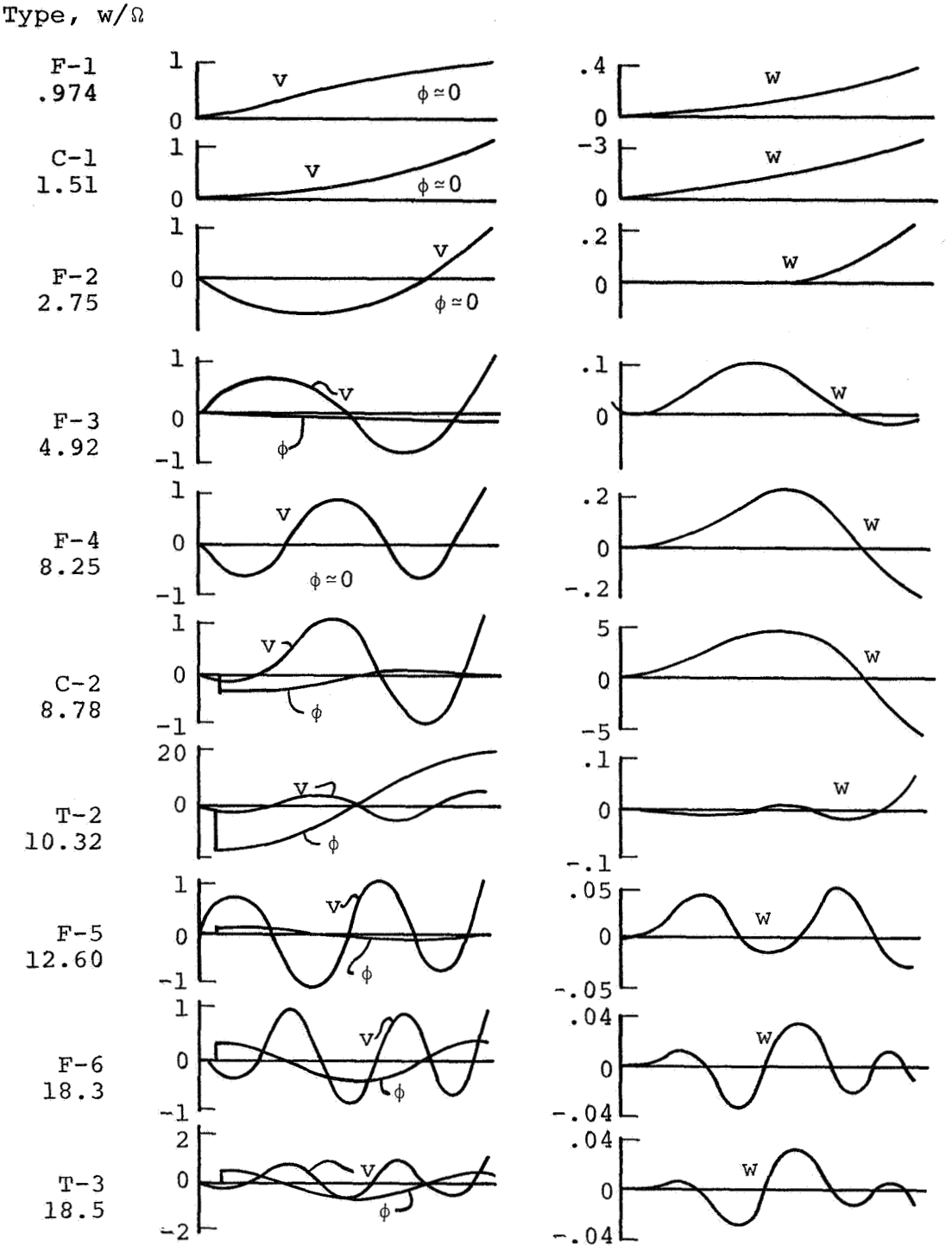

Figure 8. HU-1A coupled antisymmetric mode shapes and frequencies; v and w in m/(m v_{tip}), ϕ in rad/(m v_{tip}), Ω=32.88

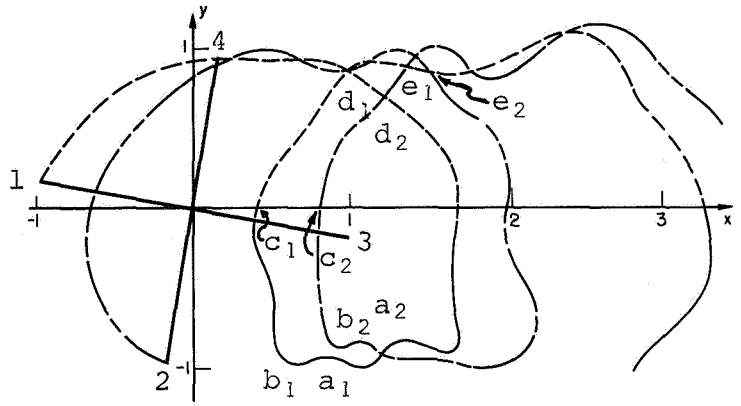

(a) plan view

Blade No.	advancing side	retreating side
1	– – –	———
2	——– – ——–	——– · ——–

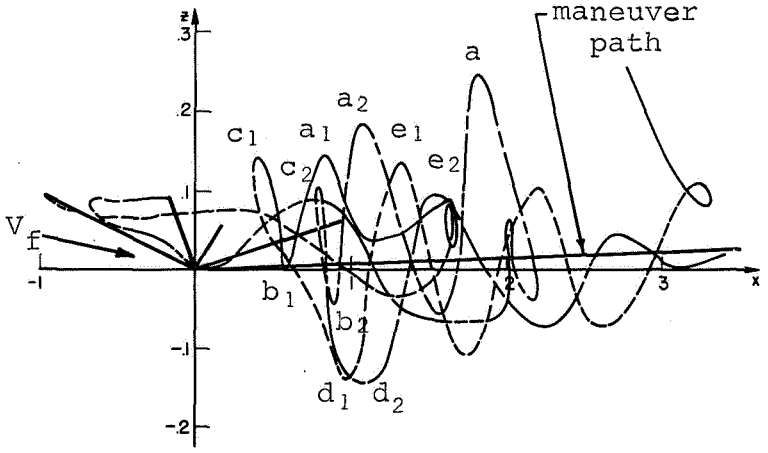

(b) side view

(c) plan view, aft portion of rotor disk, with corresponding blades and tip vortices indicated by number

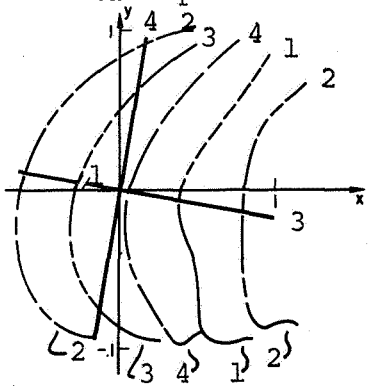

Figure 9. Wake geometry for Case 3, H-34 helicopter, right turn, μ=0.225, f_g=1.34

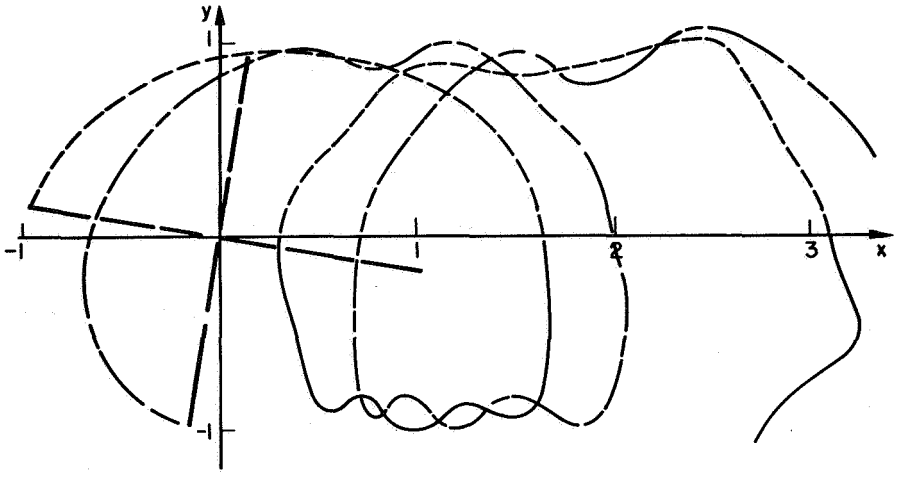

Blade No.	advancing side	retreating side
1	- - - - - -	———
2	—— - - ——	——— - - ——

(a) plan view

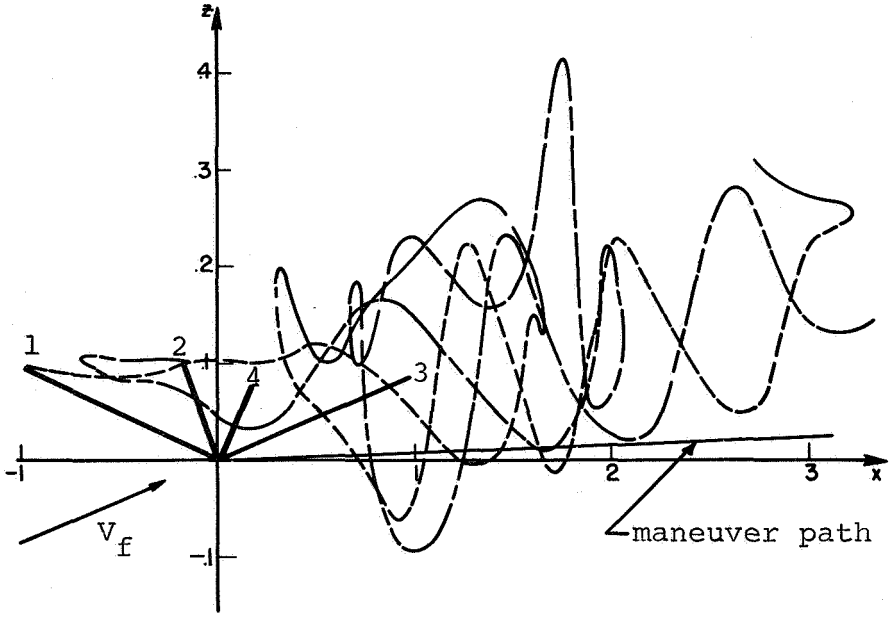

(b) side view

Figure 10. Wake geometry for Case 6, H-34 helicopter, symmetrical pull-up, μ=0.224, f_g=1.4

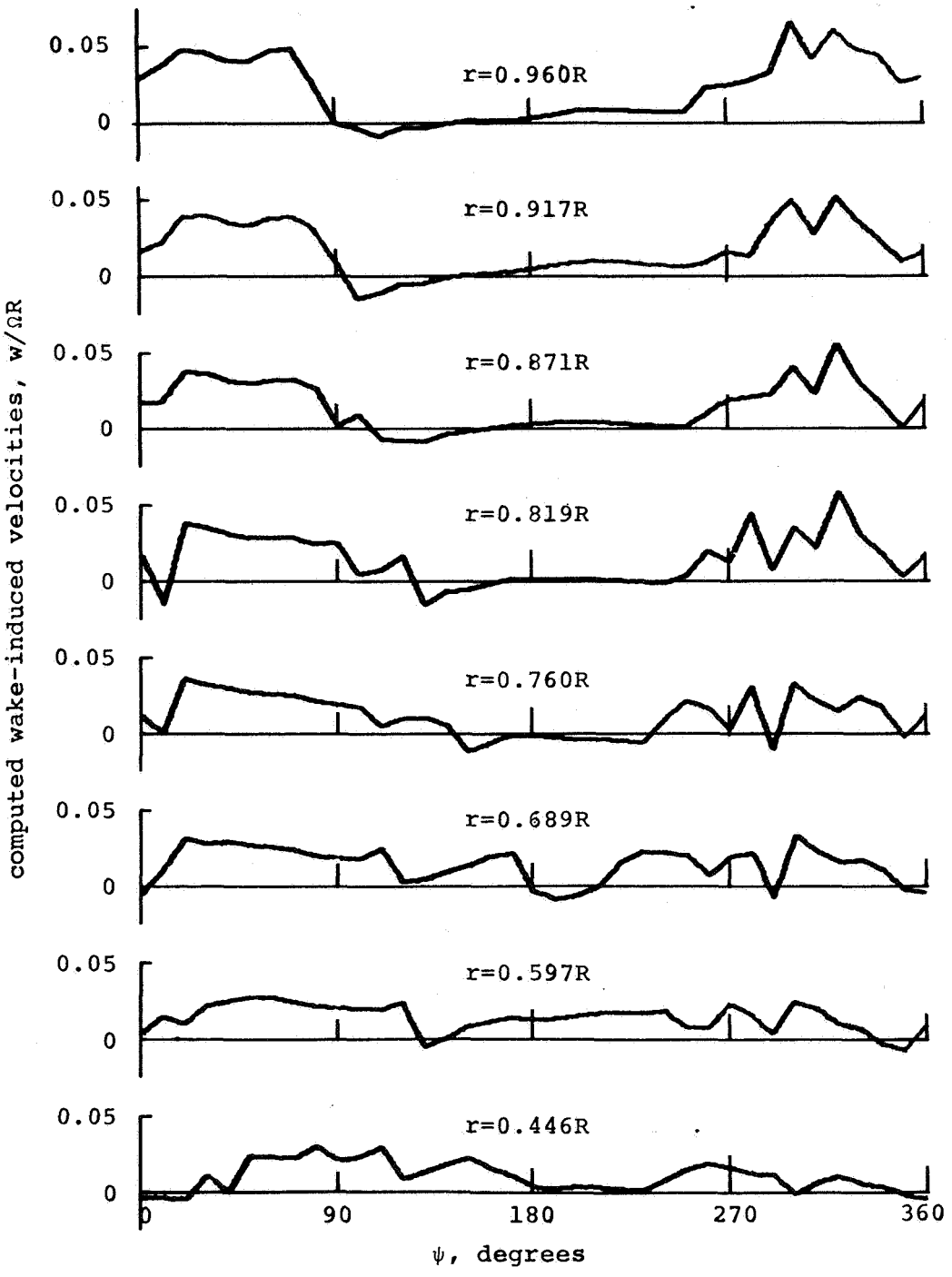

Figure 11. Computed wake-induced velocities at aerodynamic load points for Case 1, H-34, right turn, μ=0.185, f_g=1.5

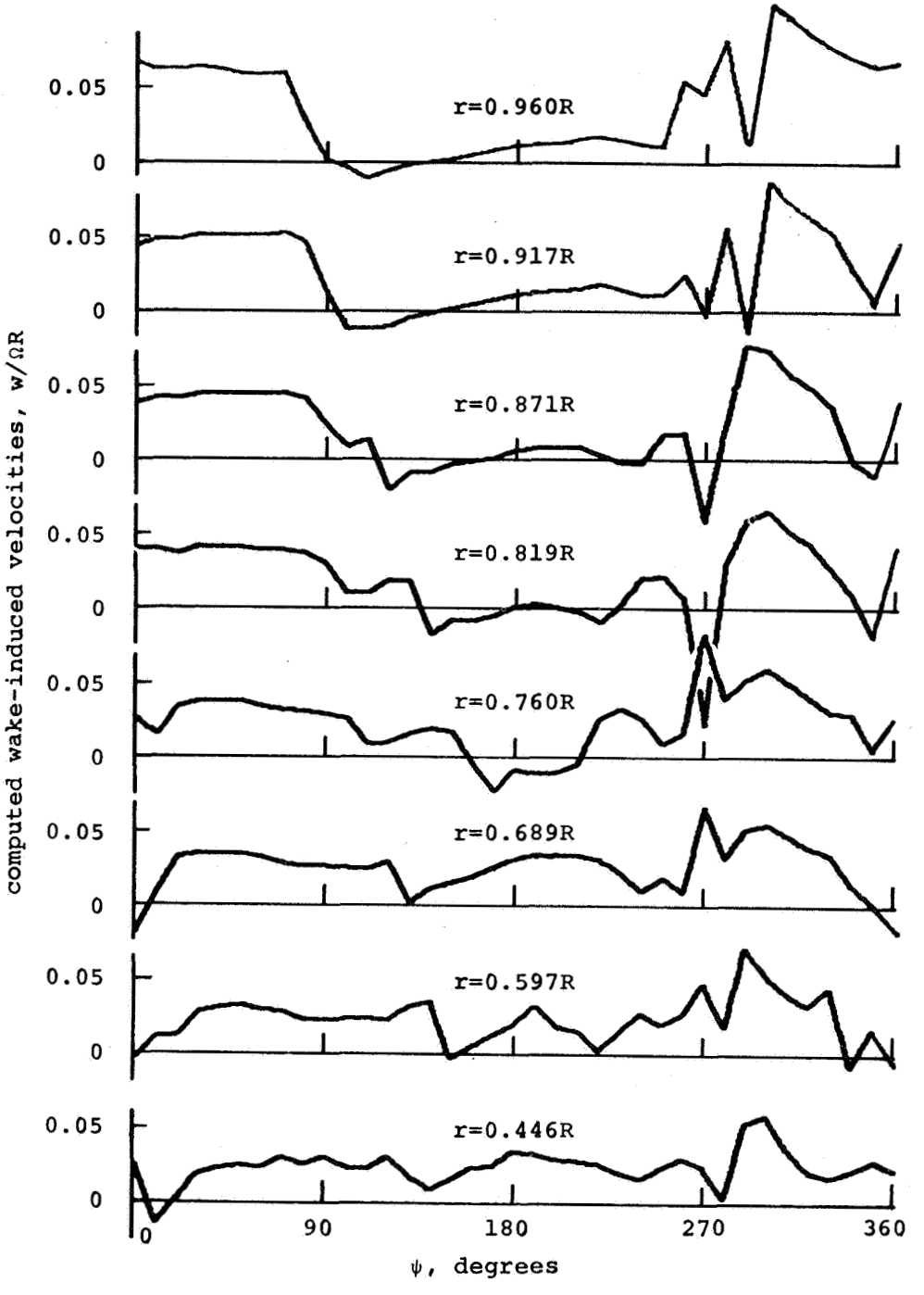

Figure 12. Computed wake-induced velocities at aerodynamic load points for Case 5, H-34, pull-up, μ=0.159, f_g=1.6

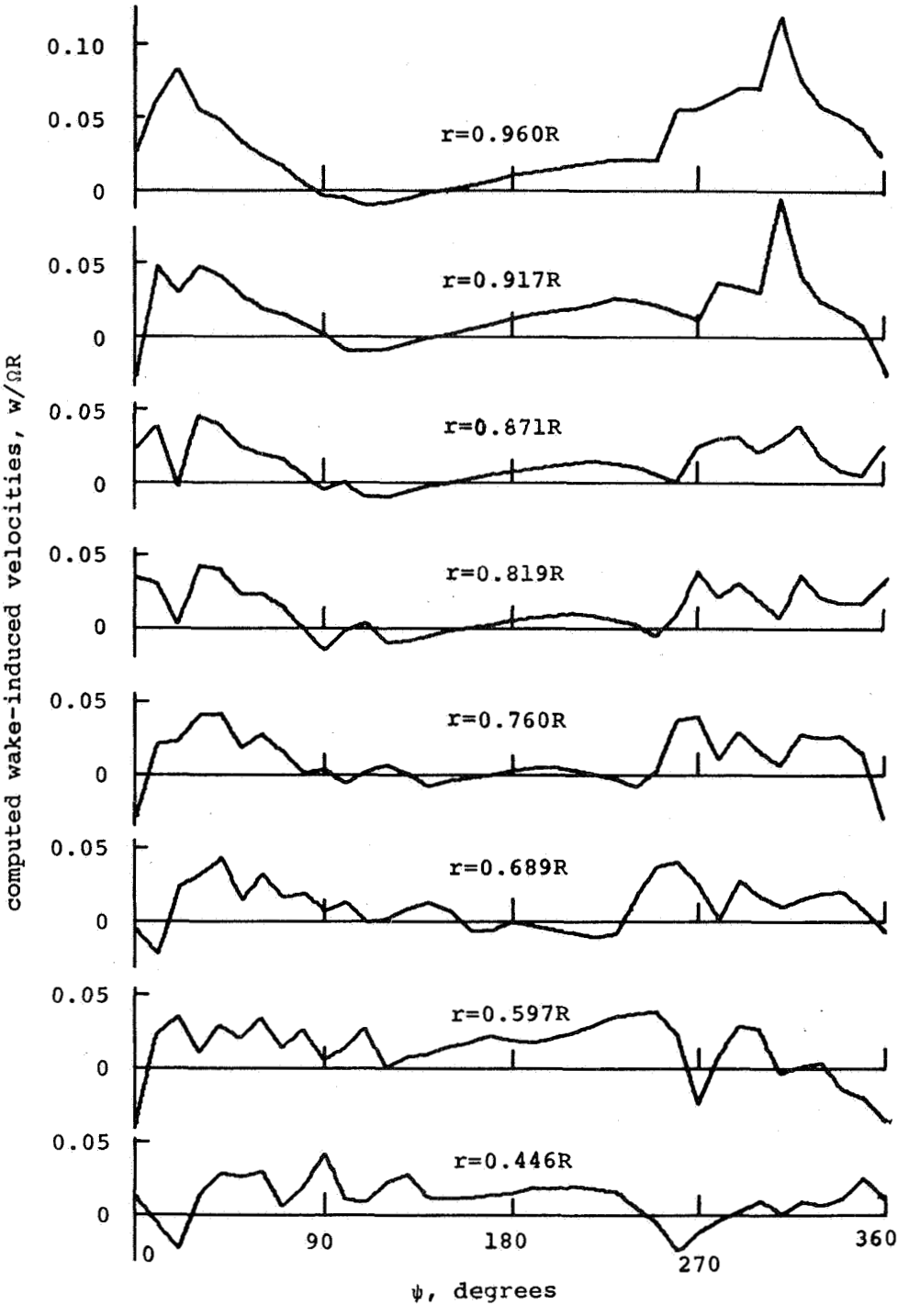

Figure 13. Computed wake-induced velocities at aerodynamic load points for Case 6, H-34, pull-up, μ=0.224, f_g=1.4

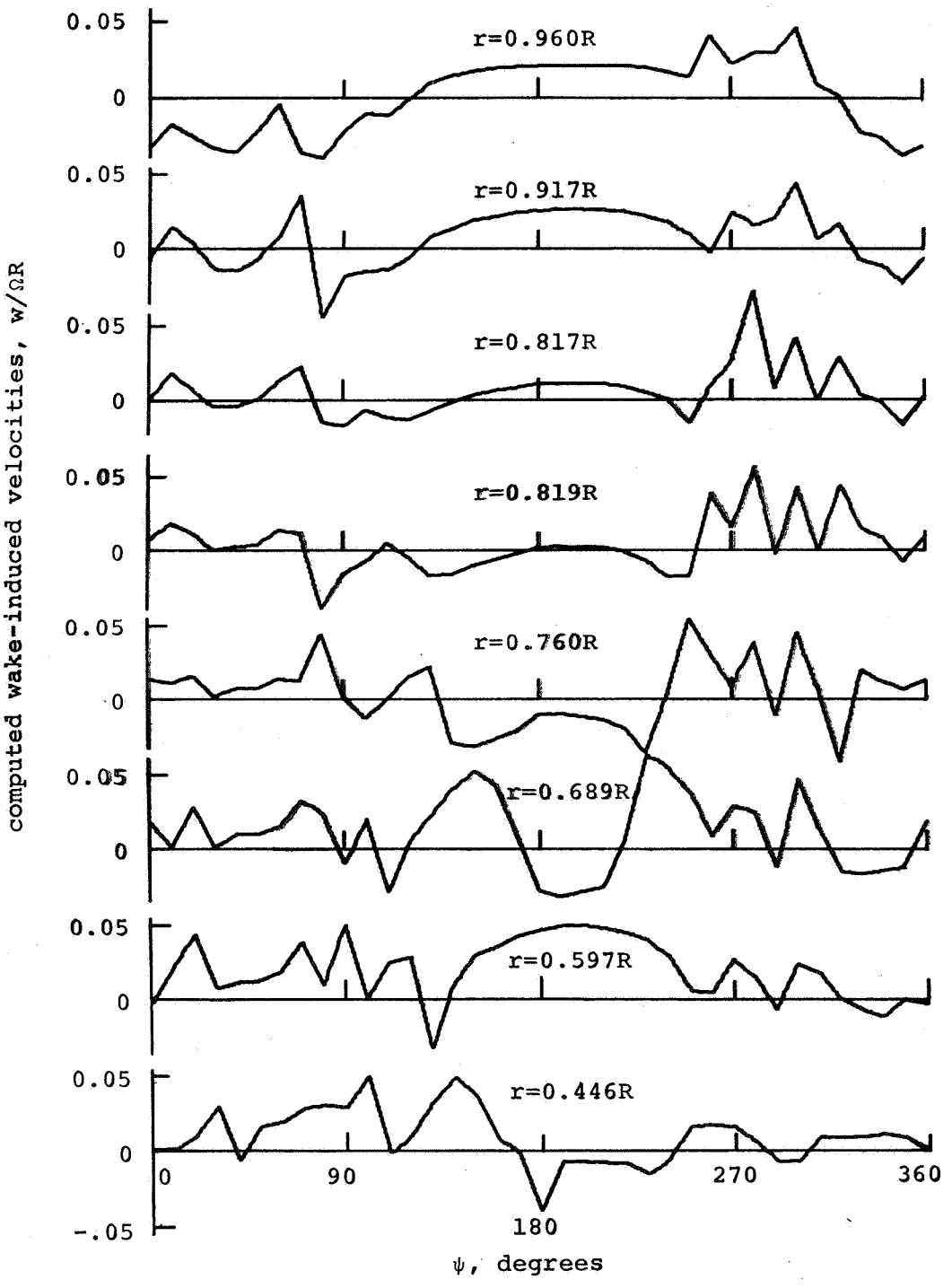

Figure 14. Computed wake-induced velocities at aerodynamic load poitns for Case 7, H-34, right roll, μ=0.20, f_g=1.0

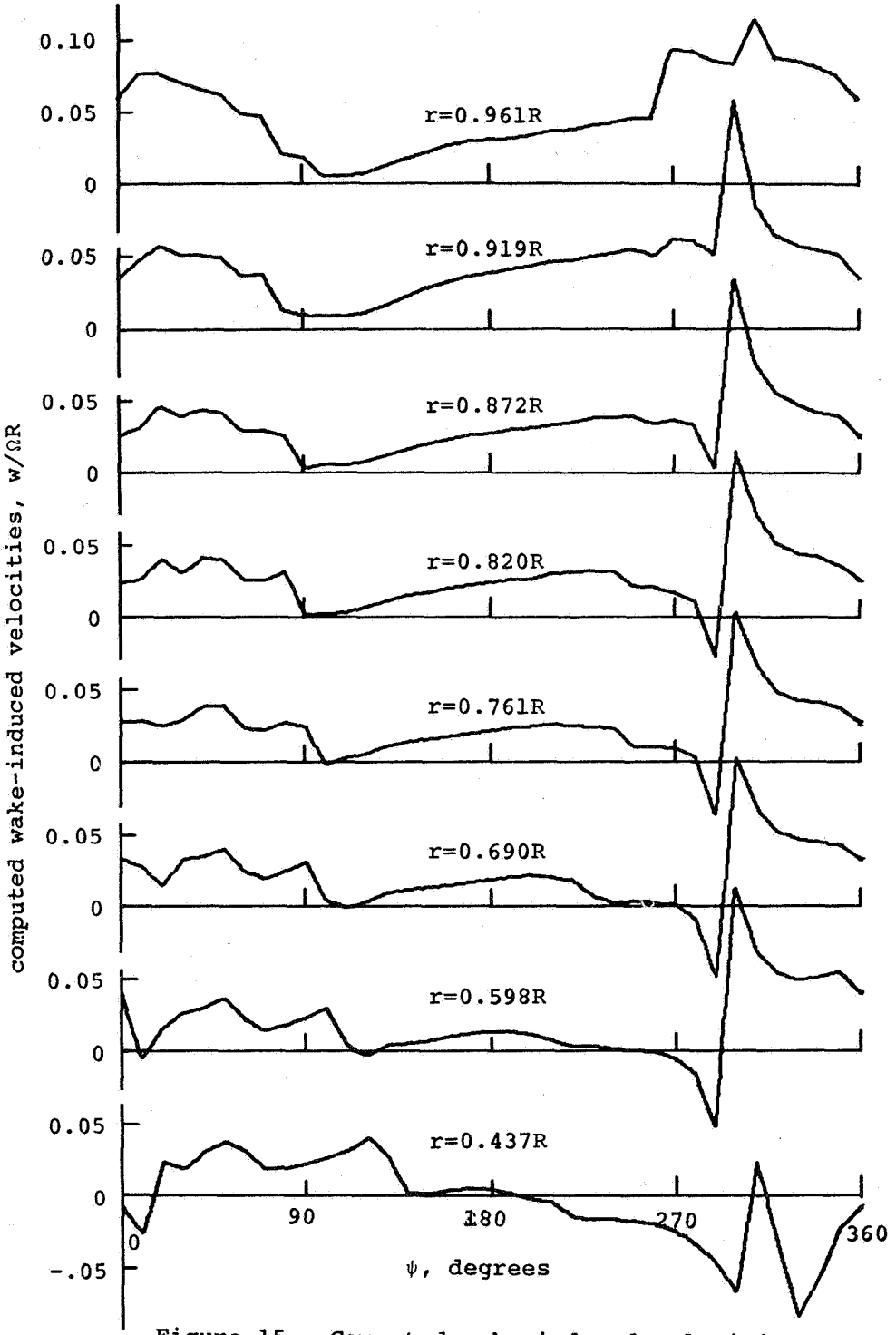

Figure 15. Computed wake-induced velocities at aerodynamic load points for Case 10, HU-1A, left turn, μ=0.24, f_g=1.5

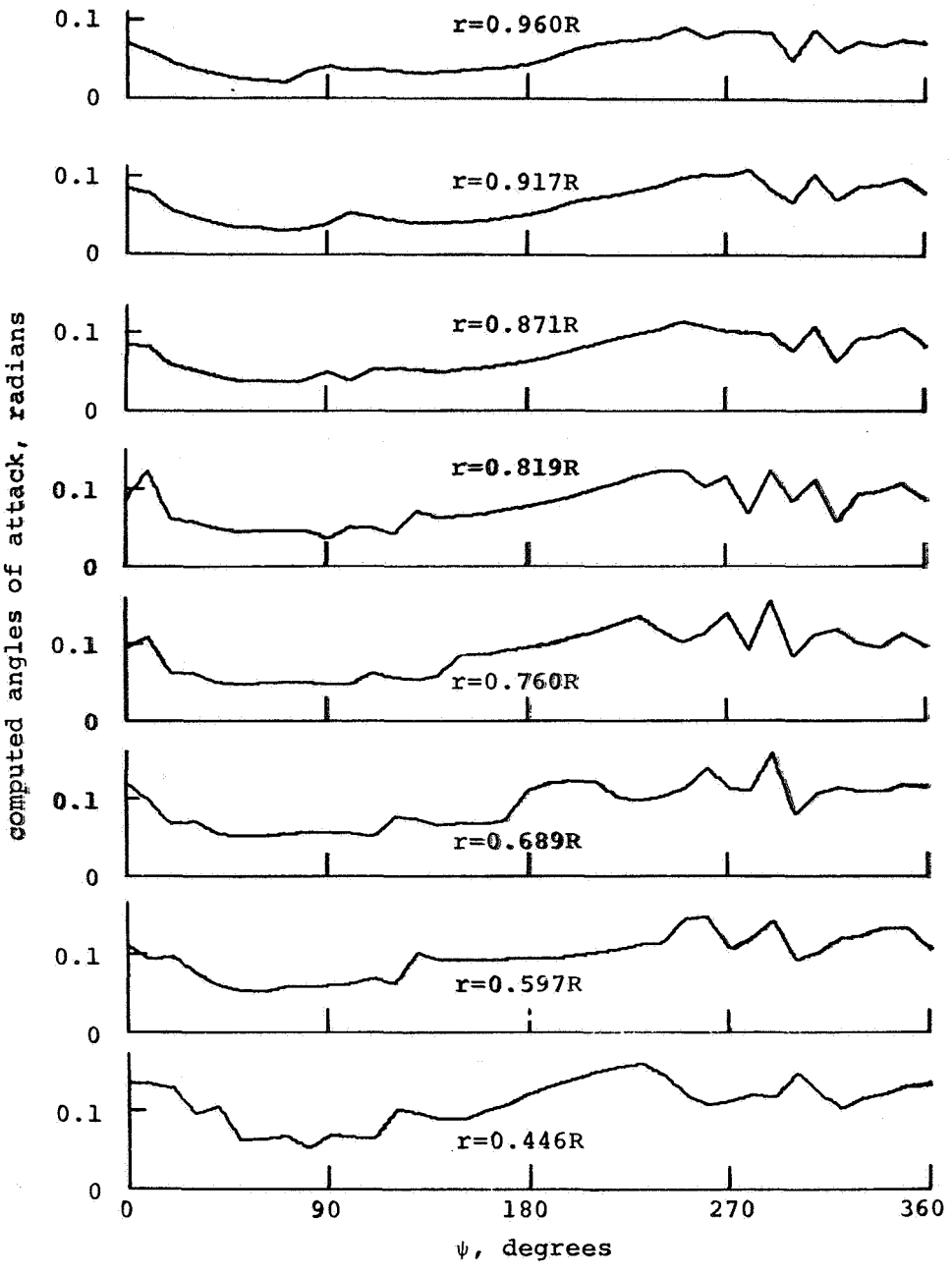

Figure 16. Computed angles of attack at aerodynamic load points for Case 1, H-34, right turn, μ=0.185, f_g=1.5

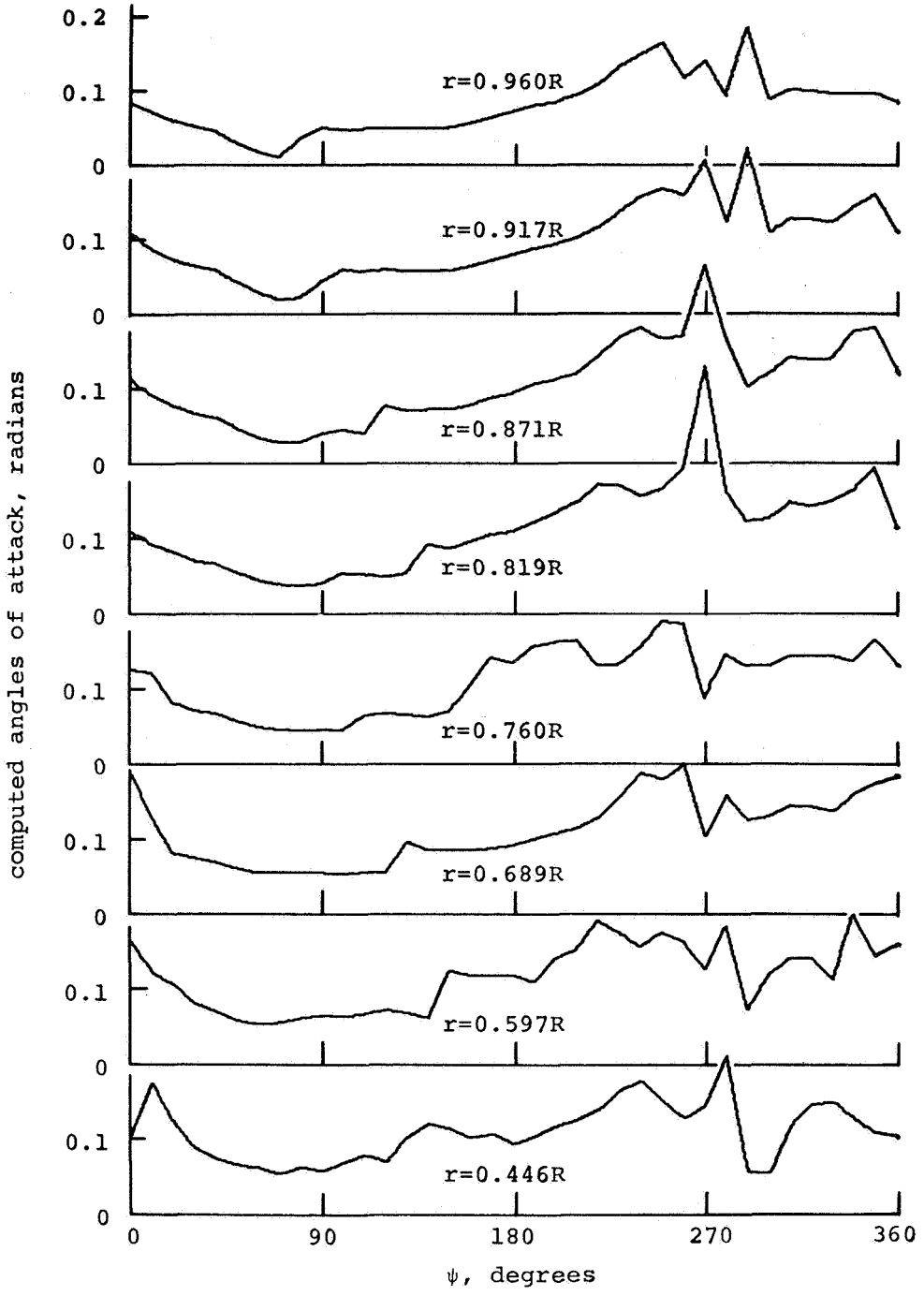

Figure 17. Computed angles of attack at aerodynamic load points for Case 5, H-34, pull-up, μ=0.159, f_g=1.6

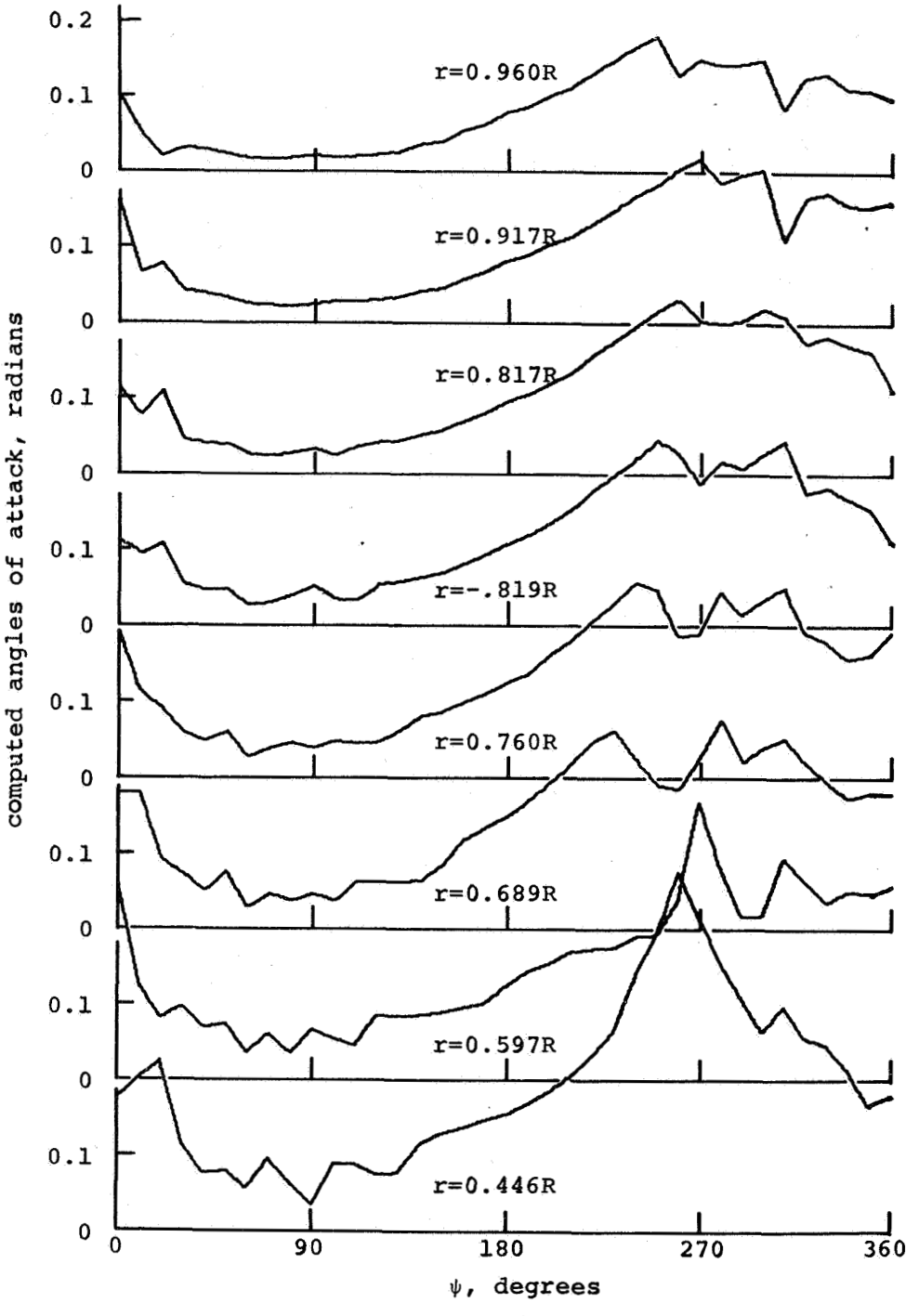

Figure 18. Computed angles of attack at aerodynamic load points for Case 6, H-34, pull-up, μ=0.224, f_g=1.4

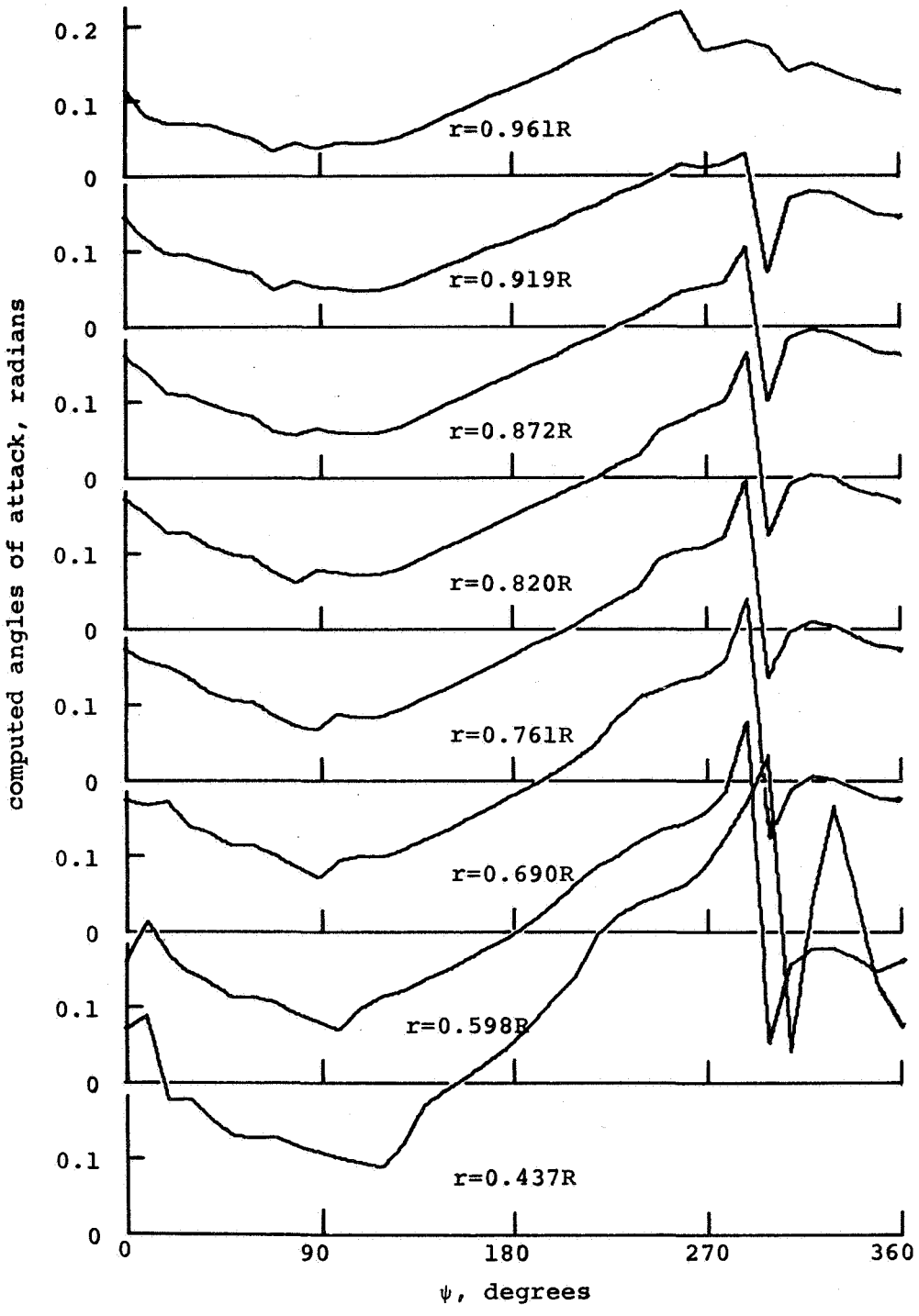

Figure 19. Computed angles of attack at aerodynamic load points for Case 10, HU-1A, left turn, μ=0.24, f_g=1.5

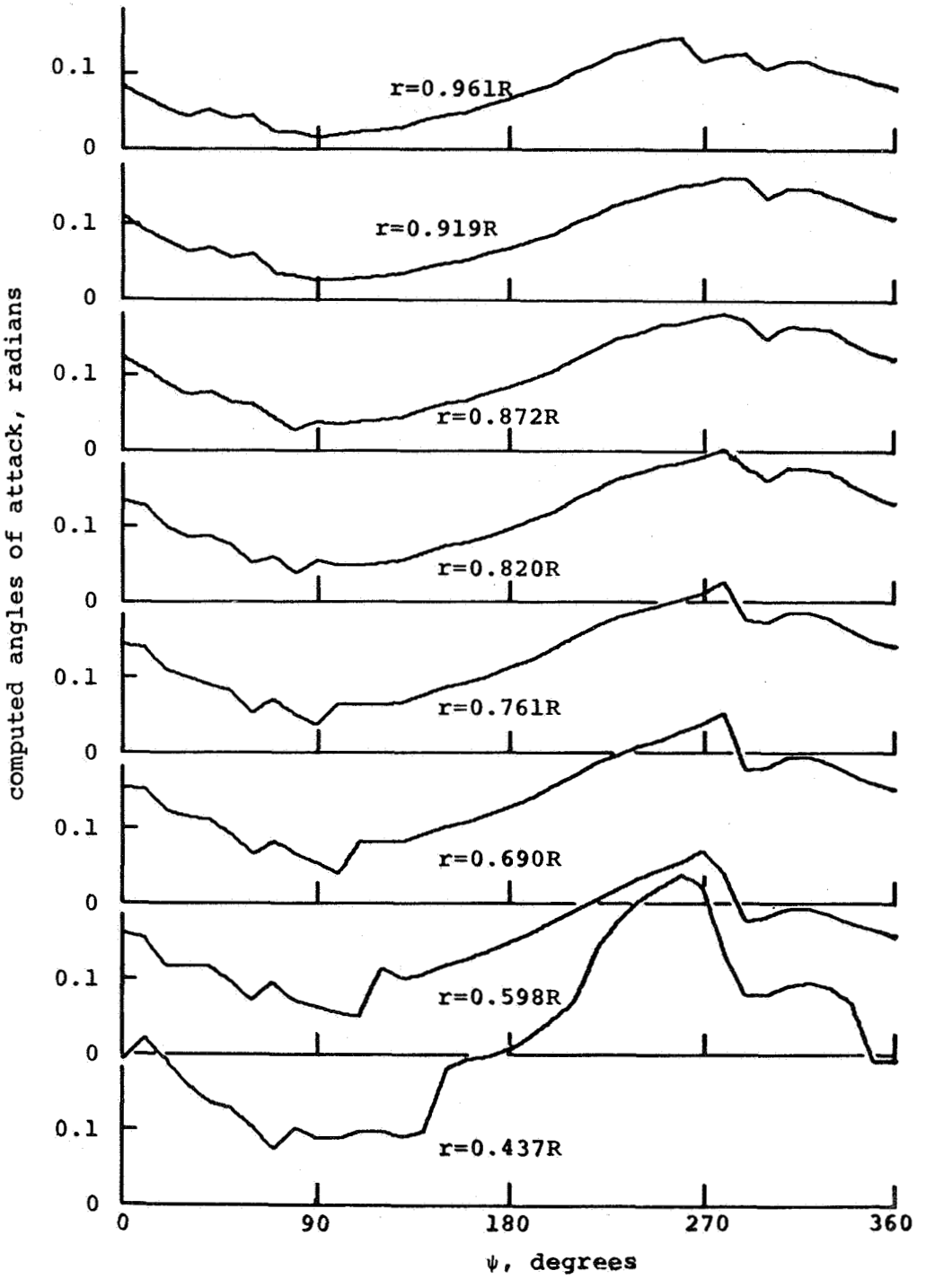

Figure 20. Computed angles of attack at aerodynamic load points for Case 11, HU-1A, pull-up, μ=0.21, f_g=1.15

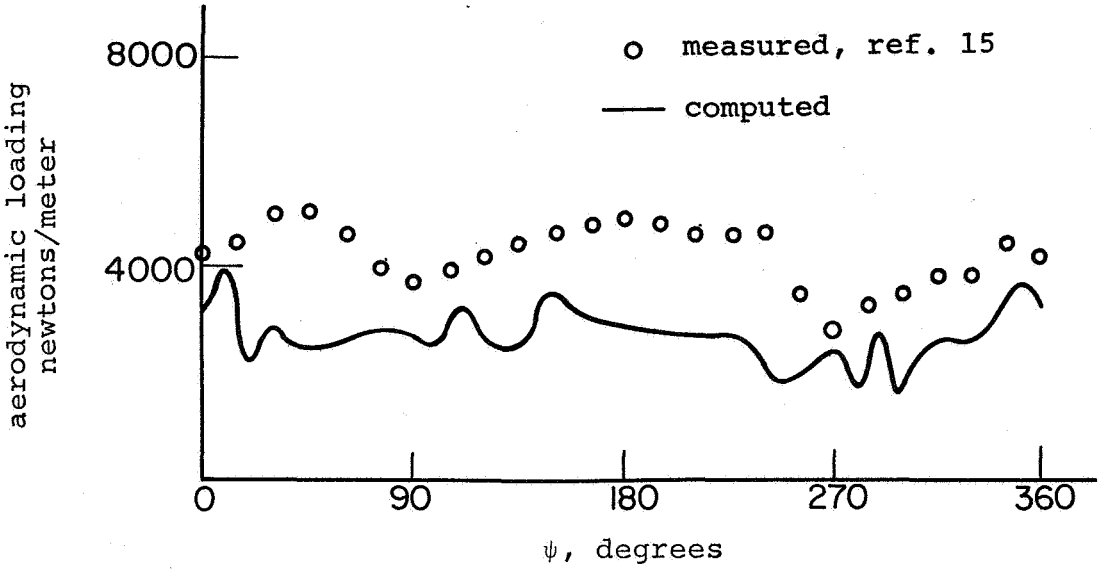

(a) loading at r≈0.75R

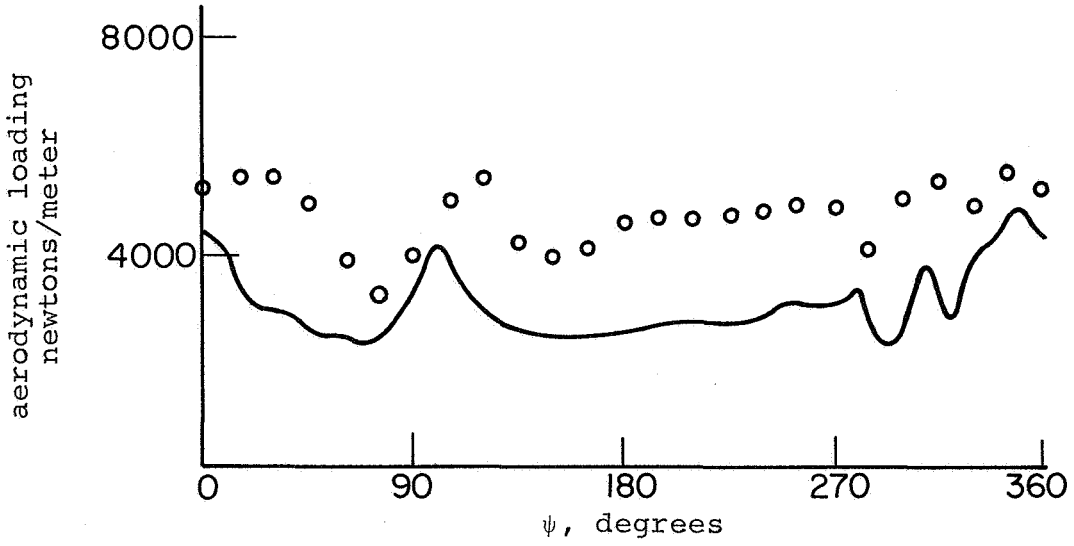

(b) loading at r≈0.90R

Figure 21. Section aerodynamic loading for Case 1, H-34, right turn, μ=0.224, f_g=1.5

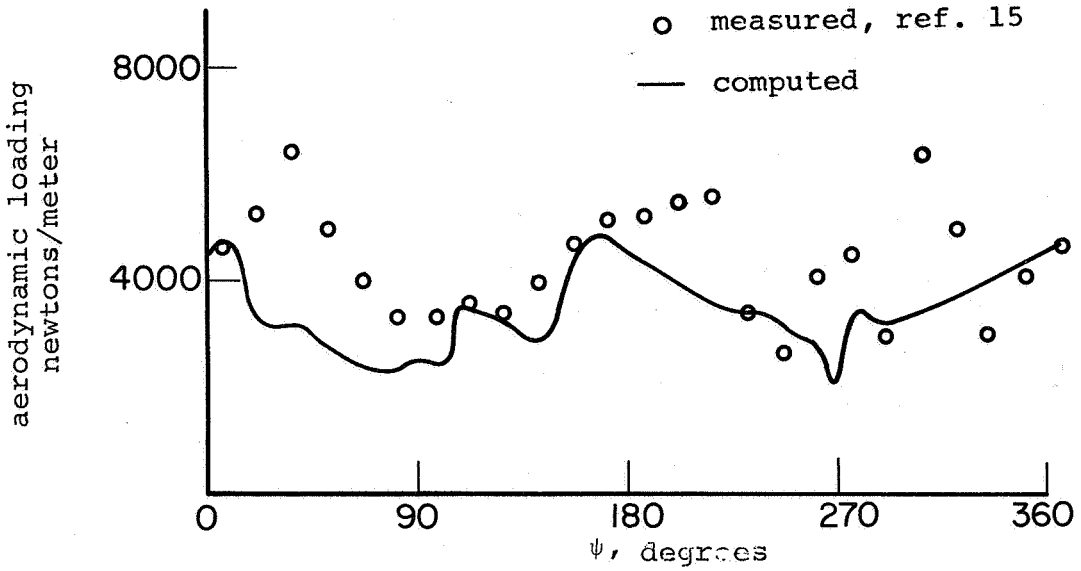

(a) loading at r≈0.75R

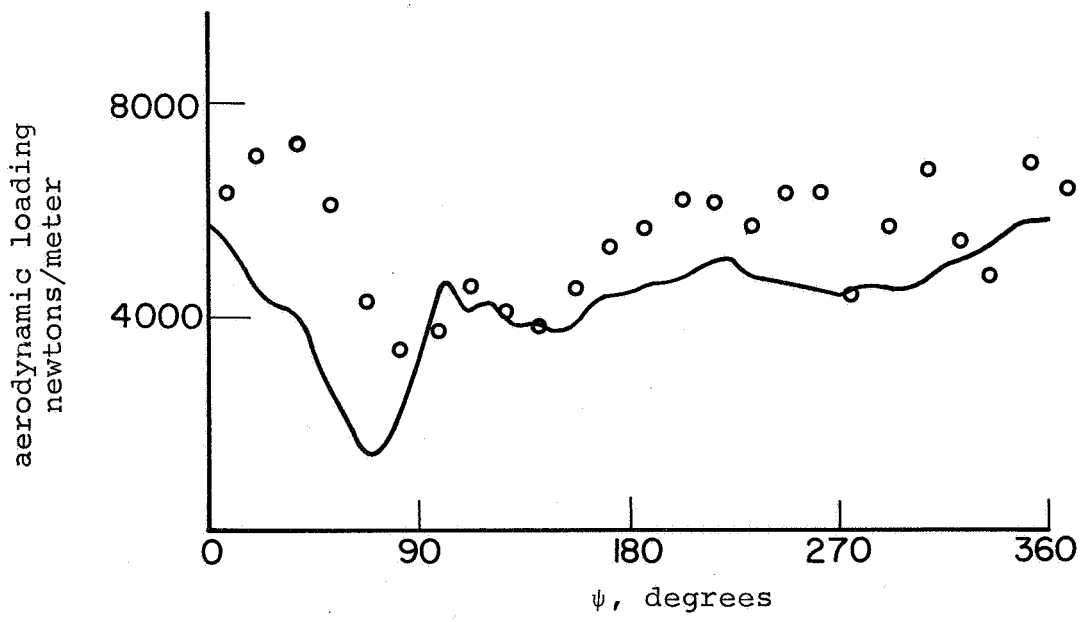

(b) loading at r≈0.90R

Figure 22. Section aerodynamic loading for Case 5, H-34 pull-up, μ=0.159, f_g=1.6

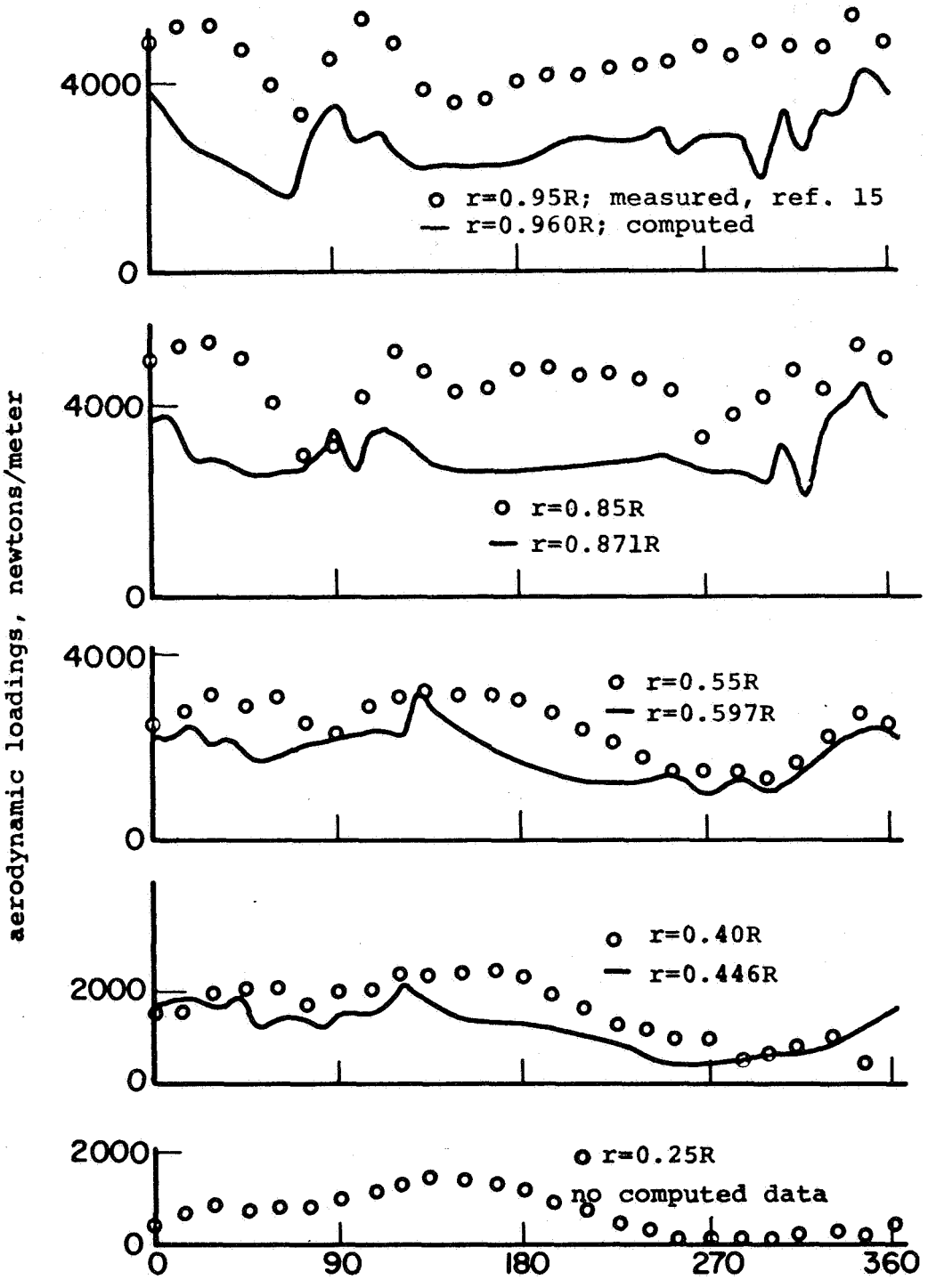

Figure 23. Section aerodynamic loading for Case 1, H-34, right turn, μ=0.185, f_g=1.5

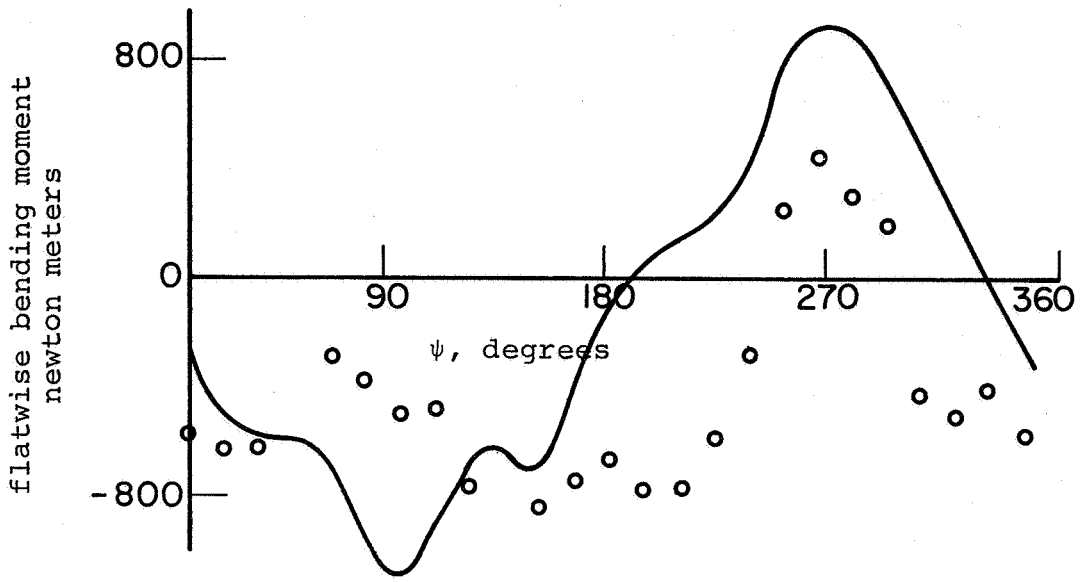

(a) flatwise moment for Case 1

o measured, ref. 15

—— computed

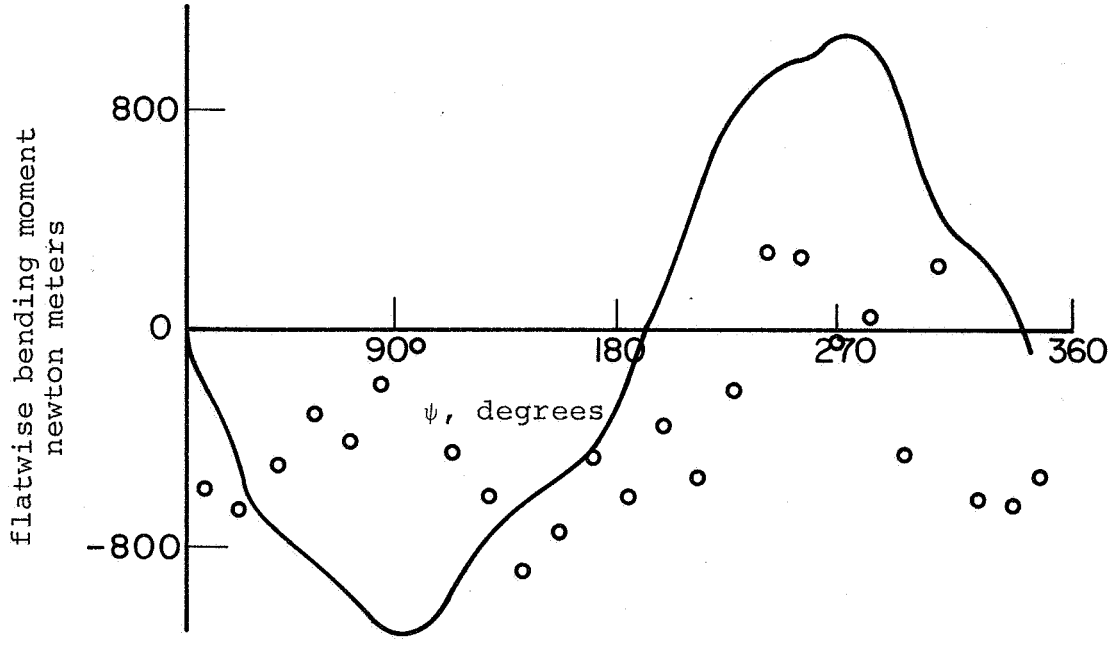

(b) flatwise moment for Case 5

Figure 24. Flatwise bending moments for Cases 1 and 5, for r≈0.65R

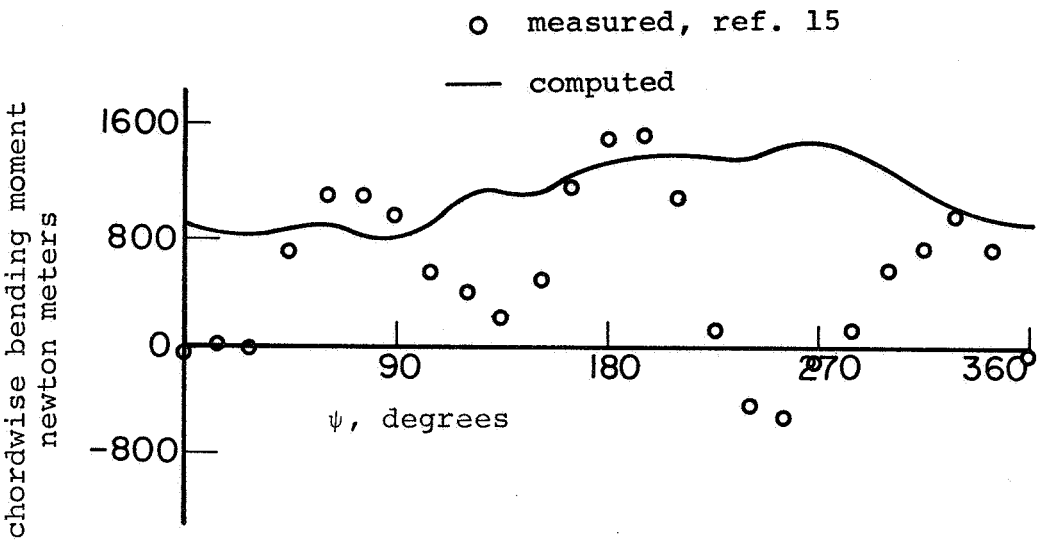

Figure 25. Chordwise bending moment for Case 1 for r≈0.575R

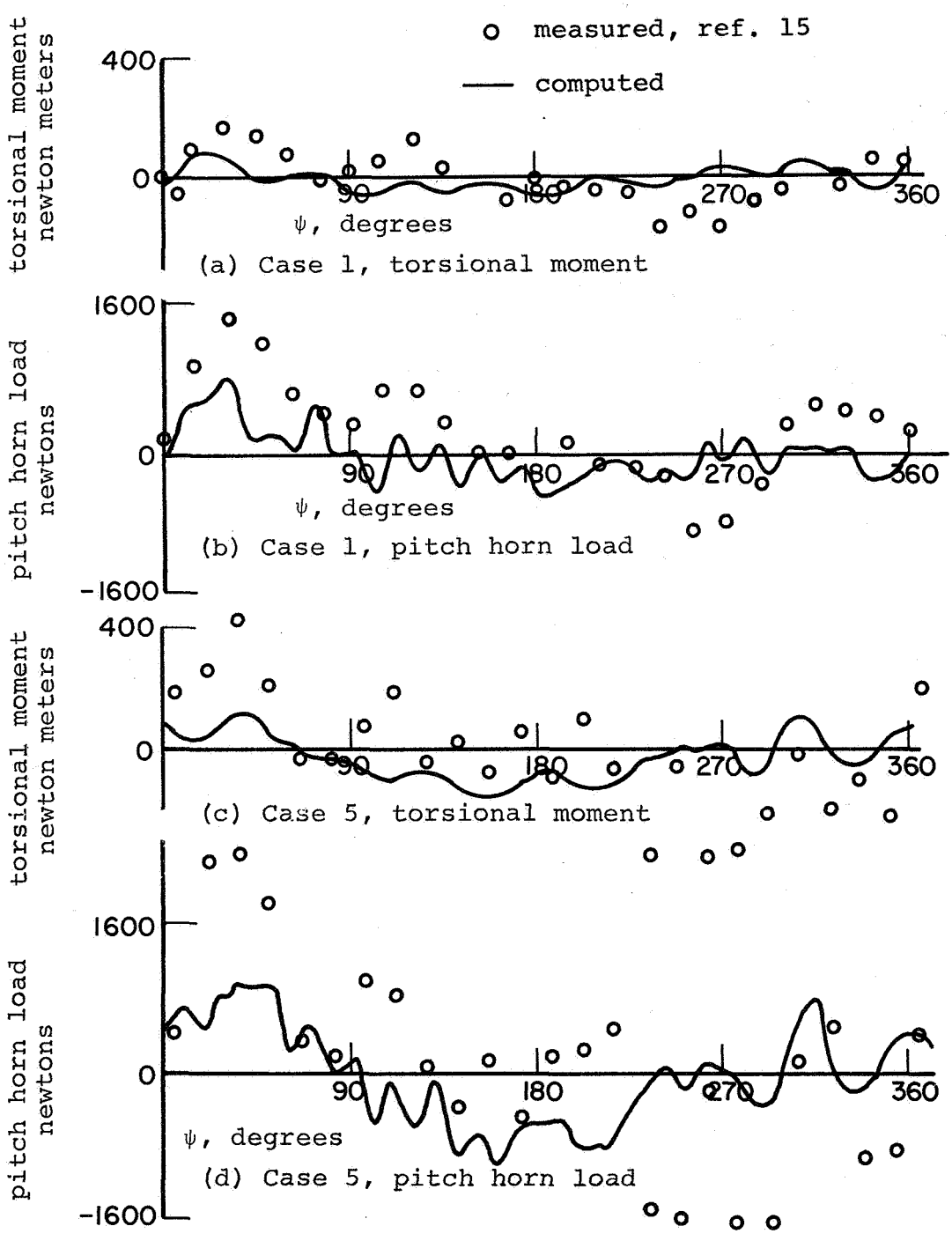

Figure 26. Torsional moments at 0.5R and pitch horn loads for Cases 1 and 5

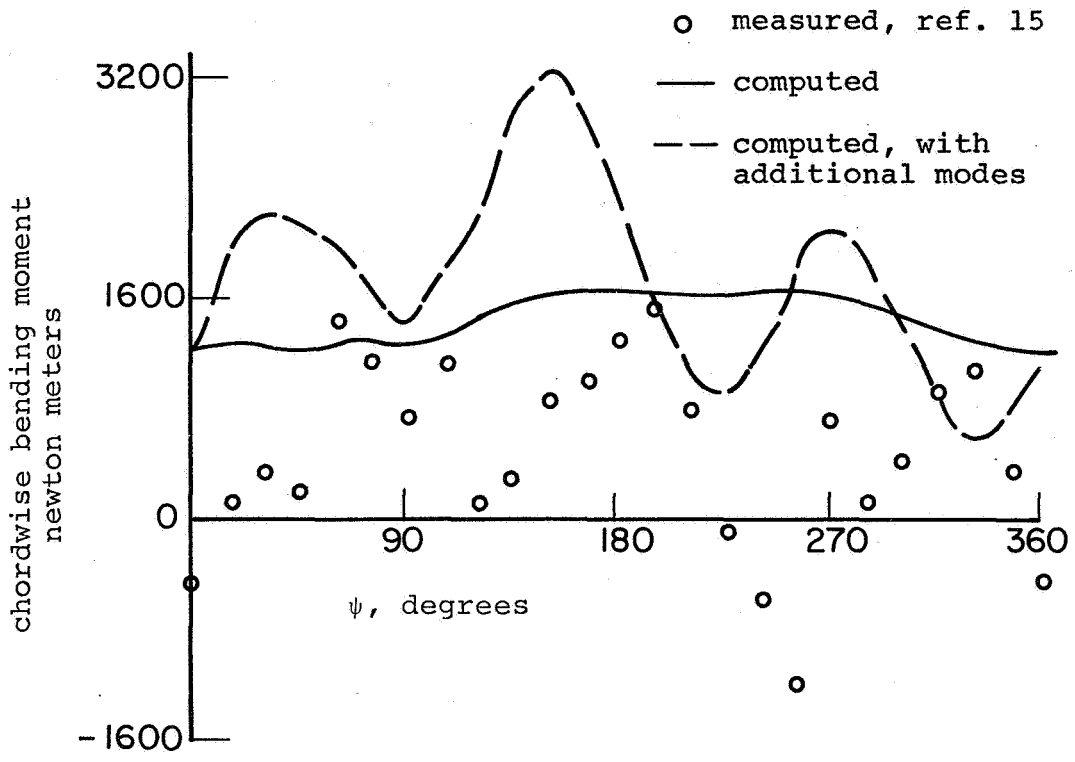

Figure 27. Chordwise bending moment for Case 6, with additional normal modes

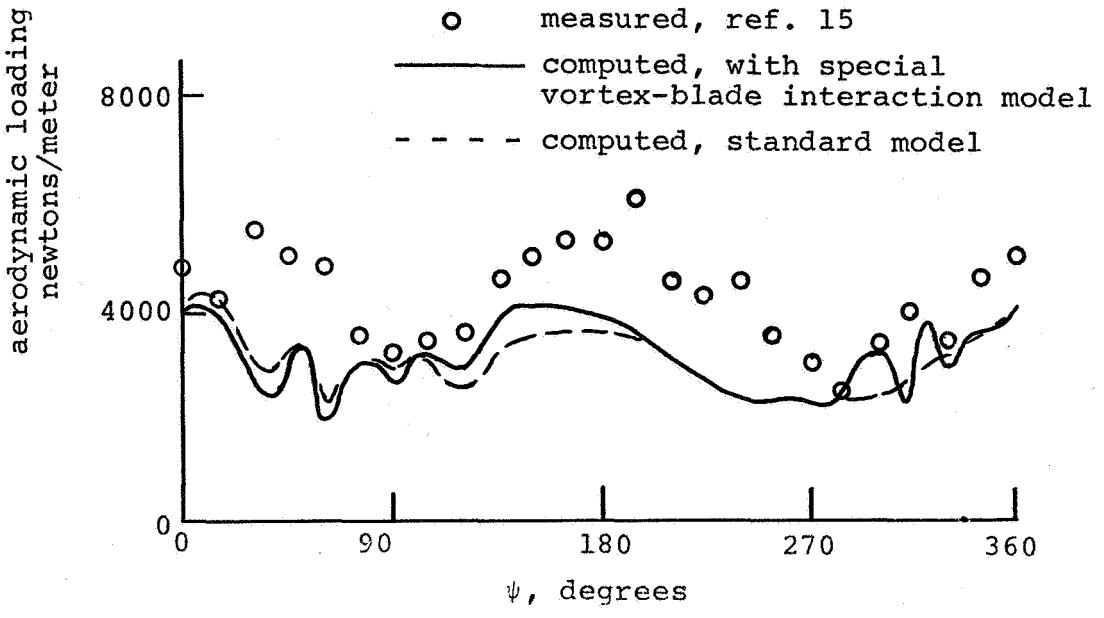

(a) loading at r=0.75R

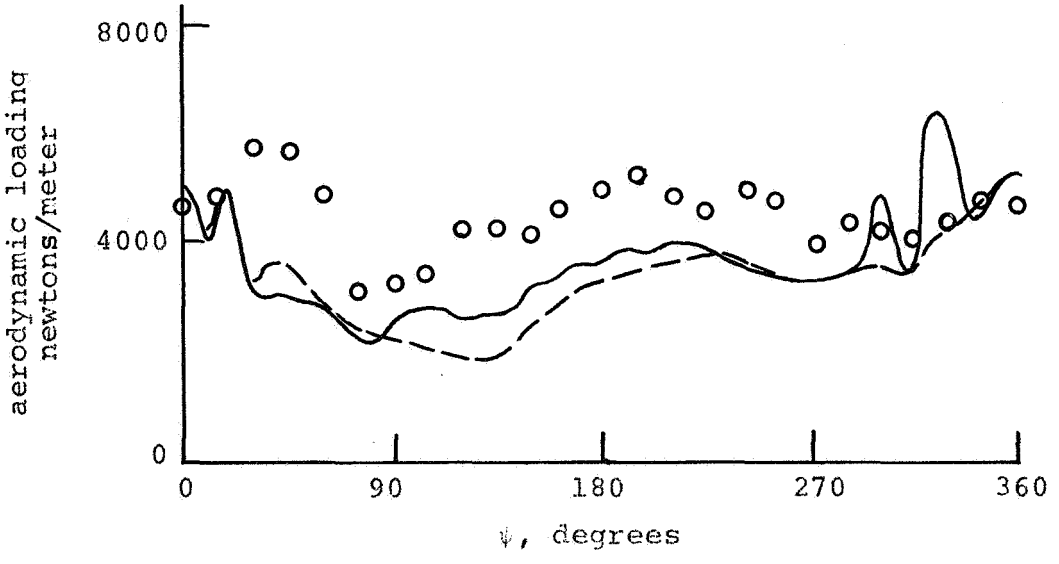

(b) loading at r=0.90R

Figure 28. Section aerodynamic loading for Case 6, H-34, pull-up, μ=0.224, f_g=1.4

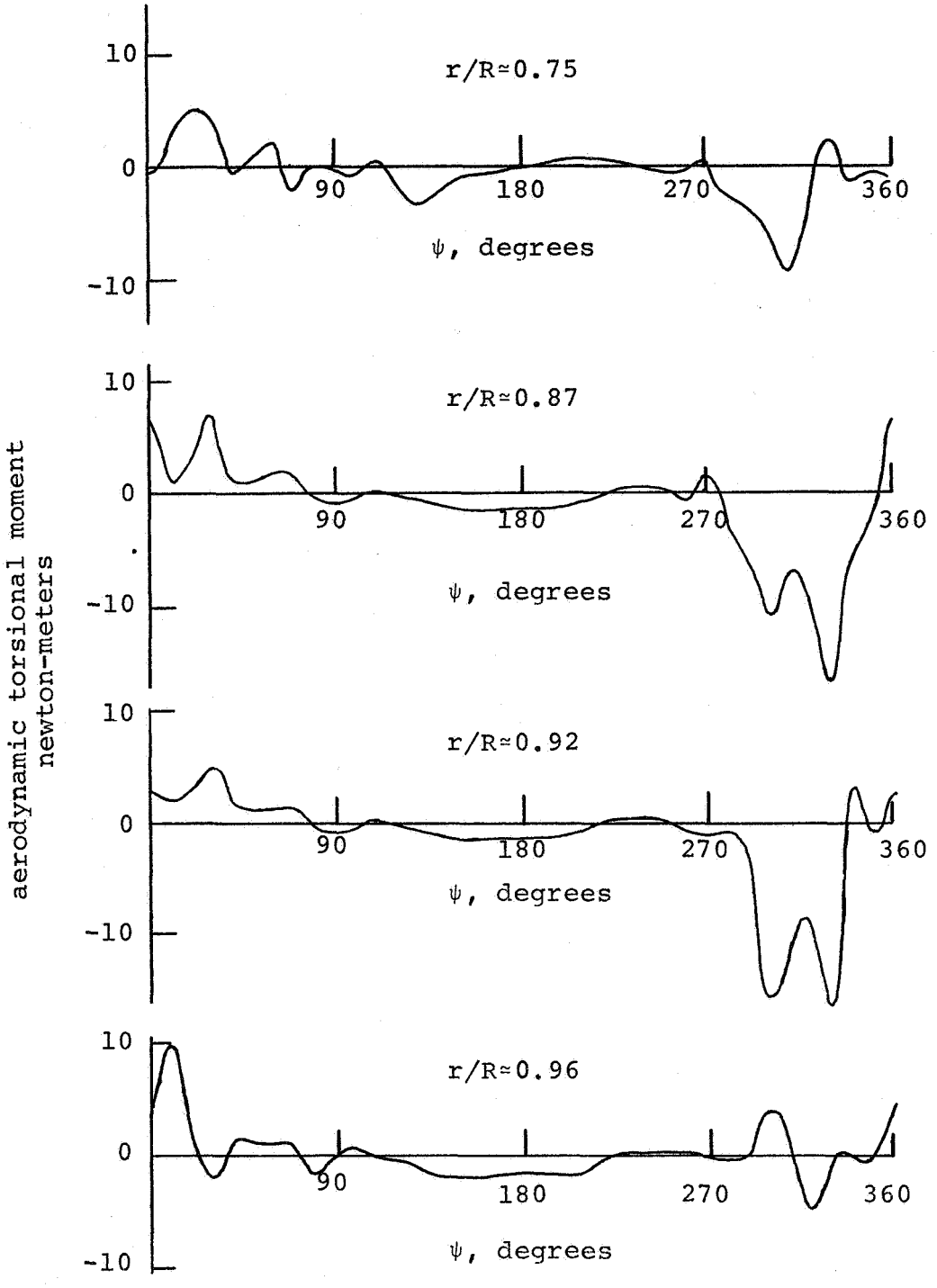

Figure 29. Computed aerodynamic torsional moment with special vortex-blade interaction model

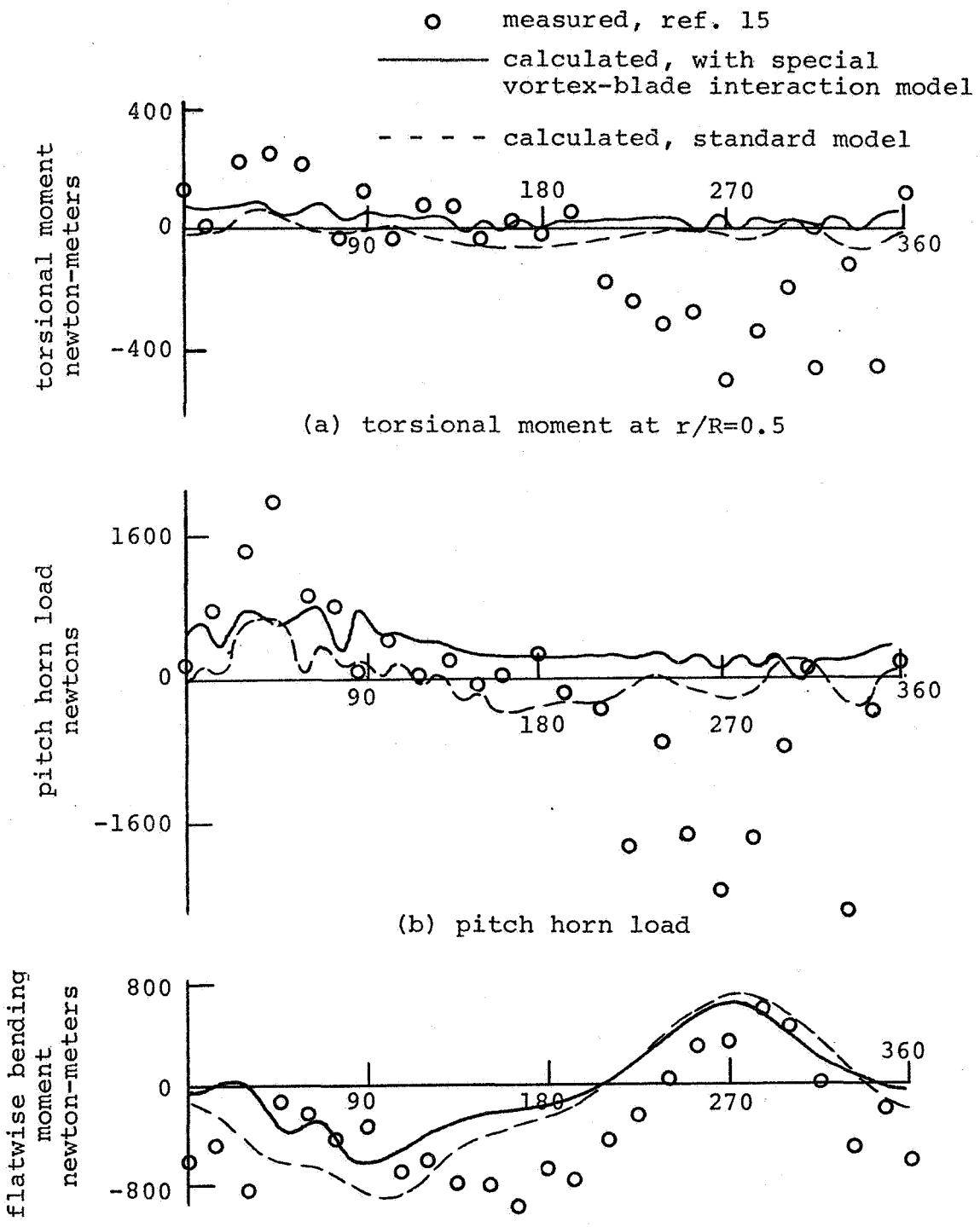

Figure 30. Blade response for Case 6

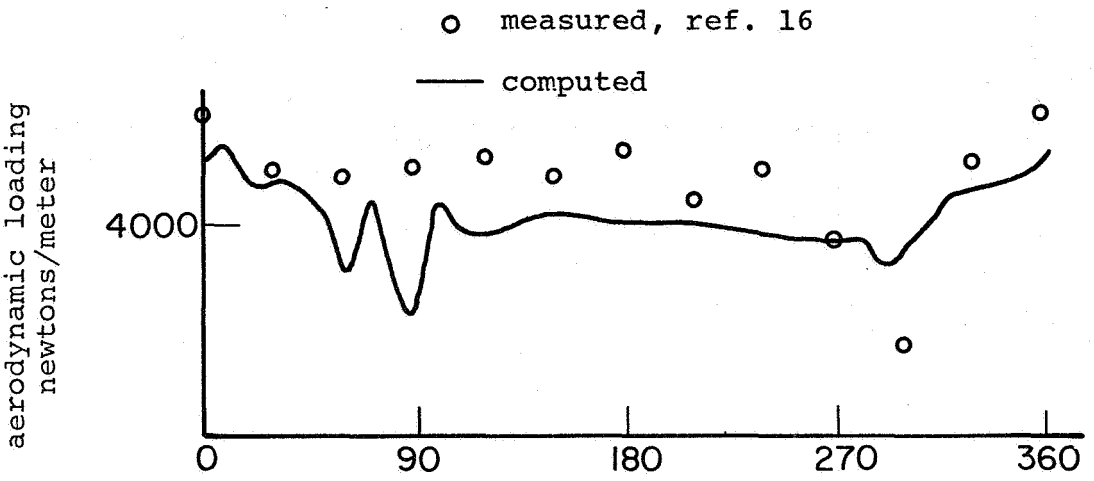

(a) loading at r≈0.75R

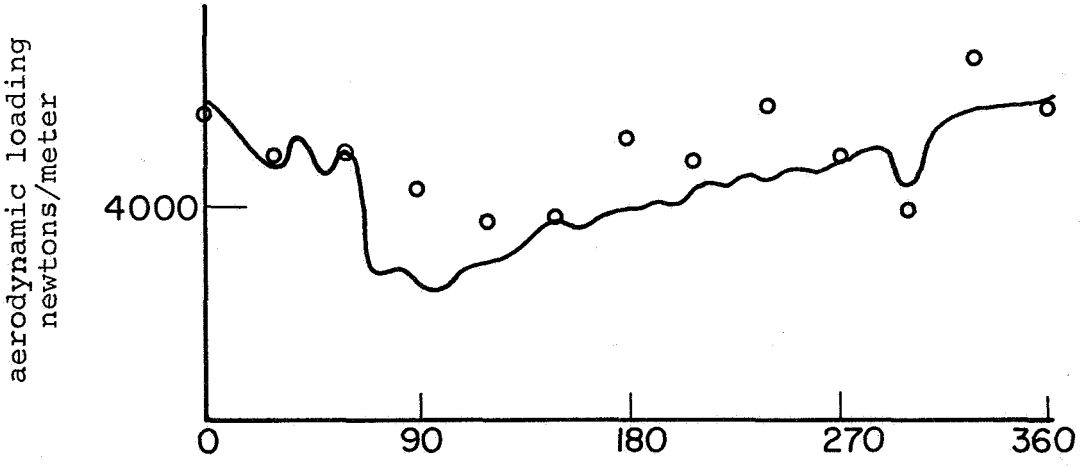

(b) loading at r≈0.90R

Figure 31. Section aerodynamic loading for Case 11, HU-1A, pull-up, μ=0.21, f_g=1.15

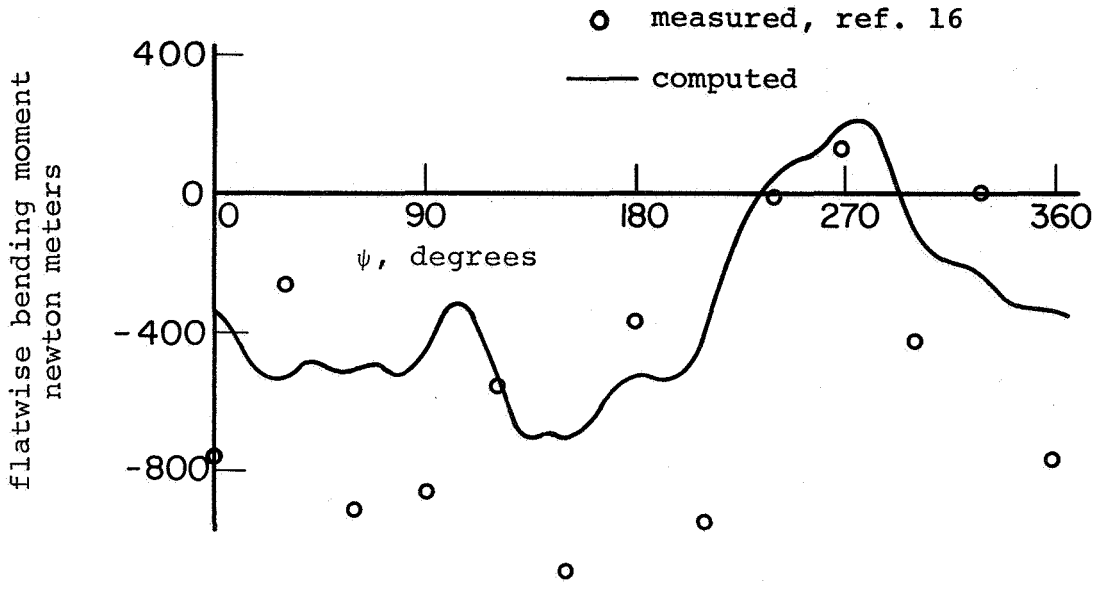

(a) flatwise bending moment for r≈0.65R

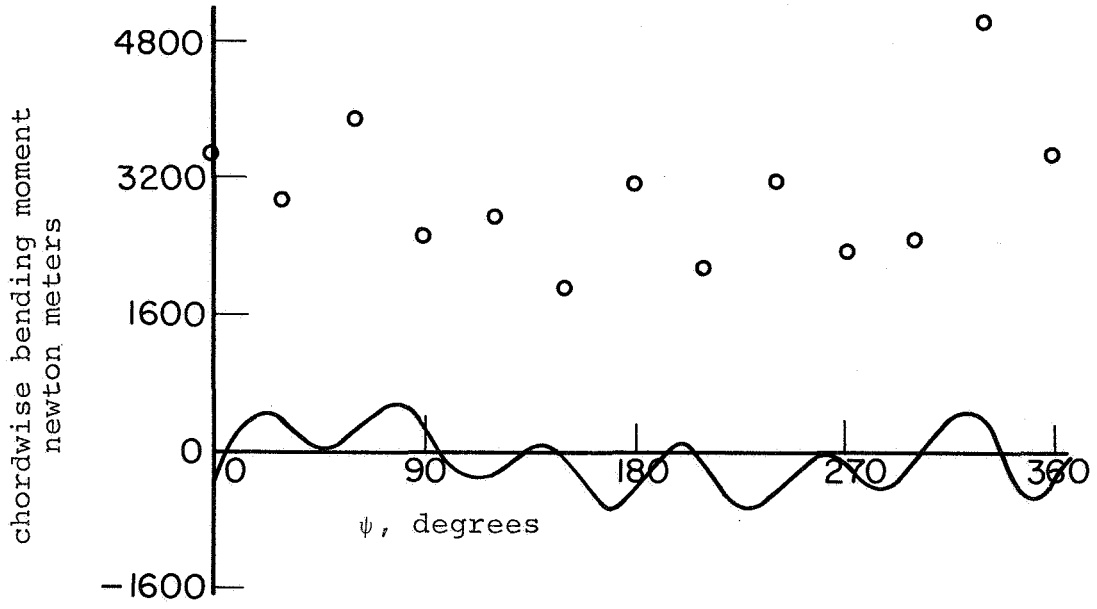

(b) chordwise bending moment for r≈0.60R

Figure 32. Bending moments for Case 11, HU-1A, pull-up, μ=0.21, f_g=1.15

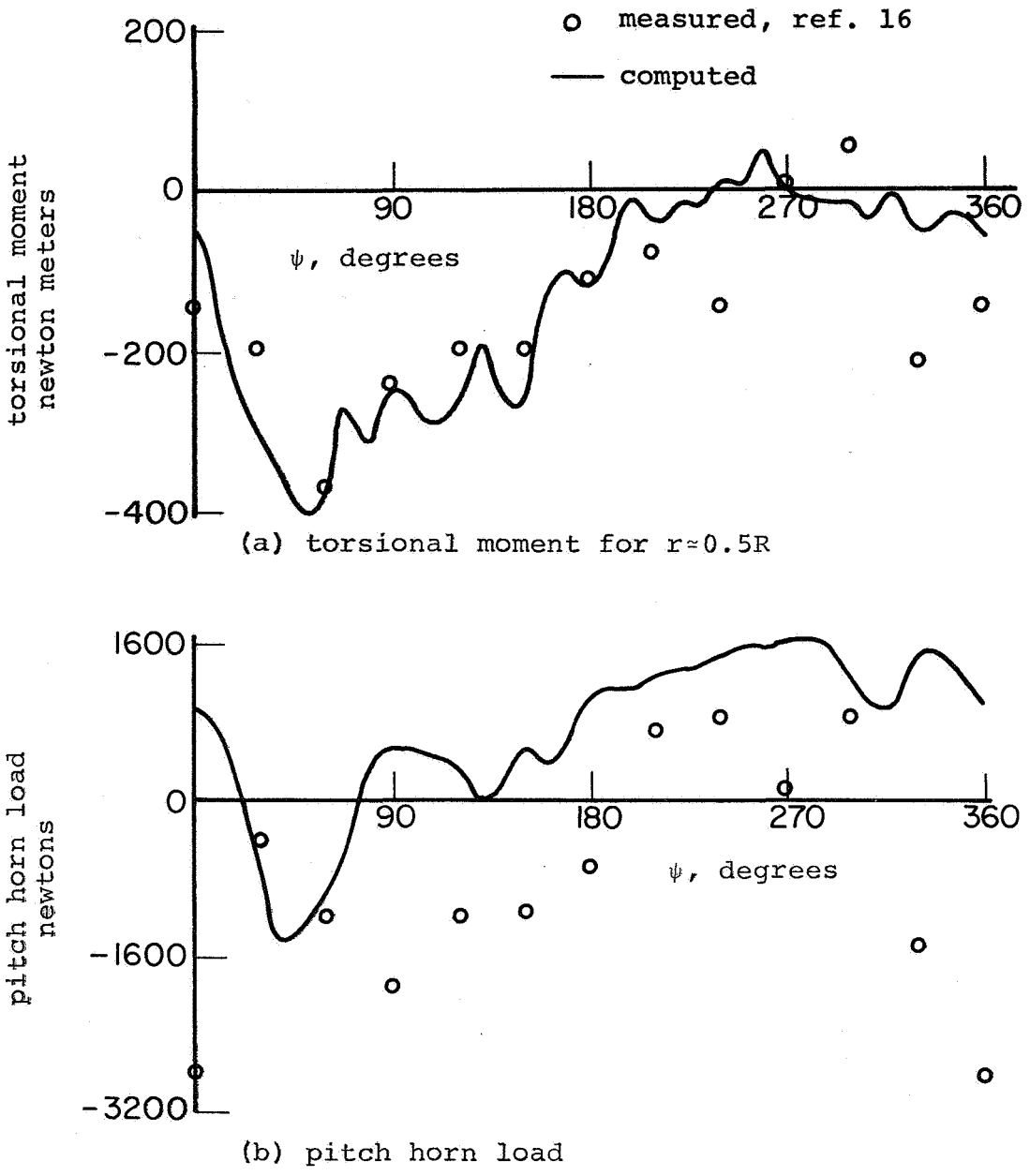

Figure 33. Torsional moment and pitch horn load for Case 11, HU-1A, pull-up, μ=0.21, f_g=1.15

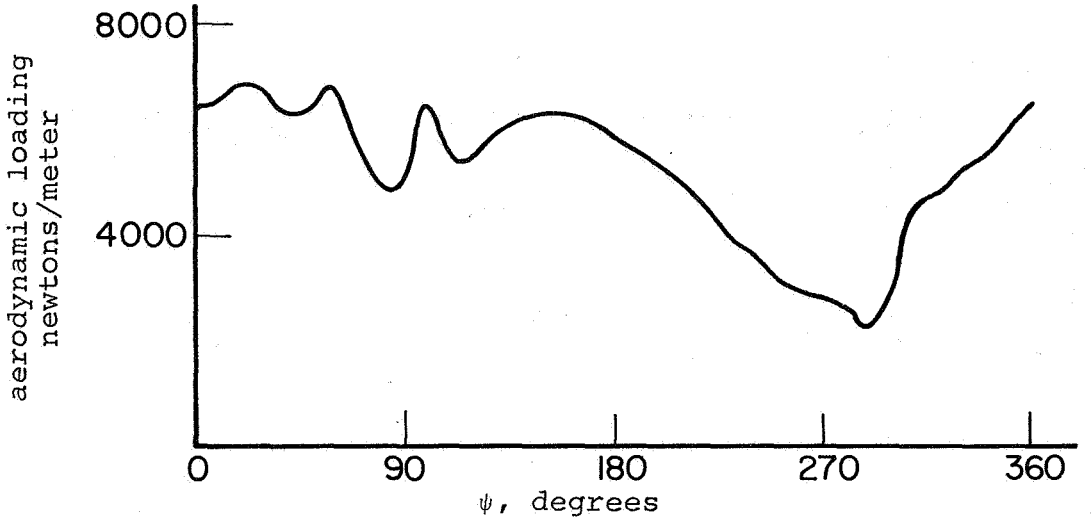

(a) loading for r≈0.75R

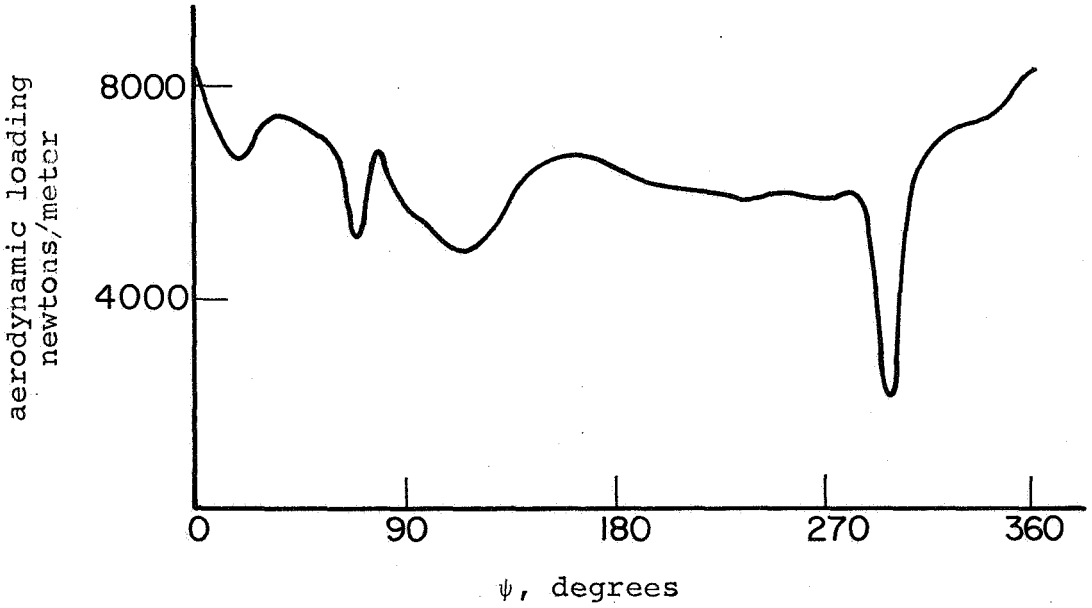

(b) loading for r≈0.90R

Figure 34. Section aerodynamic loading for Case 10, HU-1A, left turn, μ=0.24, f_g=1.5, computed only

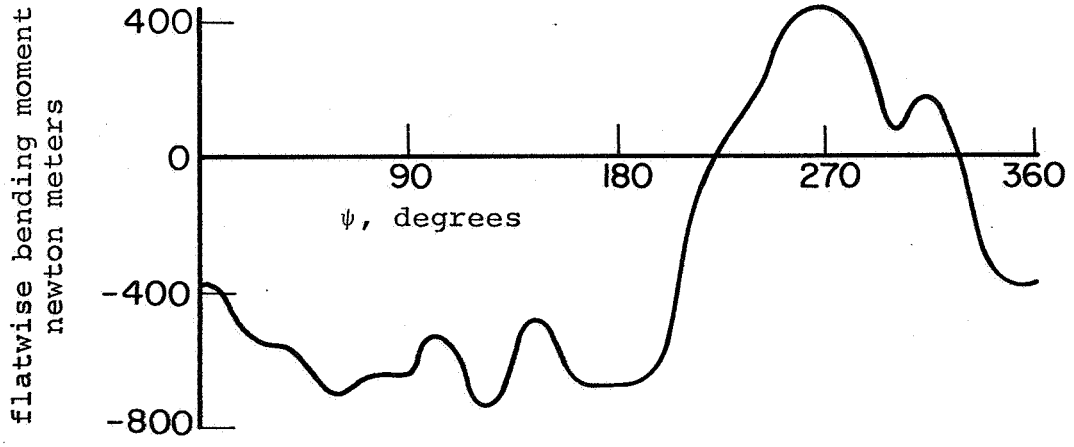

(a) flatwise bending moment for r=0.63R

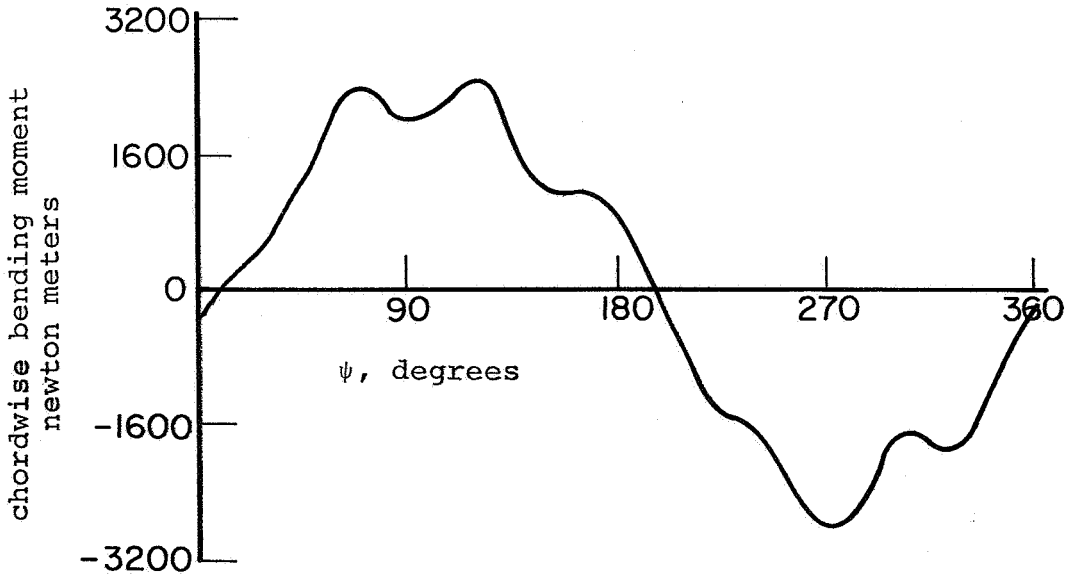

(b) chordwise bending moment for r=0.59R

Figure 35. Bending moment for Case 10, HU-1A, left turn, μ=0.24, f_g=1.5, computed only

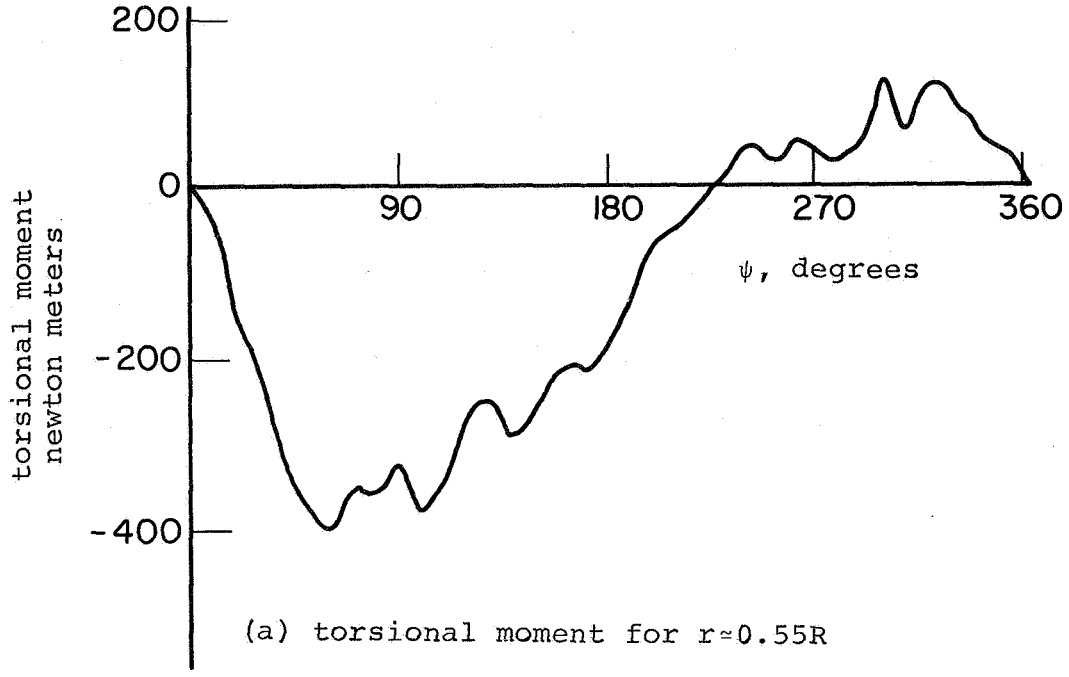

(a) torsional moment for r≈0.55R

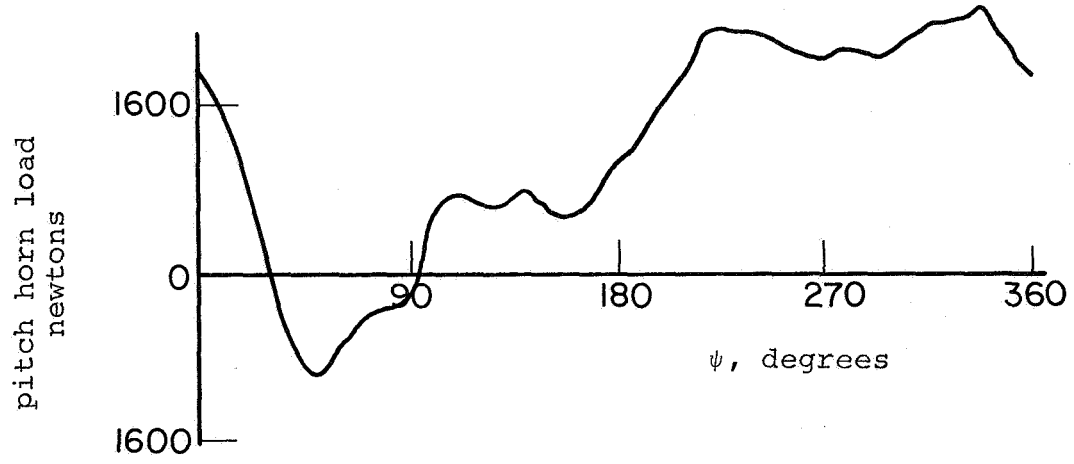

(b) pitch horn load

Figure 36. Torsional moment and pitch horn load for Case 10, HU-1A, left turn, μ=0.24, f_g=1.5, computed only

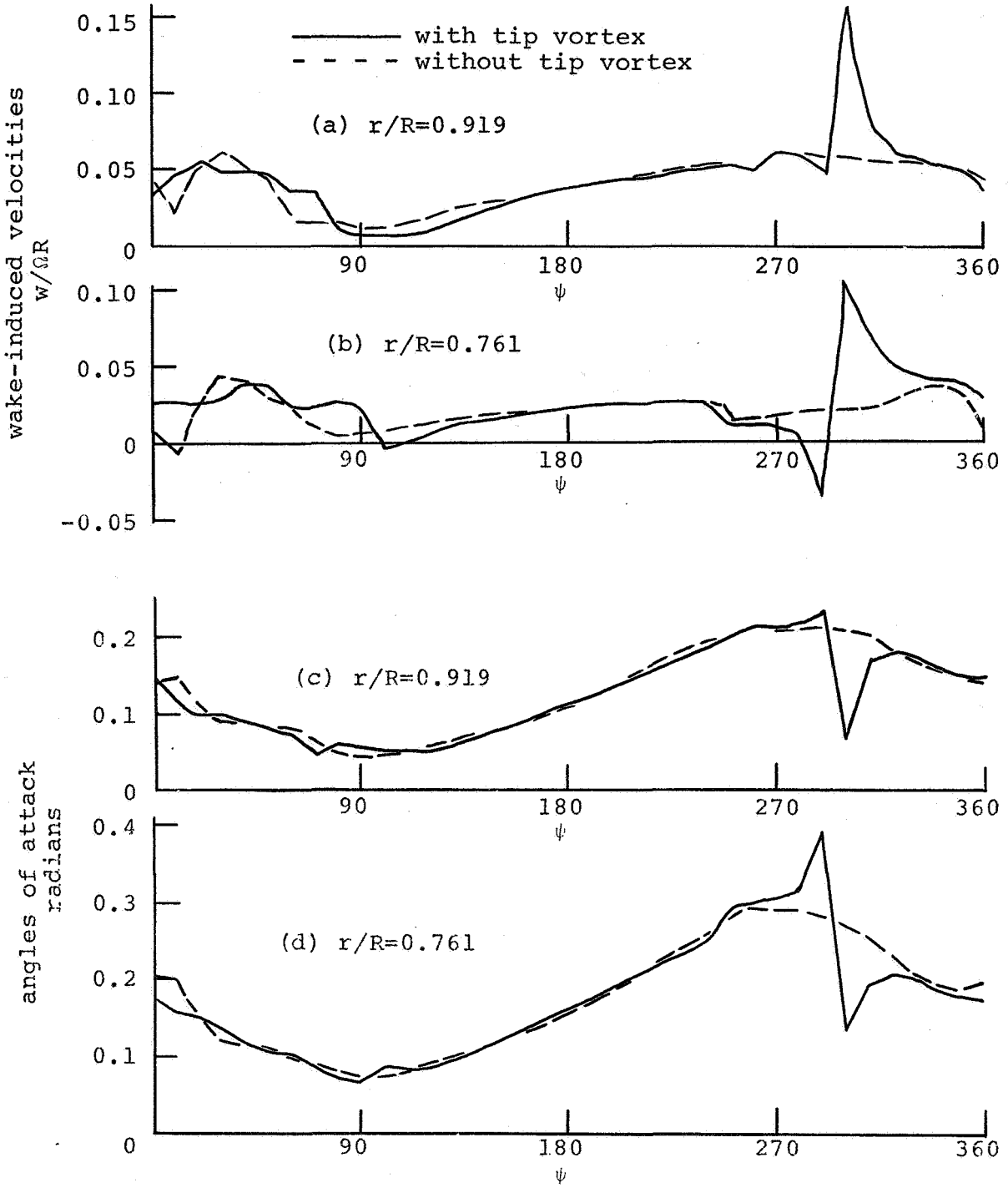

Figure 37. Case 10 computed wake-induced velocities and angles of attack with and without tip vortices

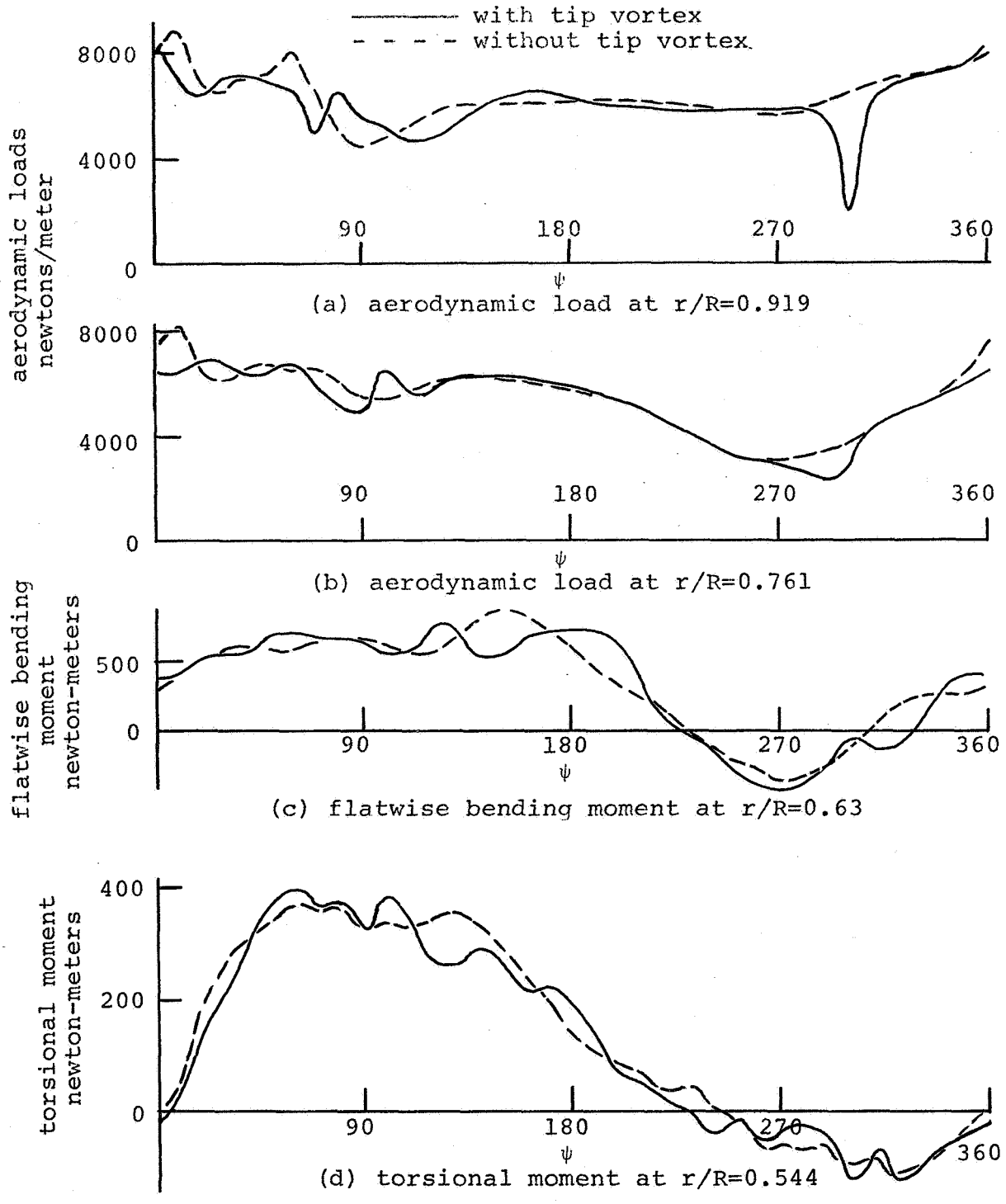

Figure 38. Computed air loads and response for Case 10 with and without the tip vortex

NATIONAL AERONAUTICS AND SPACE ADMINISTRATION
WASHINGTON, D.C. 20546

OFFICIAL BUSINESS
PENALTY FOR PRIVATE USE $300

FIRST CLASS MAIL

POSTAGE AND FEES PAID
NATIONAL AERONAUTICS AND
SPACE ADMINISTRATION
451

U.S.MAIL

POSTMASTER: If Undeliverable (Section 158 Postal Manual) Do Not Return

"The aeronautical and space activities of the United States shall be conducted so as to contribute . . . to the expansion of human knowledge of phenomena in the atmosphere and space. The Administration shall provide for the widest practicable and appropriate dissemination of information concerning its activities and the results thereof."

—NATIONAL AERONAUTICS AND SPACE ACT OF 1958

NASA SCIENTIFIC AND TECHNICAL PUBLICATIONS

TECHNICAL REPORTS: Scientific and technical information considered important, complete, and a lasting contribution to existing knowledge.

TECHNICAL NOTES: Information less broad in scope but nevertheless of importance as a contribution to existing knowledge.

TECHNICAL MEMORANDUMS: Information receiving limited distribution because of preliminary data, security classification, or other reasons. Also includes conference proceedings with either limited or unlimited distribution.

CONTRACTOR REPORTS: Scientific and technical information generated under a NASA contract or grant and considered an important contribution to existing knowledge.

TECHNICAL TRANSLATIONS: Information published in a foreign language considered to merit NASA distribution in English.

SPECIAL PUBLICATIONS: Information derived from or of value to NASA activities. Publications include final reports of major projects, monographs, data compilations, handbooks, sourcebooks, and special bibliographies.

TECHNOLOGY UTILIZATION PUBLICATIONS: Information on technology used by NASA that may be of particular interest in commercial and other non-aerospace applications. Publications include Tech Briefs, Technology Utilization Reports and Technology Surveys.

Details on the availability of these publications may be obtained from:

SCIENTIFIC AND TECHNICAL INFORMATION OFFICE

NATIONAL AERONAUTICS AND SPACE ADMINISTRATION

Washington, D.C. 20546